TILING OF CELLULAR STRUCTURES INTO THE PARTS ACCORDING TO THE DENSITY VALUES OF SIMP TOPOLOGY OPTIMIZATION

A THESIS SUBMITTED TO
THE GRADUATE SCHOOL OF NATURAL AND APPLIED SCIENCES
OF
MIDDLE EAST TECHNICAL UNIVERSITY

BY

DAMLA ÖZKAPICI HELVACI

IN PARTIAL FULFILLMENT OF THE REQUIREMENTS
FOR
THE DEGREE OF MASTER OF SCIENCE
IN
MECHANICAL ENGINEERING

SEPTEMBER 2020

Approval of the thesis:

TILING OF CELLULAR STRUCTURES INTO THE PARTS ACCORDING TO THE DENSITY VALUES OF SIMP TOPOLOGY OPTIMIZATION

submitted by **DAMLA ÖZKAPICI HELVACI** in partial fulfillment of the requirements for the degree of **Master of Science in Mechanical Engineering Department, Middle East Technical University** by,

Prof. Dr. Halil Kalıpçılar
Dean, Graduate School of **Natural and Applied Sciences** ______________

Prof. Dr. M. A. Sahir Arıkan
Head of Department, **Mechanical Engineering** ______________

Assoc. Prof. Dr. Ulaş Yaman
Supervisor, **Mechanical Engineering, METU** ______________

Examining Committee Members:

Assoc. Prof. Dr. Kıvanç Azgın
Mechanical Engineering, METU ______________

Assoc. Prof. Dr. Ulaş Yaman
Mechanical Engineering, METU ______________

Assist. Prof. Dr. Orkun Özşahin
Mechanical Engineering, METU ______________

Assoc. Prof. Dr. Yusuf Sahillioğlu
Computer Engineering, METU ______________

Assist. Prof. Dr. Eralp Demir
Manufacturing Engineering, Sabancı University ______________

Date: 24.09.2020

I hereby declare that all information in this document has been obtained and presented in accordance with academic rules and ethical conduct. I also declare that, as required by these rules and conduct, I have fully cited and referenced all material and results that are not original to this work.

Name, Surname: Damla Özkapıcı Helvacı

Signature :

ABSTRACT

TILING OF CELLULAR STRUCTURES INTO THE PARTS ACCORDING TO THE DENSITY VALUES OF SIMP TOPOLOGY OPTIMIZATION

Helvacı, Damla Özkapıcı
M.S., Department of Mechanical Engineering
Supervisor: Assoc. Prof. Dr. Ulaş Yaman

SEPTEMBER 2020, 137 pages

In this thesis, a method is proposed to enhance the performance of the parts optimized by Solid Isotropic Material with Penalization (SIMP) method. SIMP is a density-based topology optimization method which basically aims to distribute the material through the part subjected to various loads, boundary conditions and constraints in the optimum way. Thus, the part satisfies an optimization goal without violating the predefined constraints. The most prominent feature of this method is that the densities of the finite elements composing the part are either 1 or 0. The method penalizes the intermediate densities to converge to 1 or 0. One of the reasons behind the penalization is to provide a manufacturable geometry since intermediate density regions are difficult to fabricate. However, inclusion of these regions in the final topology may enhance the performance of the part. Based on this idea, a method is developed to use intermediate densities and it is applied on both 2D and 3D geometries.

The proposed method uses the density data obtained for each finite element as a result of the SIMP optimization. Then, the part is remodelled with rectangular cellular structures which have user defined dimensions. The area or volume of the cellular structures are proportional to the average density of covered elements. The main focus of the method is to generate lightweight, simple-shaped, and manufacturable geometries with satisfying performances. Besides, it proposes a novel technique to generate fully connected geometries, and also a technique to remove excess powder remaining inside the part after fabrication for 3D geometries in powder or resin based additive manufacturing machineries. The performance of the method is compared with the SIMP method for all geometries and other optimization techniques, such as homogenization and genetic algorithms through analysis and tests.

Keywords: Additive Manufacturing, Topology Optimization, SIMP, Cellular structures, Connectivity Analysis

ÖZ

SIMP TOPOLOJİ OPTİMİZASYONUNUN YOĞUNLUK DEĞERLERİNE GÖRE PARÇALARIN HÜCRESEL YAPILAR İLE KAPLANMASI

Helvacı, Damla Özkapıcı
Yüksek Lisans, Makina Mühendisliği Bölümü
Tez Yöneticisi: Doç. Dr. Ulaş Yaman

Eylül 2020 , 137 sayfa

Bu tez çalışmasında Katı İzotropik Malzeme Cezalandırma (SIMP) yaklaşımı ile topoloji optimizasyonu yapılan parçaların performansını artırmaya yönelik bir yöntem sunulmuştur. SIMP, temel olarak malzemeyi çeşitli yüklere, sınır koşullarına ve kısıtlamalara maruz kalan bir parça üzerinde en optimum şekilde dağıtmayı, böylece parçanın önceden tanımlanmış kısıtlamaları ihlal etmeden bir optimizasyon hedefini karşılamasını amaçlayan yoğunluk tabanlı bir topoloji optimizasyon yöntemidir. Bu yöntemin en belirgin özelliği, malzemeyi parçayı oluşturan sonlu elemanların özkütlesinin 1 ya da 0 olacak şekilde dağıtmasıdır. Yöntem, ara yoğunluğa sahip olan elemanların özkütlesini cezalandırma yöntemi ile 1 veya 0'a yakınsar. Cezalandırma yönteminin amaçlarından biri optimizasyon sonucunda üretilebilir bir çıktı yaratmaktır. Bunun sebebi ara yoğunluktaki elemanlara sahip bir geometrinin üretiminin genellikle mümkün olmamasıdır ama bu elemanların da optimizasyon çıktısına dahil edilmesi daha iyi performansa sahip geometrilerin oluşmasını sağlayabilir. Bu görüşten yola çıkarak, ara yoğunluğa sahip elemanların da kullanılmasını sağlayan bir yöntem geliştirilmiş ve 2 ve 3 boyutlu geometrilere uygulanmıştır.

Geliştirilen yaklaşım, SIMP optimizasyonu sonucunda her sonlu elemana atanan yoğunluk bilgisini kullanır. Optimizasyonu yapılan parça, kullanıcı tanımlı boyutlara sahip dikdörtgenel hücresel yapılar ile tekrar modellenir. Hücresel yapıların alanı veya hacmi, kapladığı sonlu elemanların özkütlelerinin ortalaması ile doğru orantılıdır. Bu yöntemin asıl amacı hafif, basit şekilli, kolayca üretilebilen ve performans açısından yeterli çıktılar oluşturmaktır. Ayrıca bu yöntem, birbirine tamamen bağlı elemanlar içeren geometrilerin oluşumu ile üç boyutlu parçalarda üretimden sonra fazlalık tozun parçanın içerisinde kalmasını engelleyen yenilikçi bir yöntem önerir. Metodun başarımı, tüm geometriler için SIMP yöntemi ile, bazı 2D geometriler içinse ek olarak homojenizasyon ve genetik algoritmlar yöntemleri ile test ve analizler aracılığı ile karşılaştırılmıştır.

Anahtar Kelimeler: Eklemeli İmalat, Topoloji Optimizasyonu, SIMP, Hücresel yapılar, Bağlantı Analizleri

To my all time favorites Sultan & Turgut Özkapıcı, Dilsu & Kerem Bahadır, Mert Helvacı and Menderes Kiper...

ACKNOWLEDGMENTS

I would like to express my sincere thanks to my supervisor, Assoc. Prof. Dr. Ulaş Yaman, for his guidance and councelling, encouragement and patience during this study.

I would like to thank my colleagues Gökhan Öztürk and Yankı Çelebi for their valuable support and technical guidance throughout the study.

I would also like to thank my colleagues Dr. Evren Tan for his help in the fabrication process, and Dr. Ferhat Sağlam for his guidance through the tests.

I am grateful to my mother, sister and husband for their valuable support and always standing by me.

TABLE OF CONTENTS

CHAPTERS

LIST OF TABLES

TABLES

LIST OF FIGURES

FIGURES

LIST OF ABBREVIATIONS AND SYMBOLS

ABBREVIATIONS

2D	2 Dimensional
2.5D	2.5 Dimensional
3D	3 Dimensional
AM	Additive Manufacturing
BESO	Bi-directional Evolutionary Structural Optimization
CAD	Computer Aided Design
CAM	Computer Aided Manufacturing
CNC	Computer Numerical Control
EBM	Electron Beam Melting
ESO	Evolutionary Structural Optimization
FEA	Finite Element Analysis
FDM	Fused Deposition Modelling
GA	Genetic Algorithms
SLM	Selective Laser Melting
SLS	Selective Laser Sintering
SIMP	Solid Isotropic Material with Penalization
SLA	Stereolithography
TO	Topology Optimization

SYMBOLS

d_x	Size of the user defined cell in x direction
d_y	Size of the user defined cell in y direction
d_r	Distance between the centers of a cell and its corner neighbor in 2D space
p_{ij}	The center point of the cell numbered as j on the i_{th} closed body
C_{ij}	The cell numbered as j on the i_{th} closed body
ρ_l	Density of a cell

CHAPTER 1

INTRODUCTION

1.1 Motivation and Problem Definition

Topology optimization is a widely used tool in designing applications. It basically aims to distribute the material through a part in the most optimum way so that the part satisfy a pre-described optimization goal, such as minimizing the weight or maximizing the stiffness. Topology optimization outputs were used as an insight into the design rather than being the design output itself until recent years, since most of the optimization results have a complex geometry which make them almost impossible to manufacture. Advances in additive manufacturing made the most important contribution to topology optimization at this point. It enables the use of optimization results directly since complex geometries can be manufactured easily by AM techniques.

Solid Isotropic Material Penalization (SIMP) is among the most popular optimization methods. Basically, it distributes the material through a part according to the finite element analysis results done in accordance with the optimization objective. At the end of the optimization, every finite element in the design domain is assigned a material whose density is either 1 or 0. There are not any elements with intermediate densities, because the method penalizes them to either converge 0 or 1. The reason for penalization is that intermediate density regions are generally not manufacturable. However, including these regions in the topology may increase the performance of the parts. Based on this idea, a method is proposed to include the intermediate density regions in the final topology and its performance is compared with the parts optimized by SIMP and other methods, such as homogenization and genetic algorithms, which also rejects intermediate densities. The performances of the parts are examined through tests and analysis and their success is measured by their load carrying capacities.

1.2 Proposed Methods and Models

The proposed method enables generation of regions with intermediate densities without violating the manufacturability constraints of the geometry. In this method, firstly, the parts are optimized by SIMP to obtain the density data assigned to each finite element. Then, the entire design domain is filled with rectangular cellular structures whose area or volume is proportional to its density. The main focus of the method is to generate easily manufacturable geometries whose performance is comparable with its SIMP optimized form.

In this study, the method is applied on both 2d and 3d geometries. A cantilever beam, a simply supported beam and a hanger geometry is used as the 2d examples. The performance of the method is compared with the SIMP optimized forms of geometries as well as the parts optimized by other techniques, in terms of their load carrying capacities.

The 3d part that the method is applied is a bracket used for connecting two rotating parts to move together. Its performance is compared with the result of the density-based optimization done in Ansys, which is a finite element analysis software.

1.3 Contributions and Novelties

The contribution and the novelties of the proposed method can be ordered as follows for 2d geometries:

- Satisfying performance with an easily manufacturable geometry
- Generating fully connected topology by adding new cells to the neighbors of the unconnected element as opposed to majority of techniques that deletes the unconnected element

and for 3d geometries:

- Generation of simple shaped geometries as an optimization result
- No post-processing required to prepare the parts for printing, i.e. ready to print results
- Easily manufacturable parts
- Satisfying performance
- Generation of fully connected topologies without deleting the unconnected element as in majority of the present methods
- Dust-free design
- Accessible internal features

1.4 The Outline of the Thesis

The focuses of the following chapters can be summarized as follows:

- Chapter 2: General information about additive manufacturing and its applications, including topology optimization, is given and related research about the topic are presented briefly
- Chapter 3: The proposed method for 2d geometries are explained and some example geometries remodelled with the proposed method are presented
- Chapter 4: The proposed method for 3d geometries are explained and an example geometry remodelled with the proposed method is presented
- Chapter 5: The results of the analysis and tests done to measure the performance of the proposed method for 2d geometries are given
- Chapter 6: The results of the analysis and tests done to measure the performance of the proposed method for 3d geometries are given
- Chapter 7: The conclusions of the thesis are summarized

CHAPTER 2

LITERATURE REVIEW

In this chapter, a general information is given about the concepts related to the thesis study. The generic additive manufacturing process, the related manufacturing methods, the advantages, the limitations and the applications of additive manufacturing including the topology optimization is explained through related studies in the literature.

2.1 Additive Manufacturing

Additive manufacturing (AM) is a transformative approach to conventional manufacturing methods. In contrast to the conventional methods that fabricate parts through subtraction of material, AM methods manufacture parts by adding layers of material on top of each other. Although it has been studied for years, developments in this area have gained momentum with the development of computer technologies like Computer Aided Design (CAD) and Computer Aided Manufacturing (CAM). AM process begins with designing of a part on CAD software. The,n the designed part is converted to an STL file, which is a common file format for all the AM processes. STL file represents the outer surface of the object with triangulated meshes. It contains no information about the color, material, units or the scale of the 3D model. In the next step, STL file is transferred to the machine software (CAM) for fabrication instructions. There, the 3D model is sliced into layers and a G-code file is generated. Finally, the machine builds the object layer by layer [1]. AM technologies can be divided into four main categories according to the state of raw material, namely liquid polymer, discrete particles, molten material and solid sheets systems. These approaches are summarized in the next section.

2.2 Additive Manufacturing Methods

Liquid based systems generally use polymers, photopolymers and hydrogels as raw material. The most well-known technology in this category is Stereolithography (SLA). SLA uses an ultraviolet light to cure the photosensitive resin at each layer. It has a relatively high building speed and good part resolution among the other AM technologies. The high cost of the resin and its supply, and the limitation of the type of material that can be used are among the disadvantages of this process [2]. Discrete particle systems use material powder and a heat source to melt powders, and fuse every layer to each other. Selective Laser Sintering (SLS), Selective Laser Melting (SLM) and Electron Beam Melting (EBM) technologies can be given as examples for powder based systems. The most distinguishing advantages of these systems are that wide range of materials can be used [3]. and support structures are not required to build parts. Additionally, fully dense and strong parts without voids can be built with these methods. However, surface finishes of the objects may not be as good [4]. Molten material systems most commonly use thermoplastics as raw material. However, metal, ceramic and wax have also been in use for a while [2]. Fused Deposition Modelling (FDM) is the most popular technology in this category. Basically, thermoplastic filaments are heated to their melting temperature and then they are extruded through a movable head onto a substrate. After the extrusion, material solidifies as it cools down and forms a layer. Objects fabricated with FDM requires support structures and does not generally have good surface quality. However, being cheap and accessible makes it a preferred method especially for “Do It Yourself” projects [5]. Solid sheet systems uses sheet form of material. Each layer is cut by laser/knife according to the shape specified by the STL file. Then, the layers are bounded to each other by the application of heat and pressure. This is a low cost process, and it does not require support structures and post-processing. Another advantage is that large scaled objects can easily be fabricated by this method. The need for the processing of the waste material and the laborious work can be considered as the disadvantages of these processes [3].

2.3 Advantages and Limitations of AM

Building objects by adding layers on top of each other, which is common to all of the above mentioned processes, offers many advantages compared to the traditional methods such as CNC machining. Firstly, considering the overall production process, AM is much faster than the CNC machining. When producing a part on CNC machinery, it may be required to change the location of the part and the tool in order to machine different features on the part [1]. For example, to fabricate a rectangular object that contains threaded holes on its two perpendicular faces, the tool should be changed to drill the hole and the object should be rotated 90 degrees to machine the hole on the other face. However, the same part can be fabricated on a single stage by using AM without the need for changing the tool or stopping the machine. Thus, reduction in process steps provides saving of time, money and energy. Besides, the material used can be recycled and used for the next printing. Therefore, AM is also an eco-friendly choice. One of the greatest advantages provided by the AM is that the complex geometries can be manufactured easily while the conventional methods remain incapable of producing such intricate artifacts [2]. Because of the accessibility limits of the machine tool that prevents the tool to touch on the surface to be machined, some geometric features may not be fabricated by CNC machining. In order to fabricate nested parts, for example, all the components comprising the part should be manufactured separately and then assembled to each other. However, such objects can be manufactured with AM in a single step.

Although AM technology has made great progress, it still has some limitations. One of its limitations is that it does not have a broad range of material to be used for manufacturing [2]. Since traditional manufacturing methods are used in industry for decades, there is an available database of materials defining their mechanical and thermal properties. Besides, all materials are standardized through industry-accepted norms. Thus, manufacturers can ensure that the material used meets the quality specifications and the industry specific standards. On the other hand, since AM is a relatively younger technology, there is a lack of information on the properties of the materials. Therefore, common global standards and properties database should be developed for AM materials. Another limitations of the AM may be the poor part accuracy and surface quality in some techniques [6]. and the limited size of materials due to small building cabin volumes. Additionally, although recycling of many materials is one of the important advantages of AM, some materials such as polymers may loss their quality after recycling. Therefore, there is still ongoing research on this issue.

2.4 Applications of AM

There are many applications of AM in industry. It is commonly used in aerospace, automotive, biomedical, bio-fabrication and energy areas. Aerospace components, for example, have generally complex geometries. They also need to be lightweight, so materials like titanium, which are hard to process by traditional methods, are commonly used. Therefore, AM is a expedient choice for such components. As an example, a compressor support case for a gas turbine engine is produced by Arcam with EBM technology using titanium alloy and the turbine blades having complex interior channels are fabricated by Concept Lazer and Morris Technology with SLM method by using Inconel 718 and cobalt chrome alloy, respectively [4]. Another example is that Daneshmand et. al used SLS in order to build wind tunnel testing model of a launch vehicle configuration [7]. This model is fabricated in a shorter time and at a lower cost by AM compared to the case fabricated by CNC machining. CRP Technology applies AM techniques in the motor sports field. It produced a titanium F1 gearbox using SLS technology. While the fabricated item has approximately 20% less weight and volume, its torsional stiffness is doubled and it consumes less power [4]. Similarly, Optomec produced titanium brackets by AM for suspension mounting using both 90% less material and reducing production time and cost. Prometal fabricated a complete intricate shaped engine block with its cooling and oil channels in just a week [4].

AM techniques are also used in biomedical field to fabricate products like tissues and orthopedic and dental implants. In these applications, patient-specific customized parts can be manufactured. For example, Adler Ortho Group produced a CE-certified hip prosthesis by using Arcam EBM technology [4]. Similarly, Concept Laser and MTT Technologies produced dental prosthesis and dental bridges respectively, by using SLM technology [4]. Another example for customized products can be given from Siemens. It produced over ten million custom hearing aid shells providing better fit to ears, and they stated that they received positive feedback from their customers [8].

2.5 Lattice Structures and Their Application Areas

The conveniences provided by AM also contributed to the emergence of new design concepts which were not considered before due to the limitations of the conventional subtractive manufacturing processes. One of the concepts in this context is the lattice structures. Lattice structures can be defined as an array of periodic patterns of unit cells and space where unit cell is the smallest feature of the structure.

Lattice structures have a wide variety of application areas due to their many advantageous properties. One of the most important advantages is that they can be highly stiff and lightweight at the same time, which makes them preferable for lightening applications. S. Moon et al. [9] used lattice structures for Unmanned Aerial Vehicle wing design and demonstrated the satisfying load-carrying capacities of these light structures by compression tests. Another study run by NASA focuses on using lattices in space structures which must handle high bending loads with the lowest mass possible [10]. They currently work with octet and cubic-octet form of lattices. It is stated that the octet lattice meet the project requirements and it is simpler to fabricate. However, the cubic-octet lattice provides a two times lighter solution. Both lattice structures are expected to reduce the mass of existing space structures by at least 20%. It is also stated that cubic-octet formed lattice provides energy absorption and thermal protection for the structure it is used. Lattice structures can handle great deformations which makes them favorable for shock absorbing applications. Schaedler et al. [11] studied the energy absorber properties of different types of metallic lattice structures and showed that lattices have better performances when compared to the conventional materials. Z. Ozdemir et al. [12] investigated the deformation behavior of lattice structures caused by dynamic loading. They showed through Hopkinson Pressure Bar tests that lattice samples can spread the impact loading and reduce the amplitude of the peak stress in time.

Lattice structures are also widely studied for the heat-exchanger applications. Light structures with high surface areas may be a perfect fit for heat transfer applications. Besides, by changing the cell geometry, size and orientation, thermal properties of the structures can be enhanced. V. Kumar et al. [13] investigated the effects of cell orientation on heat transfer properties of materials. They used five lattice structures having hexagonal shaped periodic unit cells. Each type of lattice cell have different orientations. They observed different levels of temperature drop between the inlet and the outlet of the lattices, which ensures that the orientation of cells affects heat flow characteristics of materials. The authors fabricated the parts by using EBM process. Generally, artifacts produced with powder-based AM techniques does not have a good surface quality. However, this may be advantageous for heat exchanger applications. It is observed that heat transfer increases as a rougher surface expands the surface area. In another study, M. Pelanconi et al. [14] searches for the radiative heat transfer performances of three types of ceramic lattice structures produced by SLA process with different sizes but the same surface area. The size of the cells significantly affects the radiative heat transfer. The authors showed by tests and analysis that the radial heat transfer in a tube increases by 160% to 200% when ceramic lattices are inserted inside a tube. It is possible to use ceramic lattices inserted tubes which are shortened by a third, instead of a long empty tube. Thus, lattice structures also provide a more compact solution for heat exchangers.

Another application area of lattice structures is biomedical industry. They are widely used as bio-implants. C. Emmalmann et al. [15] designed an osseo-integrative surface of a hip implant with lattice structures to avoid stress shielding and allow bone growth. When the original joint is replaced by an implant, the stress applied to the bone is generally reduced. This is because the implant used is much stiffer than the original joint. Therefore, while the bone was experiencing higher stresses before, now the applied stress is shared between the implant and the bone. Since bone development is proportional to the stress experienced, it gets weaker in time. This is called “stress shielding” [16]. In order to avoid this phenomena, the authors used an implant comprising of lattice structures. The implant is fabricated by SLM method with Ti-Al6V4 powders. While the lattice implant’s Young modulus is less than the conventional fully solid implants due to their porous form, it is demonstrated that it shows 70-90% similarity with the original joint. Thus, it managed to avoid stress shielding while functioning properly. The study also showed that it is possible to create a curved surface with high dimensional accuracy by using lattice structures.

2.6 Fabrication of Lattice Structures

Lattice structures can be manufactured both by conventional methods and AM approaches. Sheet metal forming, casting and wire bonding processes are among the traditional methods used for lattice fabrication [17]. However, these methods are only able to produce simple topologies. AM techniques, on the other hand, are not restricted with the complexity of the geometries. Artifacts with sophisticated shapes can be manufactured easily due to its layer by layer building process. There are many AM techniques in use appropriate for lattice manufacturing. Fused deposition modelling, powder bed processes such as electron beam melting, selective laser melting and selective laser sintering, and stereo-lithography are among the most common techniques for lattice fabrication [18].

Properties of the fabricated lattice structures are affected by the selected manufacturing process parameters. For example, the minimum size of the unit cell significantly depends on the particle size of powders and laser spot diameter [18]. A laser with a smaller diameter and finer powders can produce a structure with thinner struts. Additionally, the unit cell size should allow the removal of the unused material after fabrication. It is a commonly faced problem that excess powder or resin may remain in the structure during the fabrication of lattices in the powder bed and photopolymer based systems. The need for support structures is another limitation for lattice fabrication. Sections of the part that makes an angle larger than 45 degrees with respect to the building direction are called overhanging sections, and they need to be supported for a successful 3D printing process [19]. While powder bed processes do not require extra structures to be built since unused powder provides supporting function, liquid or molten material based systems such as SLA and FDM use sacrificial structures. Although they are required in most of the AM processes, use of sacrificial structures have some drawbacks. Firstly, the material used for building generally cannot be reused by the machine, resulting in material waste. Secondly, the removal of the supports after fabrication requires considerable amount of handwork and time. In addition, the need for the hand or tool access into the regions comprising supports for their removal restricts the design freedom of the lattice structures. Therefore, minimizing the number of supports in the lattice structures for the ease of manufacturing becomes the main subject to many studies. One of the most commonly used methods for this problem is topology optimization (TO).

2.7 Topology Optimization

TO is one of the specialized fields utilizing the advantages of AM. Basically, it aims to find the optimum structural layout which satisfies an optimization goal without violating the predefined constraints. Although the method suggests satisfying solutions, it was not that applicable in terms of manufacturing in recent years since the optimization usually ended up with complex geometries [20]. However, advances in AM technology led this field to develop rapidly due to the ease of manufacturing and made TO an even more studied topic.

In this context, Brackett et al. [19] used TO to generate overhang-free lattice structures. They used a filter to detect features that need support structures and then penalize them iteratively to achieve the optimum design. In a similar study, M. Langelaar [21] proposed a filter to integrate with TO process for an optimal design which is self-supporting. It is stated that in order for an element to be self supported, its density should not be larger than the element with the maximum density in its support region. The support region for an element consists of the element just below it and its direct neighbors, in the previously printed layer. Thus, the TO process tries to suggest a solution where every element is sufficiently supported by the previous layers and thus does not require support structures.

TO is not only used for minimizing the fabrication-based limitations, but also for increasing the performance of the overall part such as maximizing the compliance and/or minimizing the weight. The weight reduction is an important goal, especially in the aviation and automobile industry, to reduce the need for fuel and accordingly, CO2 emissions. Fraunhofer University, for example, developed a load-adapted wheel knuckle integrated with lattice structures through TO [22]. They stated that the volume of the knuckle is reduced by 25% and its rigidity is increased. After it is produced by SLM process, it is tested and installed on a prototype race car successfully. In another example, GE Aviation developed a fuel nozzle with a topology optimized interior channels to be used in LEAP aero-engines [23]. As a consequence, the optimized part is stronger than the conventional one, and it has 25% less weight. Altair managed to decrease the overall weight of the Airbus's passenger aircraft, A380, by 500 kg by redesigning the Droop Nose Ribs using TO [24]. Thus, fuel consumption and the CO2 emissions of the aircraft is reduced. In a study carried out by the EOS and the Airbus, CO2 emission over the life-cycle of Airbus A320 nacelle hinge bracket is reduced by 40% through weight reduction done by TO. TO is also applied to enhance the mechanical performances of artifacts. In this context, T. Gao et al. [25] used a TO based methodology for the design of a precision machine tool pedestal to avoid non-uniform creep relaxation over the structure, which may affect the machining accuracy. As a result, more uniform distribution of reaction forces is obtained in the structure. Besides, maximum displacement of the pedestal is reduced by 35% and the first natural frequency is increased by 15%. In another example, J. Zhu et al. [26] studied on minimizing the compliance of a cockpit windshield. Adverse weather conditions or incidents like bird strike may cause significant warping deformation around the windshield. The authors used TO in order to redistribute the critical loads which lead large warping deformations. They managed to reduce the strain energy from 0.16 J to 0.02 J.

2.8 Topology Optimization Methods

Several methods are used for TO. Homogenization method is one of the earliest in this field, which is introduced by Bendsøe and Kikuchi [27] in 1988. In this method, the purpose is to find the optimal distribution of micro-cells in a design domain according to a predefined optimization purpose, which is the minimum compliance for this study. The process begins with discretization of the design domain into micro-cells that consists of rectangular micro-voids. After the material properties are calculated for each micro-cell through the homogenization theory, optimization problem is solved based on the finite element analysis (FEA) done in accordance with the optimization goal. The authors applied the method on several 2D geometries for two cases. In the first case, the design variable for the problem is chosen as the size of the holes. The density of each micro-cell can be altered by changing the hole sizes. As a result, they observed a topology having many intermediate density regions, which makes the manufacturing of the structure not possible. In the second case, they introduced the orientation of the holes as the additional design variable and solved the optimization problem. The hole's size and orientation determine the optimal material distribution in the reference domain. It is shown that the majority of the micro-cells have densities 1 or 0 which implies that the resulting topology has a precise shape. Thus, it can be manufactured easily.

There are many studies employing homogenization method. As opposed to the general trend of minimizing the compliance for more stiff structures, S. Nishiwaki et al. [28] used homogenization method to maximize the compliance. They stated that flexibility may provide better performance for some structures such as compliant mechanisms which provide transmission motion through elastic deformation. In another study, L.H. Tenek et al. [29] used this method to maximize the eigen-frequencies of plates. G. Allaire et al. [30] optimized topologies for the minimum stress design. J. Yoo et al. [31] solved the optimization problem in order to enhance the performance of structures in a magnetic field by maximizing magnetic mean compliance.

Solid Isotropic Material Penalization (SIMP) is one of the most widely used density-based topology optimization methods [[32]-[33]]. It aims to find the optimal density distribution of the elements in a design domain to achieve a prescribed optimization purpose. In this method, the design variable is the density of each micro-cell. Unlike the homogenization method, it utilizes a penalization factor to avoid formation of regions with intermediate densities. As penalization factor is set to a value higher than unity, the method forces the densities of regions to converge either 1 or 0, since intermediate density regions are hard to manufacture. Thus, topologies with only solid-void elements are constructed. SIMP method is also subject to many studies. D. Tcherniak [34], for example, used the SIMP optimization to maximize the amplitude of vibrations of a resonating structure at a specific frequency. One problem the authors faced is the presence of many grey regions which imply intermediate densities.

It is stated that although the SIMP method works well for majority of static loading problems, it is not such effective for dynamic cases. Thus, in order to eliminate grey regions, the resulting designs should be subjected to post-processing in order to have fully solid-void topology. However, the change of topology may significantly affect the natural frequency of the structure. Therefore, the result may deviate from the optimal design. The authors state that they had not been able to manufacture the optimized part due to grey regions and thus could not execute any test or analysis on the part to compare with the original design. In order to utilize the regions having intermediate densities without converging their densities either 1 or 0, Yaman et al. [35] proposed a method which is called "Variable Thickness Approach" to benefit from the density field with intermediate values. They state that the reason for the SIMP to penalize intermediate densities is because of they are not manufacturable. If these regions are gained on the topology, more stiff structures may be observed. From this point of view, they applied the SIMP on a beam without penalization. After each mesh element is assigned a density value, the entire design domain is covered by a surface with varying thickness. The part of the surface corresponding to a mesh element has a thickness proportional to the density of the associated element. As a result, it is seen that the part modelled with this method has approximately 5 times higher load to weight ratio when compared to the SIMP optimized part with unity penalization. In another study, Y. Liu et al. [36] created a multi topology lattice structure optimized by the SIMP [36]. Firstly, they constructed a unit cell library which consists of different types of unit cells with different densities and Young Modulus. The properties of each type of unit cell is calculated by the homogenization method. Then, they applied the SIMP optimization for the maximum structural stiffness on both 2D and 3D geometries and find the density distribution throughout the part. After obtaining density values for each mesh element, the appropriate unit cell from the library is assigned to the associated cell. The unit cell to be assigned is selected according to its relative Young Modulus. For instance, a mesh element with a higher density should be filled with the unit cell that have larger relative Young Modulus. However, if there are multiple unit cells sharing the same Young Modulus, then the cell with the lower density relative to the Young Modulus ratio is preferred to fill the associated mesh element. Thus, an optimized multi-topology lattice structure with uniformly varying density is created.

Evolutionary Structural Optimization (ESO), Bi-directional Evolutionary Structural Optimization (BESO) and Ground Structure Method are also popular methods for topology optimization. The ESO method is firstly introduced by Xie and Steven in 1993 [37]. In this method, a structure evolves towards an optimal geometry by slowly removing the less efficient material from the ground structure. BESO method is an improved version of the ESO. It differs from the ESO by adding material to the areas experiencing high stress, for example, while removing redundant material simultaneously [[38]-[39]]. Ground Structure Method is a similar concept to ESO and BESO methods. It searches for the optimum element connectivity in a dense structure consisting of many possible connections by decreasing the number of connecting members gradually [40].

Another optimization method called Genetic Algorithms (GA) has been increasingly popular recently. It is based on the Darwin's natural selection theory. This method searches for the optimum solution consistent with the optimization goal in a population of candidate solutions. The steps of the method can be explained with the work of Jakiela et al [[41]-[42]]. The authors applied the method on cantilever plates. The process begins with a set of initial topologies which are composed of rectangular and fully solid elements. Secondly, connectivity analysis are applied on each topology to ensure cellular structures forming the part are connected to each other. If there are unconnected cells, they are removed from the structure. Then, a fitness value based on the optimization purpose is calculated for each topology. The fitness of a structure shows to what extent the optimization goal is achieved. As an analogy to the natural selection theory, less efficient solutions with lower fitnesses are eliminated while the better ones survive. Therefore, solutions with higher efficiency creates new set of topologies by changing their design characteristics. The newly generated population have a higher average fitness. It is a process that continues until the average fitness of population converges. As a result of optimization with GA, multiple topologies are created unlike the previously mentioned methods that end up with a single solution. Initial set of topologies are selected as only solid and void combinations of cellular structures. Therefore, the resulting topologies do not have regions with intermediate densities. It is also seen that although the topologies are checked for connectivity at the beginning of the process, there are still some unconnected cellular structures present in the final results.

CHAPTER 3

TILING OF CELLULAR STRUCTURES IN 2D

Many optimization methods such as homogenization, SIMP, ESO, BESO, ground structure and genetic algorithms tend to generate geometries with densities 1 and 0 only. The methods avoid intermediate density regions since these parts of the structure are almost impossible to manufacture. In this study, a method is proposed to create a fully connected and manufacturable topology consisting of intermediate density regions. The idea behind the method is that bringing the intermediate density regions to the final topology may enhance the performance of the overall structure. Based on this point of view, the proposed method is applied on 2d and 3d geometries which are optimized by the SIMP beforehand, and the performances of the resulting topologies are compared with their initial SIMP optimized forms as well as the parts optimized by other techniques, in terms of their load carrying capacities.

3.1 Application of Proposed Method on 2D Geometries

The basic steps of the method are shown in Figure 3.1. The process begins with designing the geometry to be optimized in CAD software (Rhinoceros3D). After then, the boundary and the loading conditions for the geometry are defined in a visual programming tool called Grasshopper3D, which runs with Rhinoceros3D. Then, the SIMP optimization is applied on the part in order to obtain the optimum material distribution throughout the design domain. As a result of the optimization, a density value is assigned for all the finite elements comprising the geometry. The density data is then used for remodelling of the entire domain with cellular structures, whose volumes are proportional to the densities of the regions they cover. In order to ensure that all cells comprising the part is connected to each other, connectivity analysis are applied on the part. Finally, an STL file is created for the resulting topology and the part is fabricated by the selected AM technologies. Details of these steps are given in the following sections.

In order to explain the theory behind the proposed method, a cantilever plate example in a study done by Jakiela et al. [42] is used. In the following sections, the steps of the method for the cantilever plate example are explained in detail. Additional examples for which the proposed method is applied are provided in the analysis and test results section.

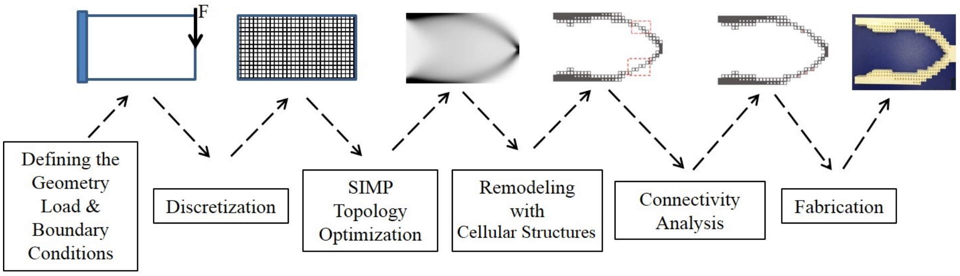

Figure 3.1: Steps of the proposed method for 2d geometries

3.1.1 Defining Geometry & Boundary Conditions

A cantilever plate geometry from the work of Jakiela et al. [42] is used as an example. The plate in the original work is scaled down for the ease of manufacturing by preserving the prescribed ratio of the edges, which is 1.6. As a result, a $96mm$ x $60mm$ rectangular plate is used as the initial geometry. It is fixed from the left edge and a unit force is applied on the middle of the right edge as shown in Figure 3.2.

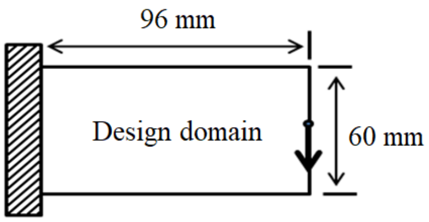

Figure 3.2: Cantilever geometry and boundary conditions

The geometry is first generated in Rhinoceros3D, which is 3D CAD software commonly used in industries such as product design, industrial design and architecture. 3D geometries are modelled by a mathematical representation technique called Non-Uniform Rational B-Splines (NURBS). Using NURBS, any shape can be generated precisely from curves to complex 3D geometries without any limitation on the complexity of parts. That's why Rhinoceros3D is highly utilized in 3D printing applications.

After generating the geometry in Rhinoceros3D, the boundary and the loading conditions of the plate are described in Grasshopper3D. Grasshopper3D is an add-on for Rhinoceros3D and used for visual programming purposes. As opposed to the text-based programming approaches, it allows to represent the scripts by visual components rather than lines of codes written as text. The algorithms are constructed by using functional blocks and monitoring their relation with each other. It is also possible to use scripting languages such as Python within Grasshopper3D.

In this study, all the coding part is done in Grasshopper3D and Rhinoceros3D is used for the visualization of the script outputs. The representation of the plate in Rhinoceros3D and the part of the script for the description of boundary and loading conditions are shown in Figure 3.3. The blocks are referred by the numbers next to them throughout the chapter.

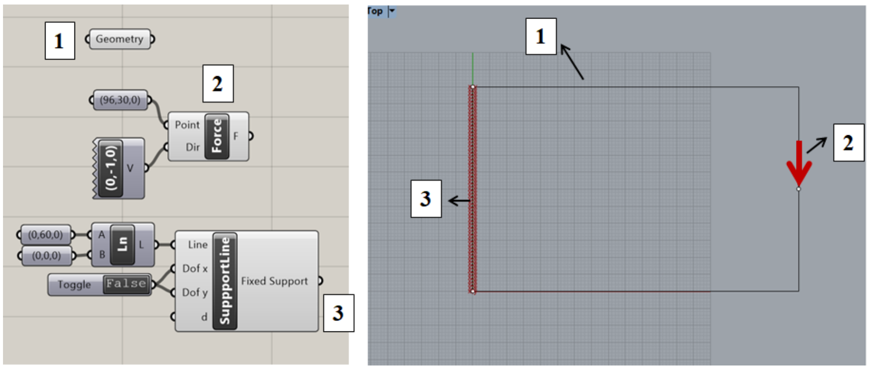

Figure 3.3: Cantilever plate geometry (1), force applied (2) and the fixed support (3) script in Grasshopper (Left) and the visualization of plate in Rhinoceros (Right)

3.1.2 SIMP Topology Optimization

SIMP optimization is done automatically by a plug-in called TopOpt developed for Grasshopper3D. TopOpt plug-in requires several inputs. The first input is the design domain. It is the area enclosed by the outer boundaries of the geometry to be optimized as shown in Figure 3.2. It is also possible to set the solid and void areas within the domain which are wanted to stay untouched after optimization. The domain is discretized into $1mm$ by $1mm$ finite elements before the optimization as shown in Figure 3.4. The next inputs are the force and supports present in the geometry. The location of the force application points and the supports, and the magnitude of the force are specified as shown in Figure 3.3. Then, the optimization settings are adjusted; volume fraction, penalization factor and minimum feature size after the optimization. Volume fraction is set as 0.25 as in [42]. In order to include intermediate density regions in the optimization result as much as possible, the SIMP is applied without any penalization. Therefore, the penalization factor is set to unity. Finally, the minimum feature size is set as $2mm$ by taking the capabilities of 3D printer into consideration. The code block for the optimization settings is shown in Figure 3.5.

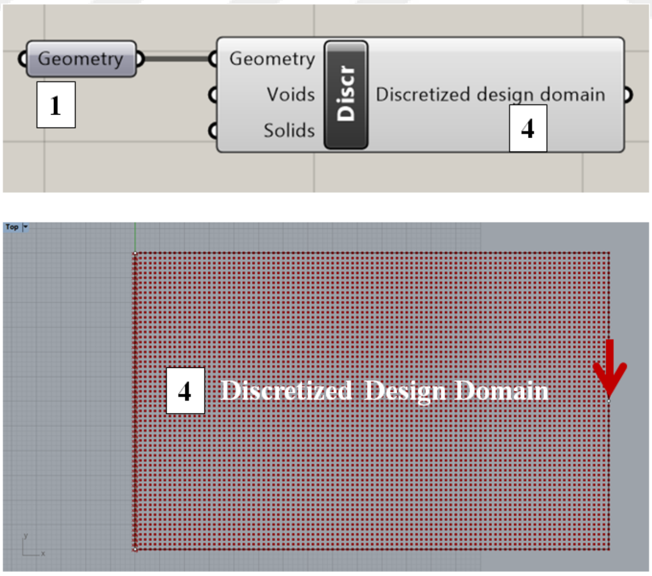

Figure 3.4: Grasshopper3D block for design domain discretization (4) in Grasshopper3D (Top) and the visualization of the discretized geometry in Rhinoceros3D (Bottom)

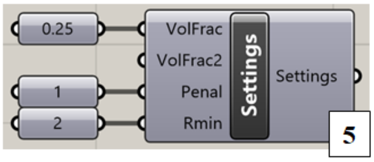

Figure 3.5: Grasshopper3D block for the optimization settings

As the last step, all the inputs are fed to the TopOpt block and the optimization is run. At the end of the optimization, a density list showing the density values of each finite element is taken as output. The optimized geometry is visualized by using the block “Preview.1Mat”. The script related to the SIMP optimization and the optimized topology can be seen in Figure 3.6.

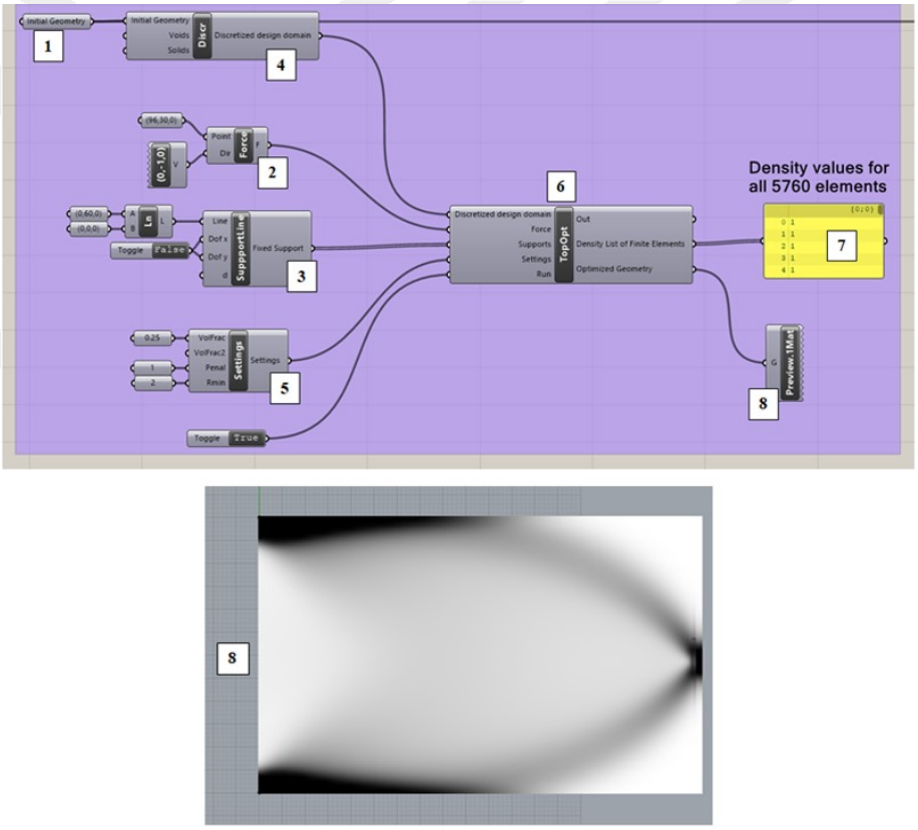

Figure 3.6: All the inputs (1-5) fed into the TopOpt module (6), density list as output (7) in Grasshopper3D (Top) and the representation of the SIMP optimized cantilever plate without any penalization in Rhinoceros3D (Bottom)

As it can be seen from Figure 3.6, the optimized geometry which is generated without any penalization has many non-manufacturable regions due to the intermediate densities. In order to compare this result with the case where penalization is performed, the SIMP method is applied on the same geometry with a penalization factor of 3. In this case, it is seen that truss-like structures are formed and the proportion of intermediate density regions is reduced significantly. The resultant topology can be seen in Figure 3.7.

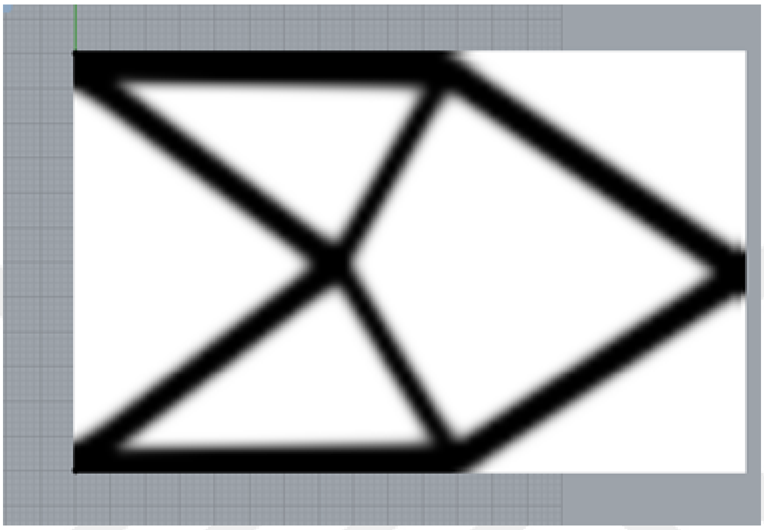

Figure 3.7: Representation of the SIMP optimized cantilever plate with a penalization factor of 3 in Rhinoceros3D

3.1.3 Remodeling with Cellular Structures

The first step after the SIMP optimization of the 2d geometry is to discretize the design domain with rectangular grids which have user defined dimensions. The size of the grids is the same as the size of the cellular structures in which the optimized geometry will later be remodelled with. In this example, $3mm$ by $3mm$ grids are used. As a next step, the average density of 9 elements covered by $3mm$ grids are calculated. The code block related to the generation of grid cells and the average density calculation are shown in Figure 3.8. The initial rectangular geometry which is defined at step 1 before the SIMP optimization, densities of finite elements created in step 4, and the user defined dimensions of grid cells to be generated in x and y directions are taken as inputs to the code block. The output is the newly discretized design domain with user defined grids and the density value of each grid in the domain.

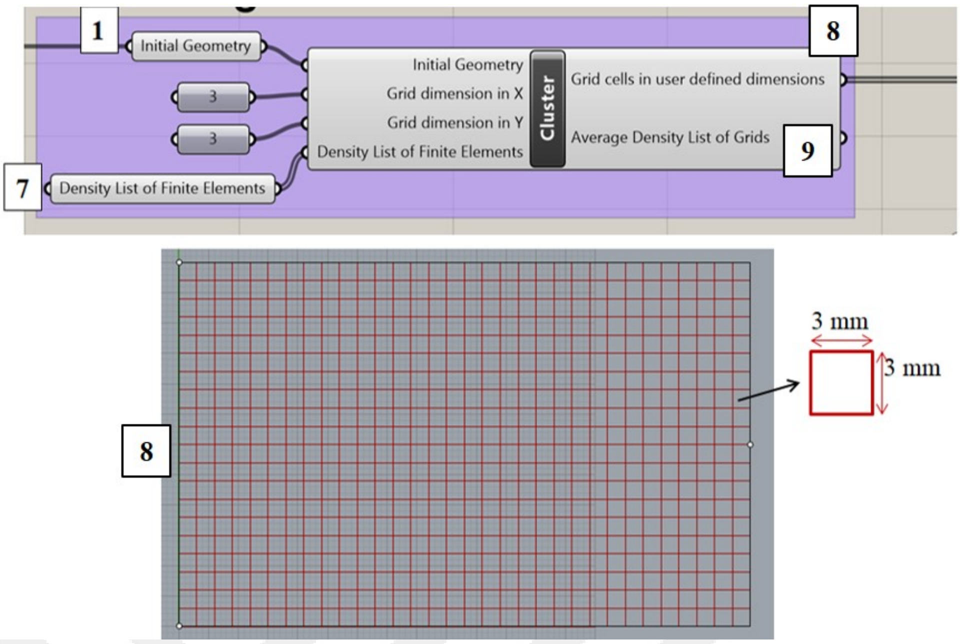

Figure 3.8: Discretization of design domain with grid cells

The next step is to fill the design domain with cellular structures. Each cellular structure covers an area proportional to its density. Three types of cellular structures that are categorized according to their densities are used. The first group of structures are fully composed of material. Their densities are less than or equal to 1 and greater than 0.75. The second group of structures have a rectangular hole in the middle. The size of the hole is the four tenths of the size of the outer dimensions of cellular structure. The second group has a density less than or equal to 0.75 and greater than 0.5. The third group of structures also have a rectangular hole with sizes seven tenths of the outer dimensions of the cellular structure. Their densities are less than or equal to 0.5 and greater than 0.25. The regions having densities less than 0.25 are left without material. The cellular structures are illustrated in Figure 3.9 and their properties are summarized in Table 3.1.

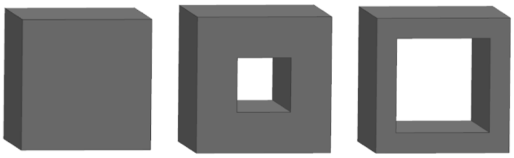

Figure 3.9: Cellular structures filling the design domain

Table 3.1: Properties of cellular structures

Properties	First	Second	Third
Outer dimensions (mm)	3x3	3x3	3x3
Inner dimensions (mm)	NA	1.2x1.2	2.1x2.1
Wall thickness (mm)	NA	0.9	0.45
Area ratio (%)	100	84	51
Density region	0.75 – 1	0.5 – 0.75	0.25-0.5

The related code block takes the grid cells in user defined dimensions, their densities as input and gives the topology remodelled with cellular structures as the output. The code block and the resulting topology are shown in Figure 3.10.

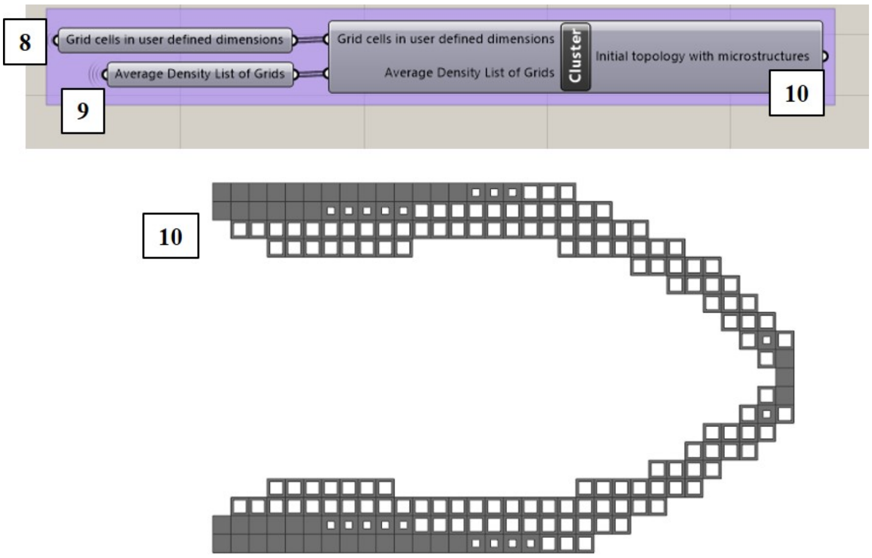

Figure 3.10: Final topology remodelled with rectangular cellular structures

3.1.4 Connectivity Analysis

In this step of the method, the resulting topology determined in the previous step is checked against any unconnected elements. A cellular structure is unconnected if it only shares a corner with the neighbor cells. Neighbor cells are the cells sharing a corner or an edge. A cellular structure has 4 edge- and 4 corner-neighbors in 2D space. Figure 3.11 shows an example of a topology consisting of multiple unconnected elements. Unconnected cells lead to a non-manifold geometry, which cannot be manufactured. Therefore, the geometry to be 3D printed should be fully connected. In contrast to many other methods that remove the unconnected element from the topology [[39], [41], [42], [43], [44], [45], [46]], the methods used in this study connects the unconnected elements by adding material. Two methods which can be used interchangeably are developed for connectivity improvement.

3.1.4.1 Method I

The algorithm used in this method is summarized below.

Input: An ordered list of grid cells with material in the topology
Output: An ordered list of grid cells with material in a connected topology
Initialize Output list as the Input list

Algorithm 1 Connectivity Analysis Method I

```
1:  for $i = 0$ to $length_{Input}$ do
2:      Find the edge- and corner-neighbors with material of the $i^{th}$ element in the Input list.
3:      Find the two common edge-neighbors of the $i^{th}$ element and its each corner-neighbor.
4:      if $\rho_{BothCommonEdgeNeighbors} \leq 0.25$ then
5:          The $i^{th}$ element and its associated corner- neighbor are unconnected.
6:          Find the common edge-neighbor (obtained in line 3) with the highest density.
7:          Find the cell with the highest density among the pair of unconnected cells, i.e. the $i^{th}$ cell or its associated corner-neighbor.
8:          Add a new cellular structure to the position of the cell obtained in line 6.
9:          Scale the newly added cell (obtained in line 8) in the same proportion as the cell obtained in line 7.
10:         Add the cell obtained in line 9 to the Output list.
11:     end if
12: end for
13: return Output
```

As an example, the unconnected topology shown in Figure 3.11 can be considered. The steps of the algorithm will be applied on a small section of this topology. The section to be analyzed is marked on Figure 3.11.

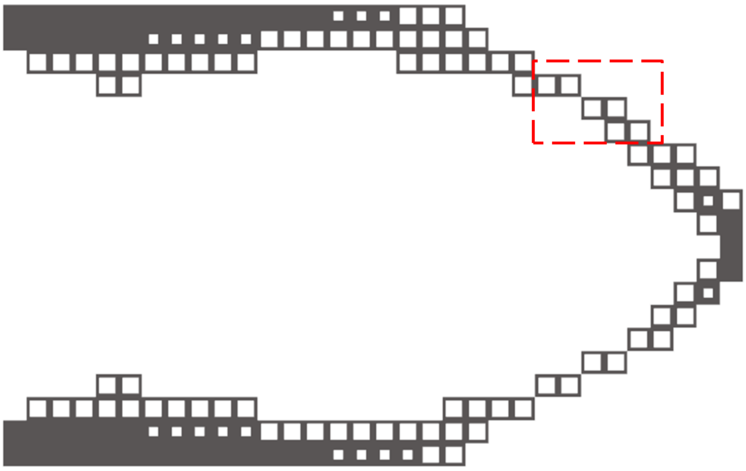

Figure 3.11: A topology with multiple unconnected elements

The algorithm begins with finding the edge- and corner-neighbors of the grid cells whose densities are larger than 0.25, in other words, the cells with a material. In order to find the neighbors of a cell, the closest 8 cells are determined as shown in Figure 3.12. The closest 8 cells to the cell number 1, namely the neighbors, are the cells numbered from 2 to 9.

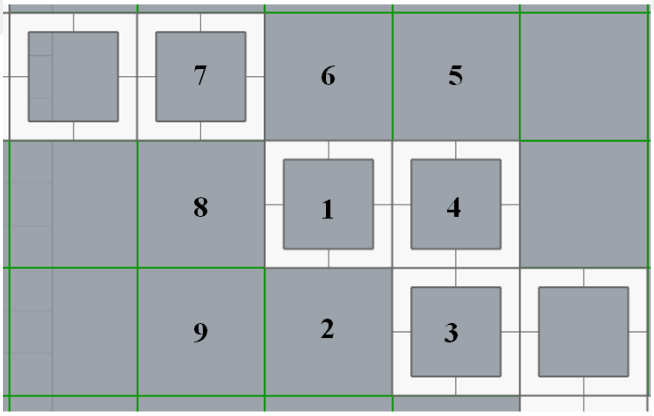

Figure 3.12: Closest 8 cells to the cell 1

Then, the distance between the centers of the cell 1 and its neighbors are calculated. If the distance is equal to the dimension of the cell in x or y direction, which is respectively shown as d_x and d_y in Figure 3.13, these cells are called to be edge-neighbors. Similarly, if the distance is equal to the square root of sum of squares of the cell dimensions, which is shown as d_r in Figure 3.13, then these cells are called to be corner-neighbors. The equation to calculate d_r is shown below.

$$\mathbf{d}_r = \sqrt{\mathbf{d}_x{}^2 + \mathbf{d}_y{}^2} \tag{3.1}$$

Thus, 2, 4, 6 and 8 are the edge-neighbors of the cell 1, while 3, 5, 7 and 9 are the corner-neighbors. The rest of the algorithm cares for the corner neighbors with material, which are 3^{rd} and the 7^{th} cells.

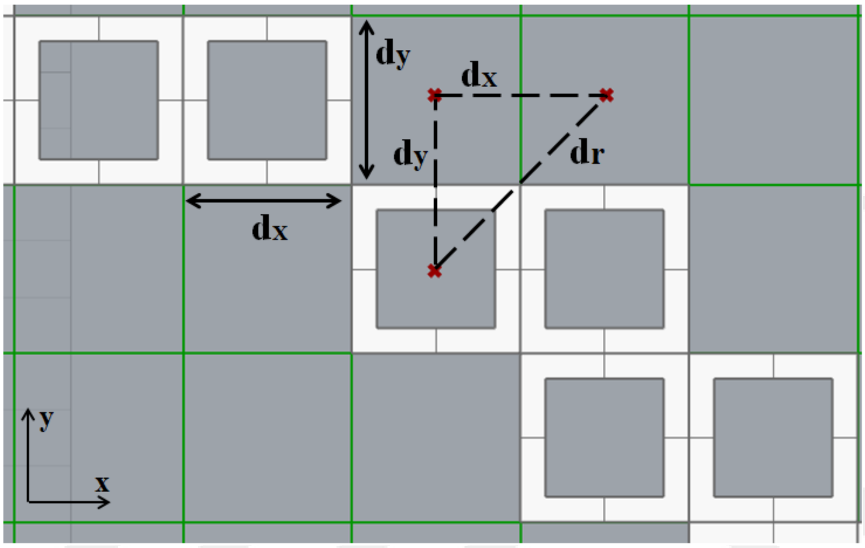

Figure 3.13: Demonstration of distance between neighbor cells

The related code block to find edge- and corner-neighbors are shown in Figure 3.14. The inputs to the block are the outputs shown in Figure 3.8, which are discretized design domain in user defined dimensions and the density list of the grids.

Figure 3.14: Code block finding the neighbors

The next step is to find the pair of unconnected cells, which corresponds to the steps 3, 4 and 5 in the algorithm. Firstly, the common edge-neighbors of the cell number 1 and its corner-neighbors are determined. In this case, cell 1 shares the 2^{nd} and 4^{th} cells as edge neighbors with the cell numbered 3. Similarly, it shares 6^{th} and 8^{th}

with the cell numbered 7. Then, densities of the pair of common edge neighbors are determined. If both cells in a pair have densities less than 0.25, which means they do not have any material, then the cell 1 is unconnected from the related corner cell. The first pair of the cells to be analyzed are the 2^{nd} and the 4^{th} cells. As it can be seen on Figure 3.12, while the 2^{nd} cell has no material, the 4^{th} cell's density is between 0.25 and 0.5. Therefore, the cells 1 and 3 are connected. However, the cells in the second pair, 6^{th} and 8^{th}, have no material, which leads cell 1 and 7 to be unconnected. The related code block in Grasshopper3D is shown in Figure 3.15. The inputs to the block comes from the outputs determined in the previous step in Figure 3.14.

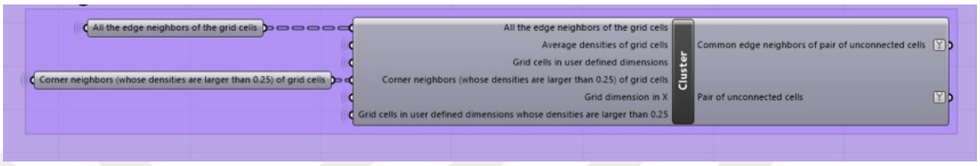

Figure 3.15: Code block finding the unconnected cells

In order to connect the unconnected pair, a new cell should be added to one of their common edge-neighbors. In this case, the cells 1 and 7 can be connected adding material to either cell 6 or 8. The decision on which cell to add material is made by comparing the densities of the cells 6 and 8. Since SIMP optimization assigns more material to the regions exposed to higher stress, the new material is added to the cell with higher density. An analysis showing the effect of the new cell's position on the performance of the structure is also presented at the end of this section. Therefore, since the cells 6 and 8 has densities of 0.29 and 0.30, respectively, the 8^{th} cell is chosen to be filled with one of the cellular structures presented in Figure 3.9.

After the location of the cellular structure to be added is chosen, which type of cellular structure to be used should be determined. At this point, the densities of the cells 1 and 7 are compared. The new cellular structure is chosen in reference to the cell with the higher density. The code blocks related to the selection of the location of the new cellular structure and the reference cell is shown in Figure 3.16. They take the outputs shown in Figure 3.15 as the inputs, and give the location of the new structure and the reference cell as outputs.

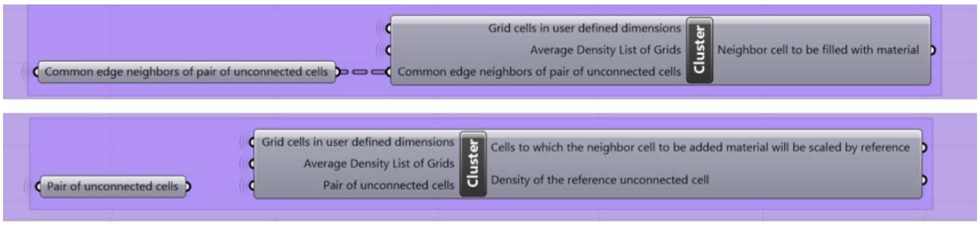

Figure 3.16: Code blocks finding the new cellular structure location and the unconnected cell

The type of the cellular structure to be added is chosen as the same as the type of the cellular structure of the reference cell. The reference cell is the cell numbered as 1, since its density, which is 0.32, is higher than the density of the 7^{th} cell, which is 0.31. A new cellular structure that is the same as the cell 1 is added to the topology. The related code block is shown in Figure 3.17. It uses the density of the reference cell and the location of the new cellular structure as the inputs and generates the new cellular structure to be added to the topology as output.

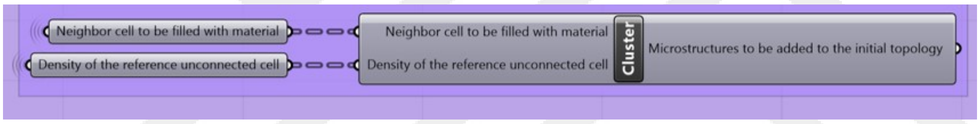

Figure 3.17: Code block for the generation of the new cellular structure

Finally, the new cellular structure and the section of the topology shown in Figure 3.12 are joined together. Thus, a fully connected geometry is obtained. The connected section of the topology is shown in Figure 3.18. The related code block is shown in Figure 3.19. The initial topology and the newly added cellular structures are taken as input, and the fully connected geometry is generated as the output.

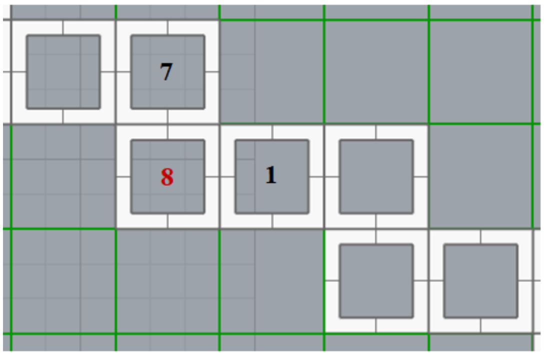

Figure 3.18: Part becomes connected with the addition of 8^{th} cell

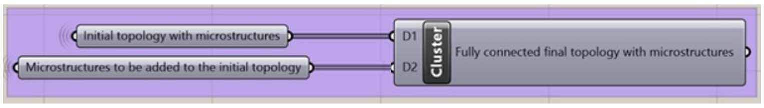

Figure 3.19: Code block generating the fully connected topology

The result of the connectivity analysis for the whole topology represented in Figure 3.11 can be seen in Figure 3.20 and Figure 3.21. Figure 3.20 shows the unconnected pair of elements and Figure 3.21 shows the fully connected geometry with newly added cellular structures.

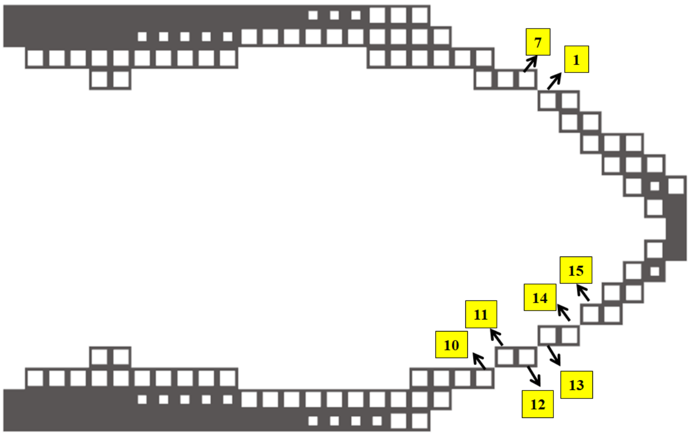

Figure 3.20: Unconnected pair of elements, which are 1&7, 10&11, 12&13 and 14&15

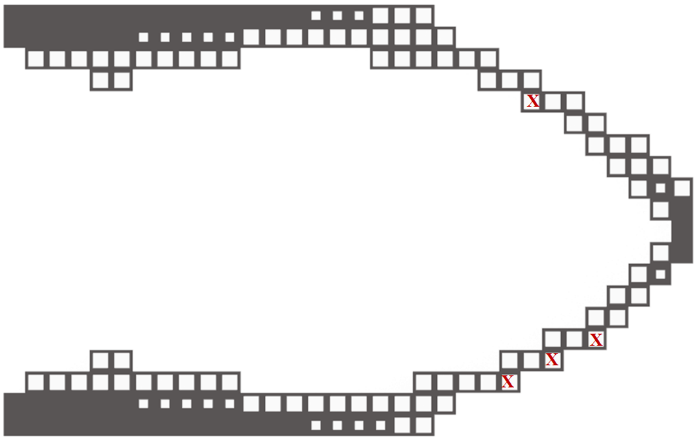

Figure 3.21: The fully connected topology after the connectivity analysis. The newly added cellular structures are tagged with x at their centers.

As discussed, the topology shown in Figure 3.21 is obtained by adding the new cell to the position of the unconnected cells' common neighbor with the highest density. In order to see the effect of the position of the new cell, a new topology is created by adding the new cell to the common neighbor with the least density, and structural analysis are performed on both geometries. It is seen that while the topology shown in Figure 3.21 starts yielding under a force of 67.5 N, the topology employing the least density rule for the addition of new cells yields under 55.5 N. Therefore, in all methods given under the section of "Connectivity Analysis" throughout the thesis, new cells are added to the neighbor cell with the highest density. The boundary conditions and the safety regions of the geometries are shown in Figure 3.22 and Figure 3.23 respectively.

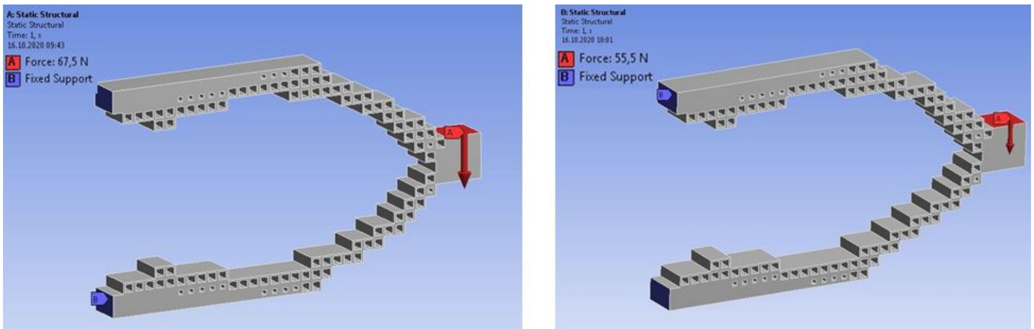

Figure 3.22: The fully connected topologies containing the new cells added to the position of the unconnected cell pairs' common neighbours with the highest (left) and least (right) density.

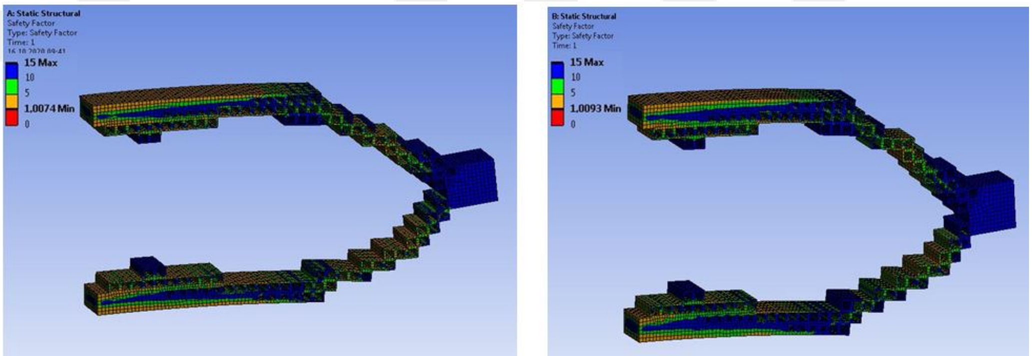

Figure 3.23: Safety regions of the fully connected topologies containing the new cells added to the position of the unconnected cell pairs' common neighbours with the highest (left) and least (right) density.

3.1.4.2 Method II

This method uses the algorithm summarized below.

Input: A list of closed bodies in a topology "*ClosedBodies*", grid cells covered by the closed bodies "*GridCells*" and independent bodies "*IndependentBodies*"

Output: A list of grid cells covered by the closed body in a connected topology, *ConnectedGridCells*

Initialize *ConnectedGridCells* list as the *GridCells* list, *IndependentBodies* list as an empty list

Algorithm 2 Connectivity Analysis Method II

```
Require: $C \longrightarrow$ closed body
Require: $p_C \,\&\, p_M \longrightarrow$ the closest points of the independent and main bodies
 1: for $i = 0$ to $length_{ClosedBodies}$ do
 2:     Find the area of $C_i$.
 3: end for
 4: Append the closed body, $C$, with the highest area in the ClosedBodies list to the
    MainBody list.
 5: Append the other closed bodies in the ClosedBodies list to the IndependentBodies
    list.
 6: for $i = 0$ to $length_{IndependentBodies}$ do
 7:     if $||p_{C_i} - p_M|| < edgelength * \sqrt{5}$ then
 8:         Add a new cellular structure to one of the $C_i$'s closest neighbors to $M$.
 9:         Add the newly added cellular structure to the ConnectedGridCells list.
10:     else
11:         Delete $C_i$ from the ClosedBodies list.
12:     end if
13: end for
14: Set the MainBody list to empty.
15: Set the IndependentBodies list to empty.
16: Append the closed body, $C$, with the highest area in the ClosedBodies list to the
    MainBody list.
17: Append the other closed bodies in the ClosedBodies list to the IndependentBodies
    list.
18: Find the intersection points between the closed bodies in the IndependentBodies
    list and the closed body in the MainBody list.
19: Find the self intersection points of the closed body in the MainBody list.
20: Find the four closest grid cells to the intersection points.
21: Find the cell (obtained in line 20) with the highest density.
22: Add a new cellular structure to the position of the cell obtained in Line 21.
23: Add the newly added cellular structure to the ConnectedGridCells list.
24: return ConnectedGridCells
```

The algorithm is applied on the example geometry shown in Figure 3.24. As it can be seen from the figure, the topology has many unconnected elements which are enclosed by red rectangles.

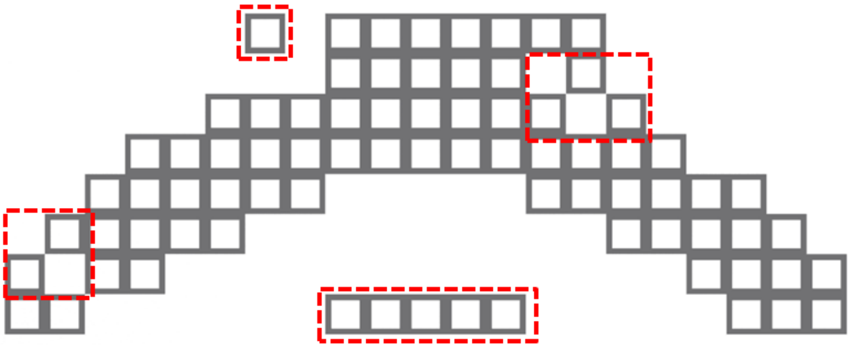

Figure 3.24: A topology with multiple unconnected elements

The algorithm begins with finding the closed regions in the geometry. There are 4 closed regions as shown in Figure 3.25.

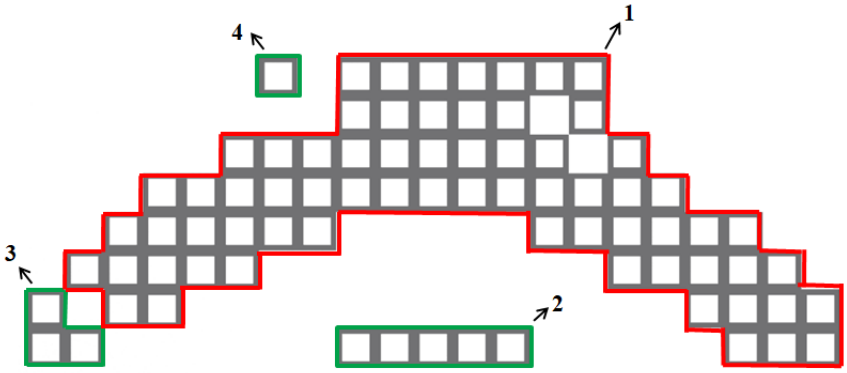

Figure 3.25: Closed regions in the geometry

Then, the region with the highest area is determined. As it can be seen in Figure 3.25, the region numbered as 1 has the largest area among others. Therefore, it is called the main body. The other regions numbered as 2, 3 and 4 are called as independent bodies. The related Grasshopper3D code block to determine the closed, main and the independent bodies are shown in Figure 3.26. The code block takes the outputs of the block shown in Figure 3.8, which are “Grid cells in user defined dimensions” and the “Average density list”, and gives the closed, main and the independent bodies as outputs.

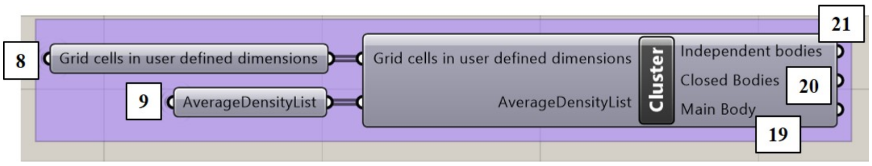

Figure 3.26: Code block for the determination of the closed, main and the independent bodies

The first objective of the algorithm is to connect the independent bodies to the main body. In this regard, firstly, the closest points of the main and the independent bodies are determined as shown in Figure 3.27. Then, the distances between the pair of closest points, namely, p_{11}-p_{31}, p_{12}-p_{32}, p_{13}-p_{21}, p_{14}-p_{22}, p_{15}-p_{41}, are calculated.

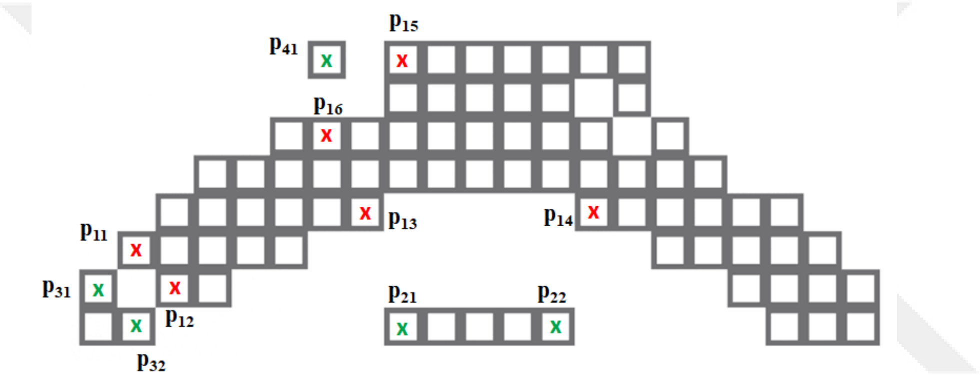

Figure 3.27: Closest pair of points of the main and the independent bodies

The related Grasshopper3D code block for the determination of closest points of the main and the independent bodies and the distance between points is shown in Figure 3.28.

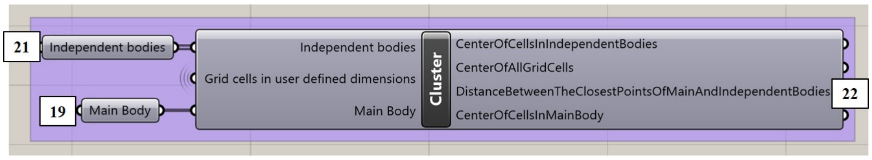

Figure 3.28: Code block finding the distance between the closest points of the main and the independent bodies

If the distance between the pair of closest points is less than or equal to the square root of 5 times the cell's edge length, it can be attached to the main body; else the independent body is deleted from the topology. In this example, the pairs p_{11}-p_{31}, p_{12}-p_{32} and p_{15}-p_{41} fulfill the distance condition while the pairs p_{13}-p_{21} and p_{14}-p_{22} do not. Therefore, the independent body numbered as 2 in Figure 3.25 is deleted from the topology, and the others are continued to be processed for attaching on the main structure.

The next step is to choose the locations of the cellular structures to be added. The independent body numbered as 3 can be connected to the main body by adding a cellular structure to one of the grid cells shown as a, b and c in Figure 3.29. In a similar way, the independent body numbered as 4 can be connected to the main body via the grid cells marked as d and e. The position of the cellular structures are selected randomly among the possible cell locations. In this example, cellular structures are added to the grids marked as a and d. The densities of the cellular structures are equal to the average densities of the cells to which it is attached. Therefore, the densities of cell a and cell d are equal to the average of the densities of C_{11}-C_{31} and C_{16}-C_{41}, respectively.

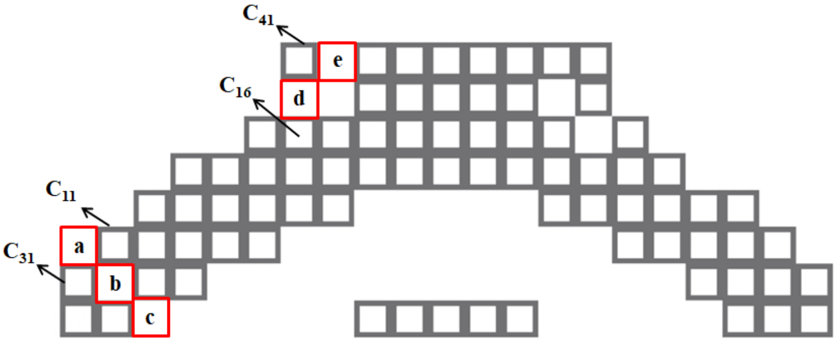

Figure 3.29: Possible locations of cellular structures to be added in order to attach the independent bodies to the main structure

The related Grasshopper3D code block for the addition of new cellular structures to the topology and the deletion of the independent bodies, which are far from the main body, is shown in Figure 3.30.

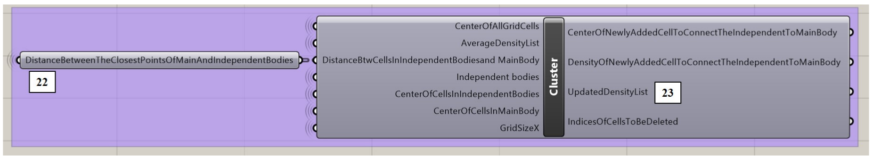

Figure 3.30: Code block for the addition of new cellular structures and the deletion of the distant independent bodies

The resulting topology is shown in Figure 3.31.

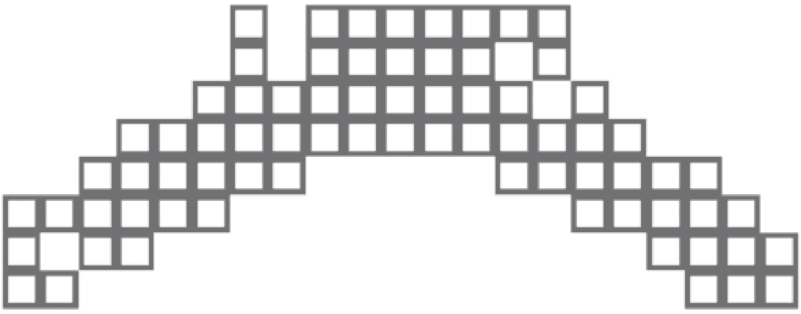

Figure 3.31: Updated topology after addition of cellular structures to the independent bodies close to the main structure and deletion of the distant independent bodies

In this step, the topology is checked for any intersections within and between the bodies. In this example, the updated topology do not contain any independent bodies. However, the main body intersects itself at three points marked as 1,2 and 3 in Figure 3.32. Since the cells marked as f&g, h&i and i&j shares only the points 1, 2 and 3 respectively, they are unconnected to each other.

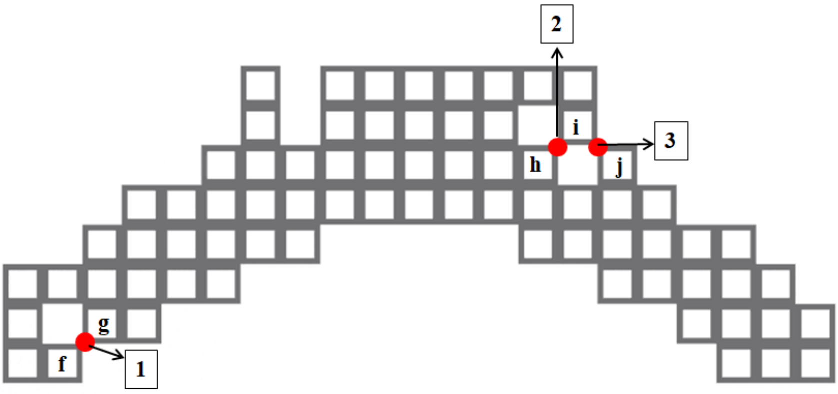

Figure 3.32: Self intersection points within the main body

The related Grasshopper3D code block to determine the unconnected cells sharing only a corner is shown in Figure 3.33.

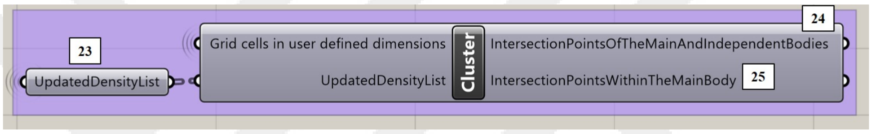

Figure 3.33: Code block to find the unconnected elements sharing only a corner

In order to connect the unconnected pair of cells to the topology, firstly the closest four grid cells to the intersection points are determined as shown in Figure 3.34. While the two of the closest cells, f&g for the intersection point 1 for example, have material, the other cells, k&l, are empty.

In order to connect the pair of cells with material, a new cellular structure is added to the empty grid cell with the highest density. In this example, the grid cell marked as l, n and o has a higher density when compared to k, m and n, respectively ($\rho_l > \rho_k$, $\rho_n > \rho_m$ & $\rho_o > \rho_n$ where ρ is the density). Therefore, the new cellular structures are added in places of the cells l, n and o.

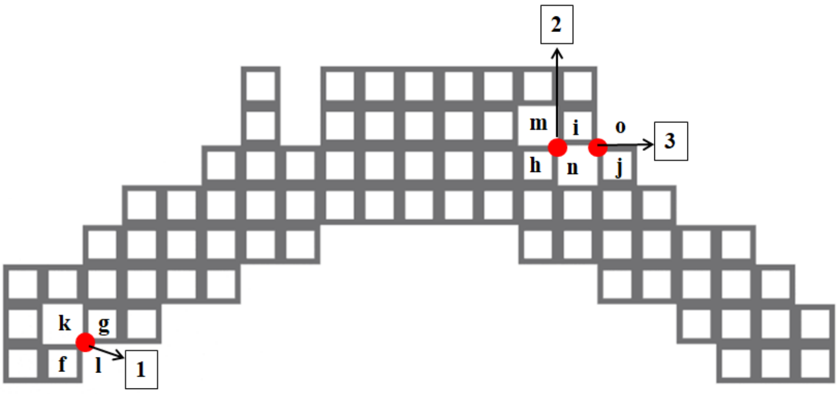

Figure 3.34: Closest four cells to the intersection points 1, 2 and 3

The next step is to select one of the three types of cellular structures shown in Figure 3.9. The type of the cellular structure to be added is chosen according to average of the densities of the unconnected pair of cells with material, namely f&g, h&i and i&j. Since the average densities of the pairs are 0.45, 0.29 and 0.35, respectively, the third type of cellular structure is added to the cells l, n and o.

The related Grasshopper3D code block to connect the cells sharing only a corner to each other is shown in Figure 3.35. It gives the density and the position of the cellular structures to be added to the topology as output.

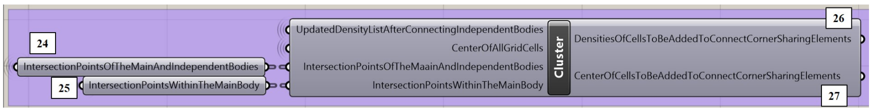

Figure 3.35: Code block to add new cellular structures for the connection of cells sharing only a corner

The final fully connected topology is shown in Figure 3.36.

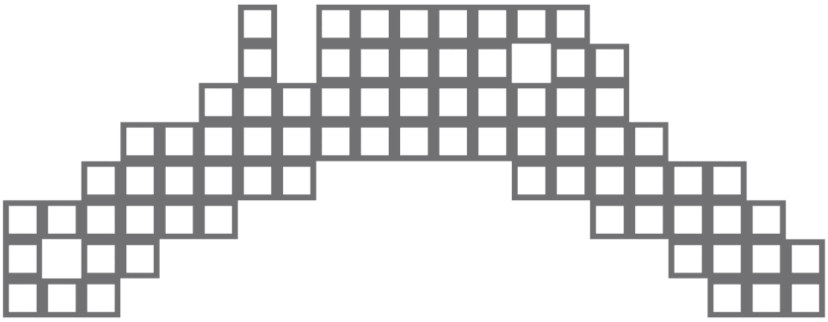

Figure 3.36: Fully connected final topology

The related Grasshopper3D code block to generate the final fully connected topology is shown in Figure 3.37.

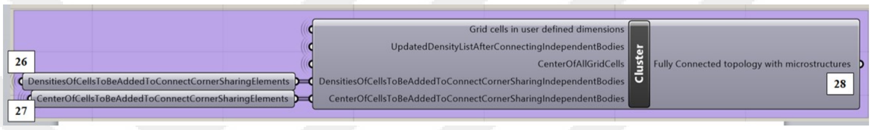

Figure 3.37: Code block for the generation of fully connected final topology

CHAPTER 4

TILING OF CELLULAR STRUCTURES IN 3D

The procedure for the application of the proposed method on 3d geometries are summarized in Figure 4.1. The process begins with the generation of a geometry on 3d CAD software. Then, the geometry is transferred to the finite element analysis software, Ansys. There, it is analyzed for the stress distribution throughout its design domain according to the predefined boundary conditions. Then, the analysis model is transferred to the Topology Optimization module of Ansys. After adjusting the optimization settings, the geometry is optimized according to an optimization objective. Finally, the optimized topology is remodelled with cellular structures in Grasshopper3D in a way that it is fully connected and it can be cleaned from the powders/resin when it is fabricated with resin- and powder-based AM methods.

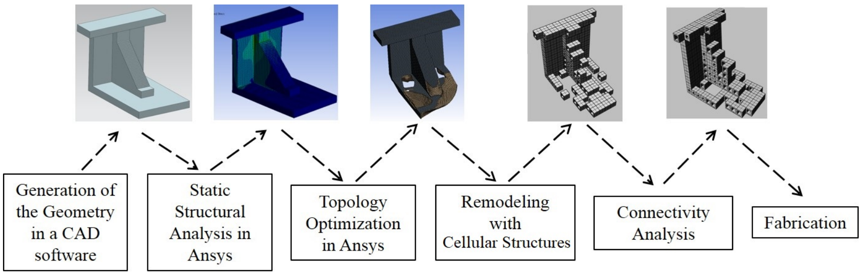

Figure 4.1: Steps of the proposed method for 3D geometries

4.1 Modeling of Geometries

In this study, Unigraphics NX is used as the CAD software. An example geometry to be optimized is shown in Figure 4.2. It is a bracket used for connecting two moving structures to rotate together. The bracket is mounted onto the moving parts via the holes shown as 1 and 2 in the figure. One of the limitations of the proposed method is that it is only applied on geometries that do not contain round and angled features due to the constraints of the topology optimization module utilized. These features can be included in the final topology by post processing. Therefore, the original geometry in Figure 4.2 is approximated as shown in Figure 4.3.

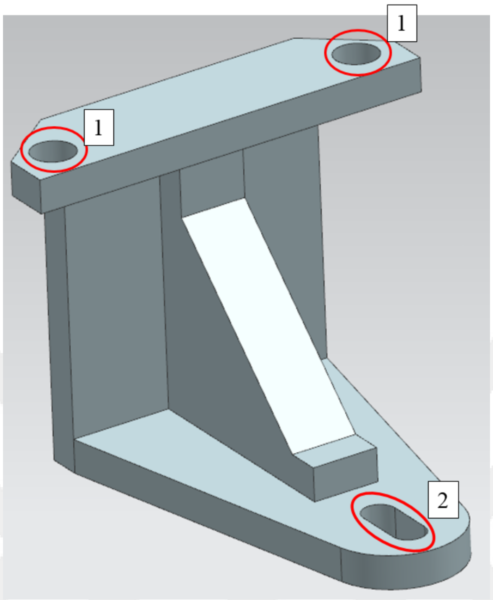

Figure 4.2: Original bracket geometry

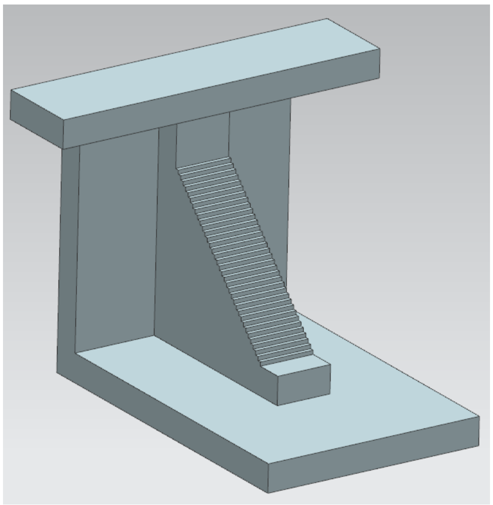

Figure 4.3: Approximated bracket geometry

4.2 Static Structural Analysis of the Geometry

After the geometry is modelled in CAD software, it is transferred to the Static Structural Module of Ansys. The user interface of the Static Structural Module is shown in Figure 4.4. In order to perform analysis of the part, the data inputs shown in the analysis tree, which is taken into a frame in the figure, should be set in a top-down order.

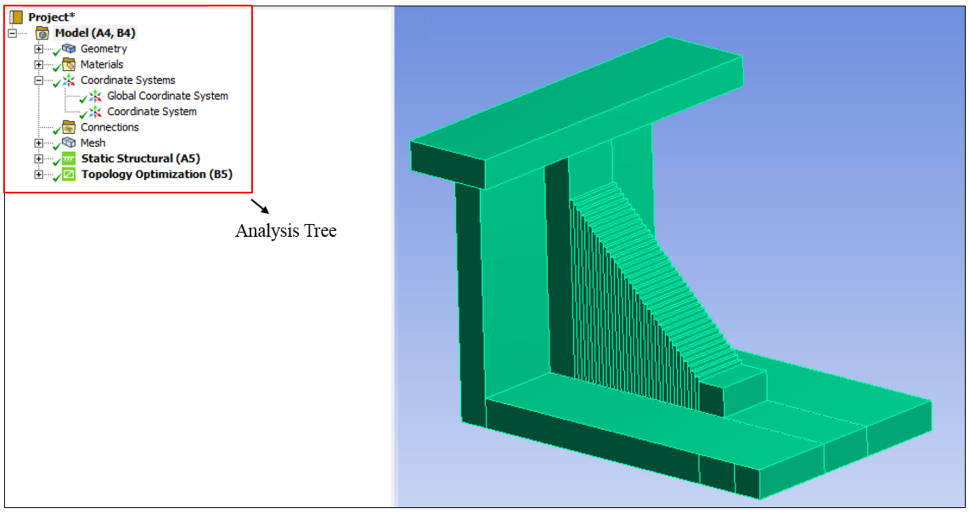

Figure 4.4: Static Structural Module interface and the analysis tree

The first step after importing the geometry is to assign material to the part. Since the part is intended to be produced with the Arcam EBM machine, which is a metal powder based 3D printer, titanium Ti6Al4V is assigned as the material. The properties of Ti6Al4V are shown in Table 4.1 as it is provided by Arcam [47].

Table 4.1: Properties of Ti6Al64V

Properties	Ti6Al6V
Yield Strength (Rp 0.2)	950 MPa
Ultimate Tensile Strength (Rm)	1020 MPa
Modulus of Elasticity	120 GPa

Secondly, a reference coordinate system is set to be used in the upcoming steps. The location of the coordinate system is shown in Figure 4.5.

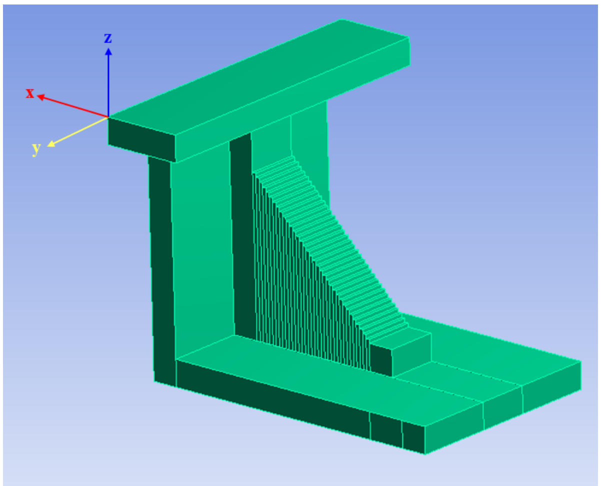

Figure 4.5: Reference coordinate system

Then, the geometry is meshed prior to the finite element analysis. The size and the type of the mesh affect the topology optimization result in the later stage of the approach. This method requires uniform rectangular meshing of the entire body. Therefore, the geometry is discretized into $1mm$ by $1mm$ elements as shown in Figure 4.6. As a result, there are total of 85652 finite mesh elements.

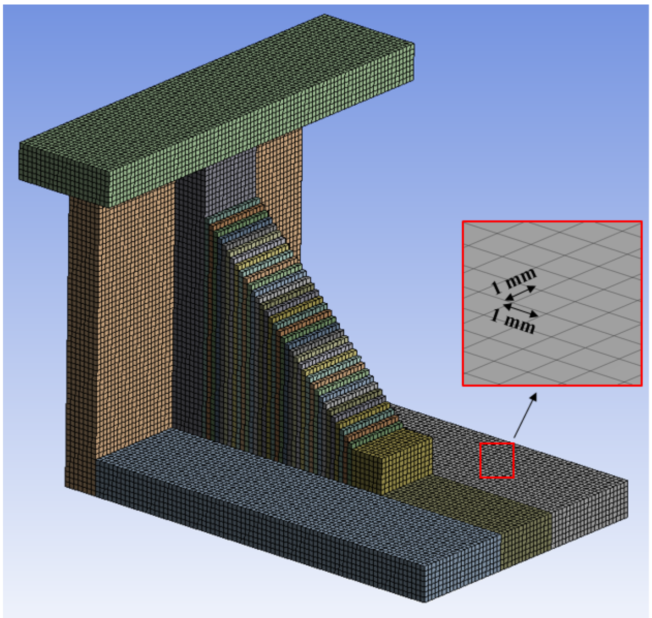

Figure 4.6: Meshed geometry

The next step is to set the boundary conditions for the geometry. The part is fixed from the surface marked as A and a load of $123N$ is applied on the surface marked as B in accordance with the working scenario of the part as illustrated in Figure 4.7.

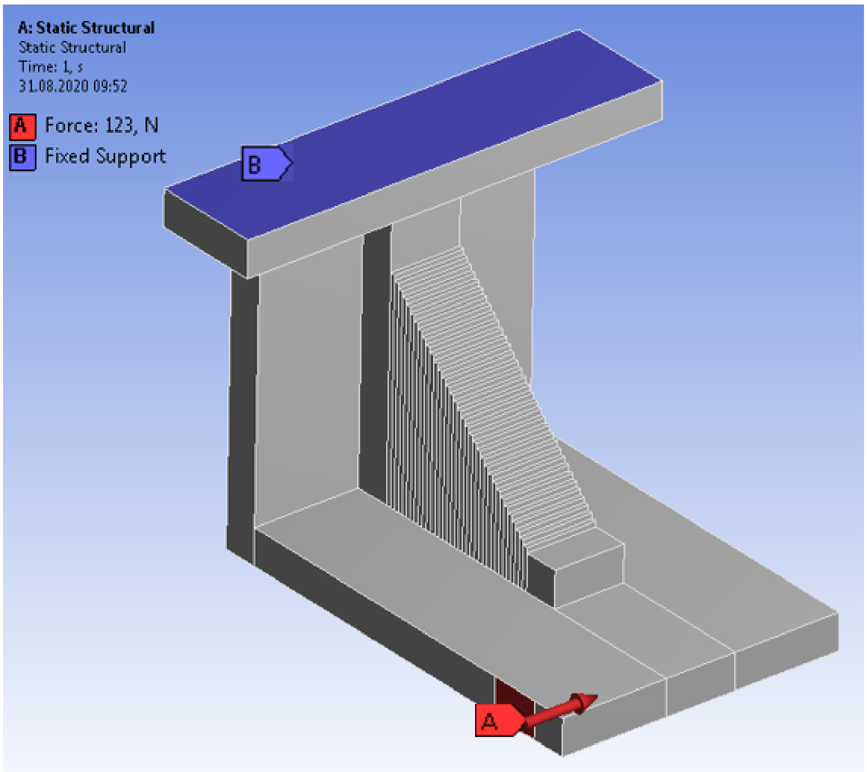

Figure 4.7: Boundary conditions for the geometry

Finally, the analysis problem is solved for the stress distribution and the deformation throughout the design domain. The results of the analysis are shown in Figure 4.8 and Figure 4.9.

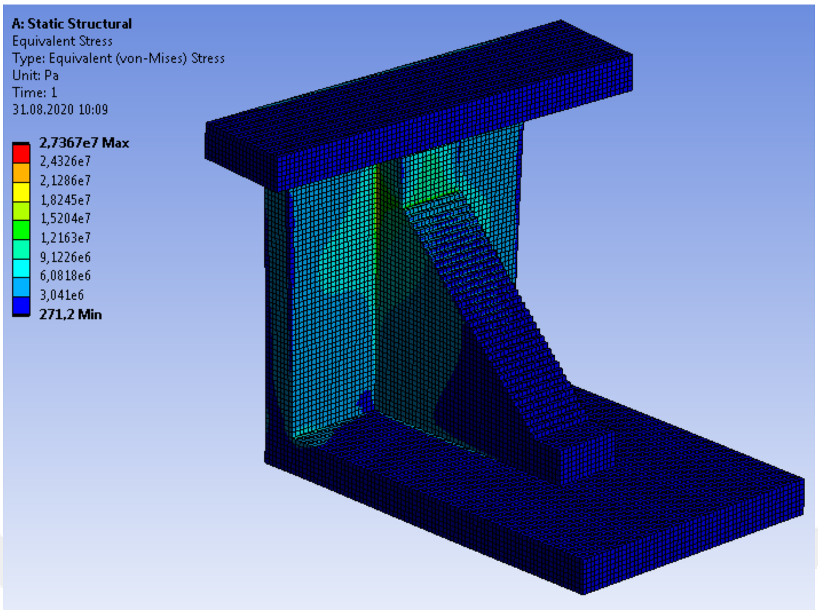

Figure 4.8: Stress distribution through the part

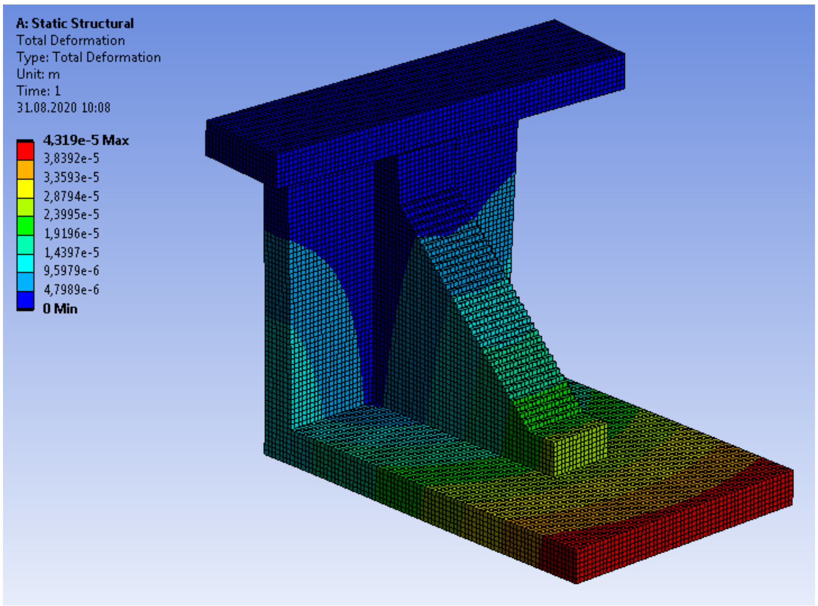

Figure 4.9: Total deformation through the part

4.3 Topology Optimization in Ansys

After the structural analysis of the part is completed, it is transferred to the Topology Optimization module of Ansys. This module takes the geometry, boundary conditions and the analysis results obtained in the previous step as the inputs. The interface of the Topology Optimization module is shown in Figure 4.10.

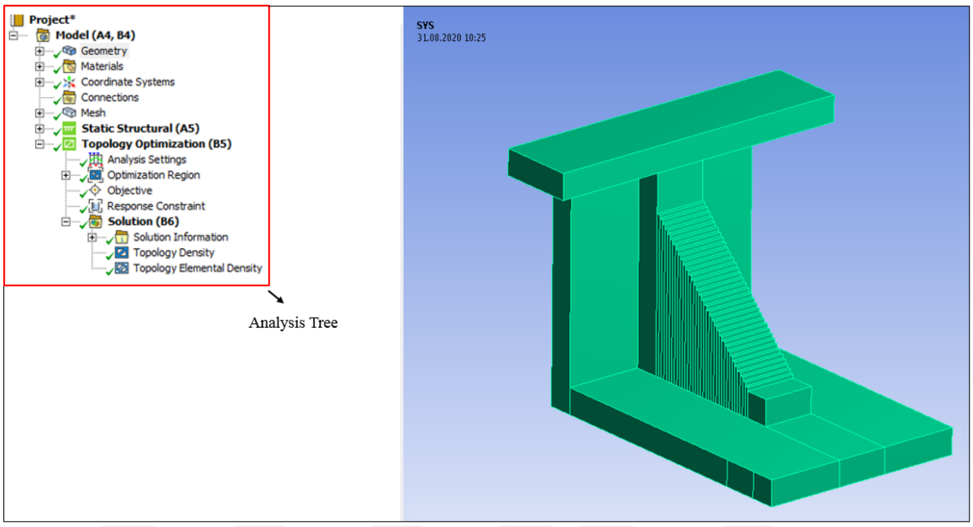

Figure 4.10: Topology Optimization module interface and the analysis tree

As it can be seen from Figure 4.10, Topology Optimization component is added to the analysis tree. As in the Static Structural module, the analysis setting are done in a top-down order. Firstly, the optimization region, which defines the regions to be used for optimization, is set as shown in Figure 4.11. In this example, the part body covering the surface with the fixed support condition and the surface on which the force is applied are extruded from the optimization while the remaining bodies are included. The exclusion and the optimization regions are marked with C and D in the following figure.

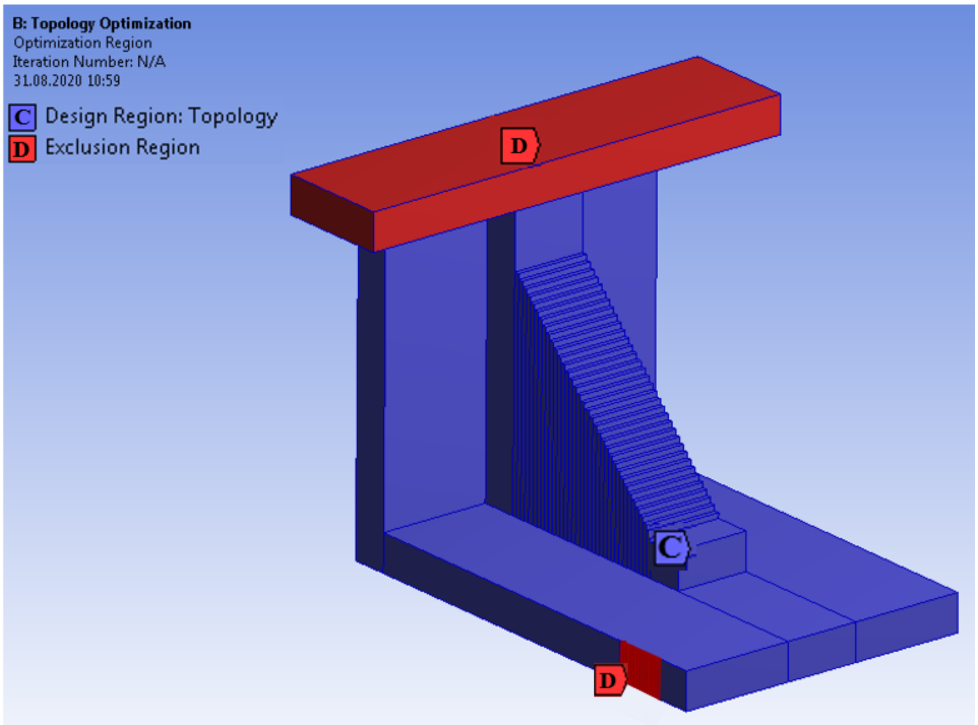

Figure 4.11: Inclusion (C) and exclusion (D) regions for the optimization problem

Secondly, the optimization objective is set. There are three possible objective options in Ansys, which are compliance, mass and volume minimization. In this example, the objective is set as the compliance minimization. Then, the constraints for the optimization problem are defined. 50% of the volume constraint is set for this example. Finally, topology optimization problem is solved for the optimum density distribution throughout the design region. As a result, each finite element is assigned a density value between 0 and 1. The elements with densities larger than 0.4 are filled with material while the others are left empty. The optimum topology is generated after 20 iterations. The result is shown in Figure 4.12.

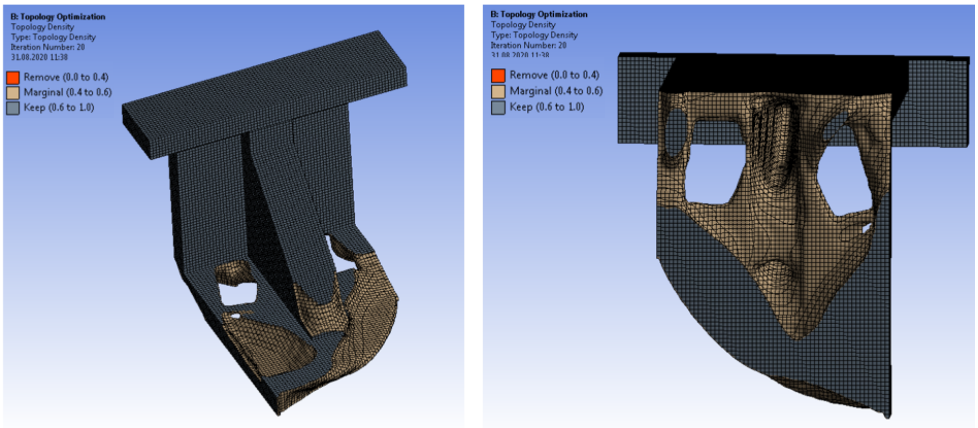

Figure 4.12: Topology optimization result

The topology optimization result can also be visualized by finite elements as shown in Figure 4.13.

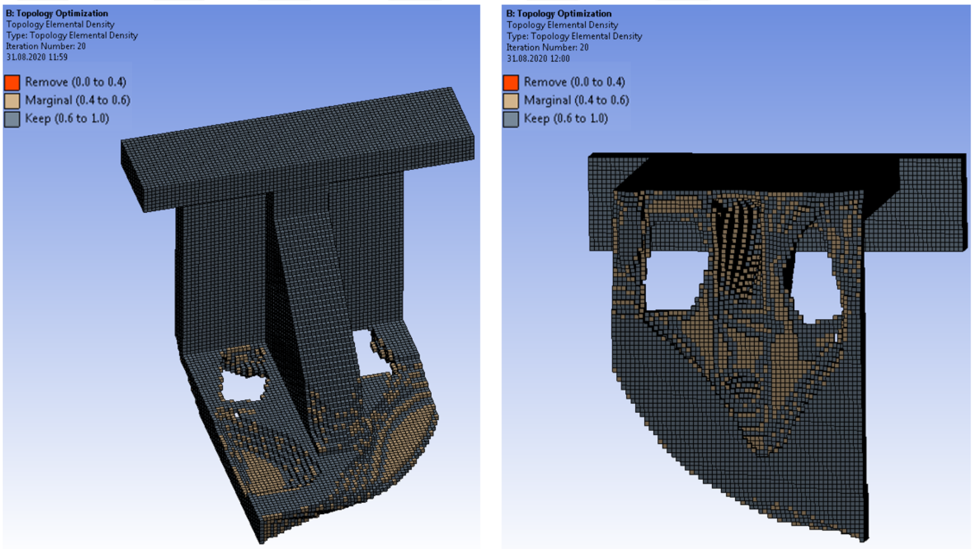

Figure 4.13: Topology optimization result (Elemental representation)

After the topology optimization, output data files are exported to be used in Grasshopper3D function blocks where the optimized topology is remodelled with cellular structures. The first data to be exported is the element ids of all the finite elements (85652 of them) comprising the geometry and their corresponding density values. The second data consist of the element ids and the ids of all the nodes covered by the corresponding element. Each finite element in the topology consists of 20 nodes as shown in Figure 4.14. The last output is the x, y and z coordinates of all the nodes according to the reference coordinate system shown in Figure 4.5. There are total of 380710 nodes in this topology.

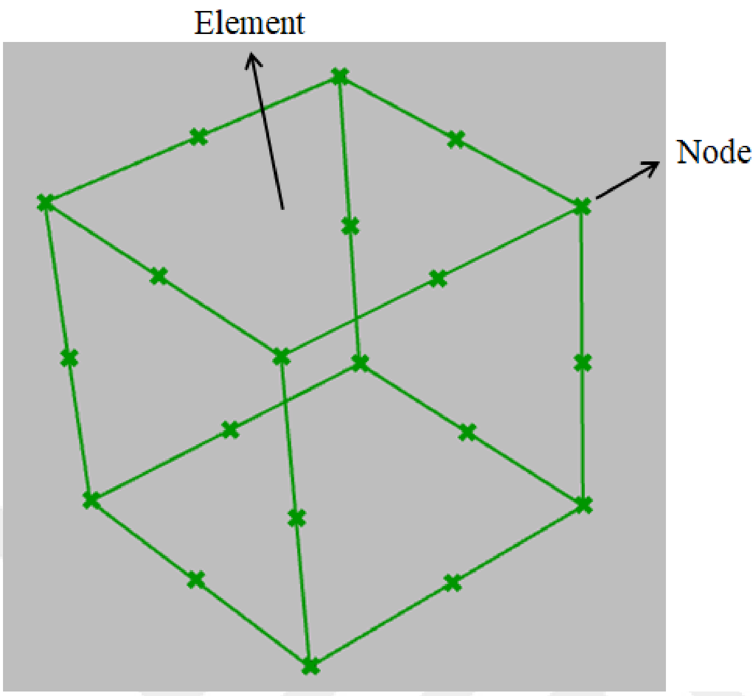

Figure 4.14: Nodes on a finite element

4.4 Remodeling with Cellular Structures

The first step is to create a bounding box enclosing the original geometry shown in Figure 4.3 as illustrated in Figure 4.15. The dimensions of the bounding box is the same as the outer dimensions of the original geometry.

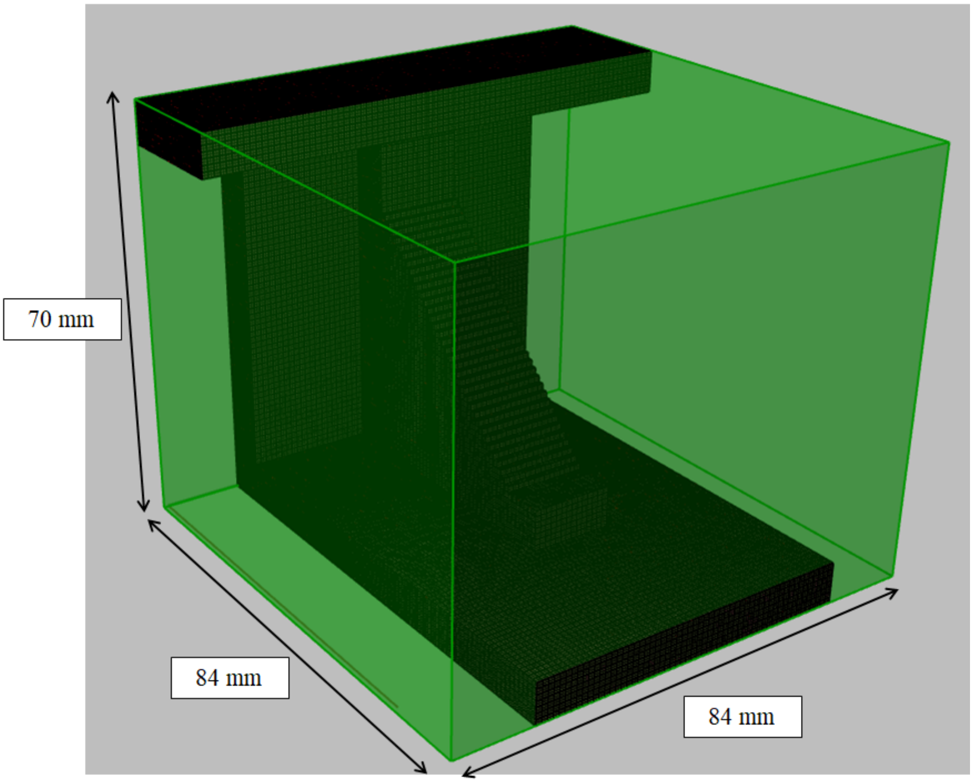

Figure 4.15: Bounding box of the original geometry

The generated bounding box is discretized into rectangular cells that have user defined dimensions. The size of the unit cells is the same as the size of the cellular structures in which the optimized geometry will later be remodelled with. In this example, $7mm$ by $7mm$ cells are used. The next step is to calculate the density of each unit cell. Since there are total of 343 finite elements in a unite cell, the density of each unit cell is equal to the average densities of the 343 elements covered by the corresponding unit cell. The discretized bounding box, user defined unit cells and the finite elements are shown in Figure 4.16.

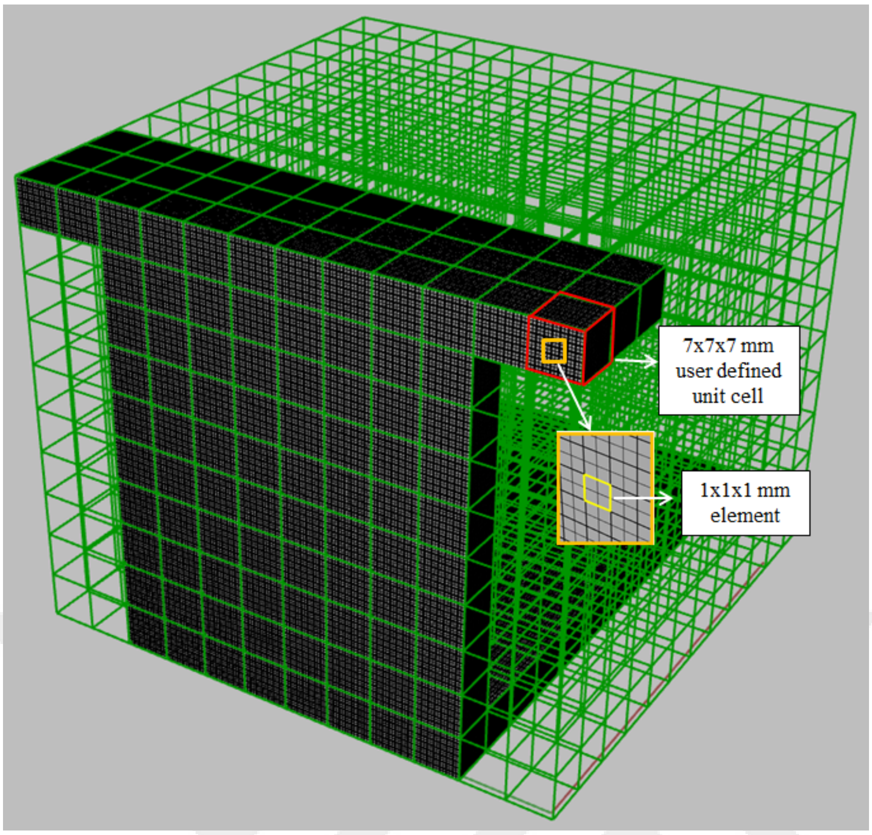

Figure 4.16: The discretized bounding box

The density data for each finite element is obtained in the previous step as a result of the topology optimization done in Ansys. This data comprises of element ids and their corresponding density values. However, there is no information about the locations of the elements. The only way to find the position of each element is to use the other two output data files obtained in the previous step which include the id numbers of nodes covered by each element and the coordinates of each node according to the reference coordinate system shown in Figure 4.5. Since every element contains 20 nodes, the x, y and z coordinates of each element is calculated as follows.

$$\mathbf{e}_{i_{xyz}} = \frac{\mathbf{n}_{i1_{xyz}} + \mathbf{n}_{i2_{xyz}} + \ldots + \mathbf{n}_{i20_{xyz}}}{20} \tag{4.1}$$

where i is ranging from 1 to the total number of elements in the bounding box, e_i refers to the x coordinate of the element with an id of i, n_{i1}, for example, refers to the x coordinate of the first node in the element with an id i. In a similar way, the density for each element is calculated as follows.

$$\rho_{e_i} = \frac{\rho_{ni_1} + \rho_{ni_2} + ... + \rho_{ni_{20}}}{20} \tag{4.2}$$

where ρ_{ei} refers to density of the element with an id i and $\rho_{n_{i_1}}$, for example, refers to density of the first node in the element with an id i. After the density of each element is calculated, the average densities of all the elements covered by each unit cell is calculated to find the density of unit cells. Then, the bounding box is filled with cellular structures. Each cellular structure covers a volume proportional to its density. Three types of cellular structures that are categorized according to their densities are used. The first group of structures are fully composed of material. Their densities are less than or equal to 1 and greater than 0.75. The second group of structures have a rectangular hole in the middle. The size of the hole is the four tenths of the size of the outer dimensions of cellular structure. The second group has a density less than or equal to 0.75 and greater than 0.5. The third group of structures also have a rectangular hole with sizes seven tenths of the outer dimensions of the cellular structure. Their densities are less than or equal to 0.5 and greater than 0.25. The regions having densities less than 0.25 are left without material. The cellular structures are illustrated in Figure 4.17 and their properties are summarized in Table 4.2.

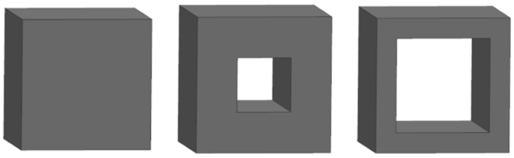

Figure 4.17: Cellular structures filling the bounding box

Table 4.2: Properties of cellular structures

Properties	First	Second	Third
Outer dimensions (mm)	7x7	7x7	7x7
Inner dimensions (mm)	NA	2.8x2.8	4.9x4.9
Wall thickness (mm)	NA	2.10	1.05
Area ratio (%)	100	84	51
Density region	0.75 – 1	0.5 – 0.75	0.25-0.5

The related code block takes the dimensions of a unit cell and the bounding box as inputs. Then, it performs the operations of generating the bounding box and discretization of it into unit cells and calculation of the densities of unit cells. Finally, it gives the topology remodelled with cellular structures as the output. The code block and the resulting topology are shown in Figure 4.18.

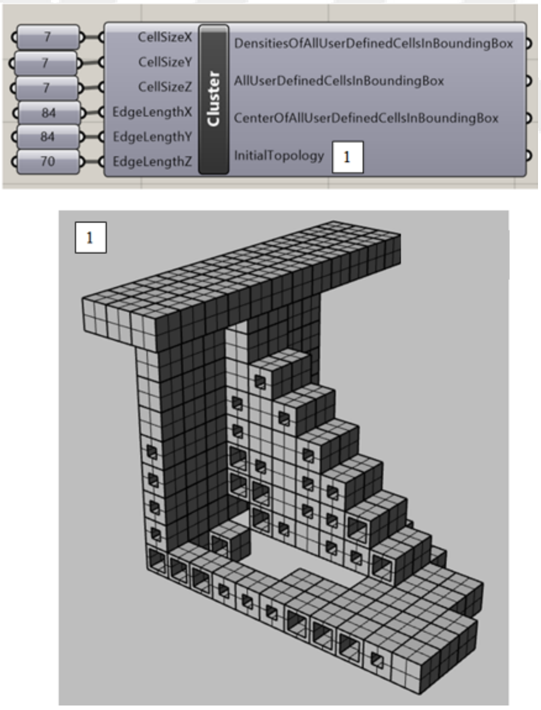

Figure 4.18: Grasshopper3D code block for the generation of the initial topology with cellular structures (top) and the visualization of the topology (bottom)

4.5 Connectivity Analysis

In this step, the resulting topology determined in the previous step is checked against any unconnected elements. A cellular structure is unconnected if it only shares a corner or an edge with the neighbor cells. A cellular structure, for example, has 12 edge, 8 corner and 6 surface neighbors in 3D space. The algorithm used in this method is summarized as follows.

```
**Input:** An ordered list of cells with material in a topology
**Output:** An ordered list of cells with material in a connected topology
Initialize Output list as the Input list
```

Algorithm 3 Connectivity Analysis of the Resulting Topology

```
for $i = 0$ to $length_{Input}$ do
    Find the edge-, corner- and surface-neighbors with material of the $i^{th}$ element in the Input list.
    if the $i^{th}$ element in the Input list and its corner neighbors share only a corner then
        The $i^{th}$ element and its associated corner-neighbor are unconnected.
        Add a new surface-neighbor to the unconnected corner-neighbor so that the new cell shares an edge with the $i^{th}$ element.
        Append the newly added surface-neighbor to the Output list.
    end if
end for
for $i = 0$ to $length_{Output}$ do
    Find the edge-, corner- and surface-neighbors with material of the $i^{th}$ element in the Output list.
    if the $i^{th}$ element in the Output list and its edge neighbors share only an edge then
        The $i^{th}$ element and its associated edge-neighbor are unconnected.
        Add a new surface-neighbor to the unconnected edge-neighbor so that the new cell shares a surface with the $i^{th}$ element.
        Append the newly added surface-neighbor to the Output list.
    end if
end for
for $i = 0$ to $length_{Output}$ do
    if the $i^{th}$ element in the Output list does not have any neighbors with material and is within a cell distance to the closest element in the Output list then
        The $i^{th}$ element is unconnected.
        Add new surface-neighbors to the unconnected $i^{th}$ element so that the new cells share a surface with the other elements in the Output list.
    end if
end for
return Output
```

Since the topology shown in Figure 4.18 does not contain any unconnected surface elements, the algorithm steps are demonstrated on another example geometry shown in Figure 4.19, which have all types of unconnected elements.

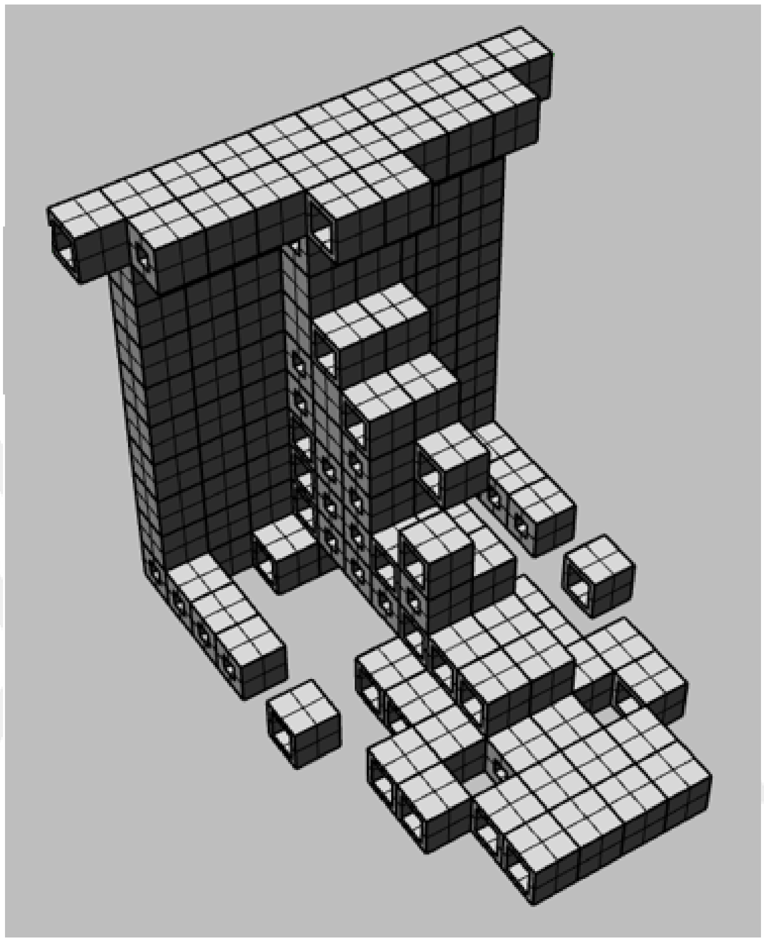

Figure 4.19: Example topology with unconnected cells

Firstly, the section of the example geometry shown in Figure 4.20 is analysed. The cell marked as 1 has a surface neighbor marked as 2, two edge neighbors marked as 3 and 4, and a corner neighbor marked as 5. Since the 5^{th} cell shares only a corner with the 1^{st} cell, they are unconnected. The Grasshopper3D code block to find all the neighbors of a cell and, if any, its unconnected corner neighbor is shown in Figure 4.21.

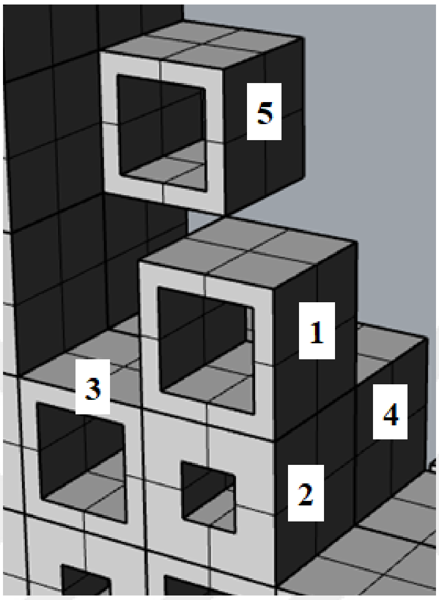

Figure 4.20: Corner neighbor (5), surface neighbor (2) and the edge neighbors (3 & 4) of the main cell marked as 1

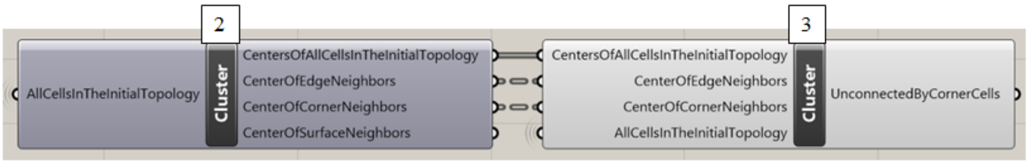

Figure 4.21: Grasshopper3D code block to find all the neighbors of a cell (2) and the unconnected corner neighbor (3)

In order to connect the corner neighbor to the main cell, firstly a new surface neighbor is added to the 5^{th} cell in a way that it shares an edge with the 1^{st} cell. In this case, there are three possible surface neighbors to be added which are marked as 6, 7 and 8 in Figure 4.22.

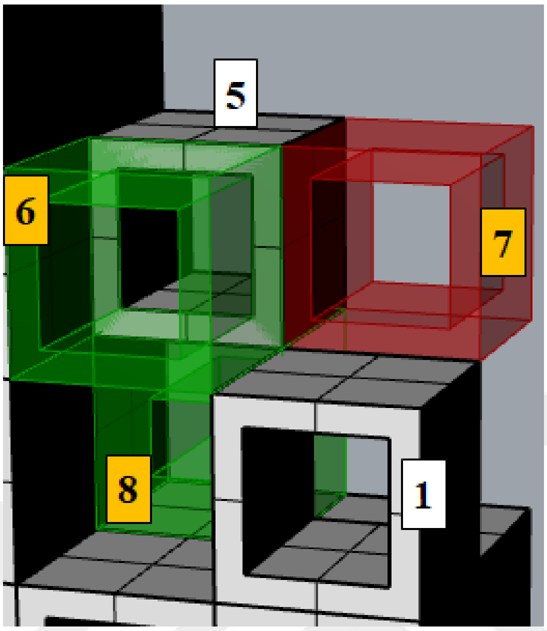

Figure 4.22: Three possible surface neighbors (6, 7 & 8) to be added to the 5^{th} cell to make it share an edge with the main cell (1).

The cell with the highest density is selected among the 6^{th}, 7^{th} and 8^{th} cells as the new surface neighbor of cell 5. In this example, cell 7 has the highest density. Therefore, the unconnected corner cell is made connected to the main cell by an edge as shown in Figure 4.23. The Grasshopper3D code block to add new surface neighbors to the unconnected cells and modify the topology shown in Figure 4.19 in a way that it contains no unconnected corner cells is shown in Figure 4.24.

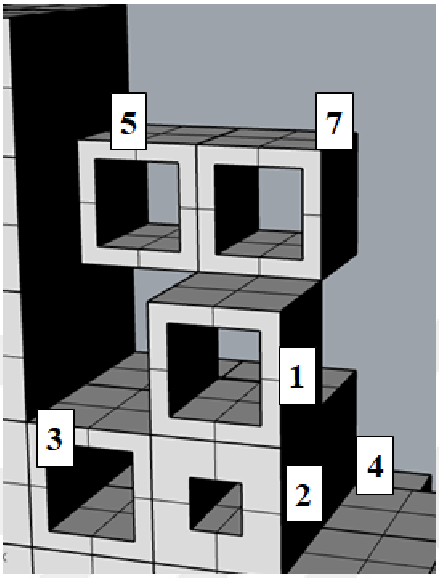

Figure 4.23: 7^{th} cell is added to the topology to connect the 5^{th} and the 1^{st} cell by an edge.

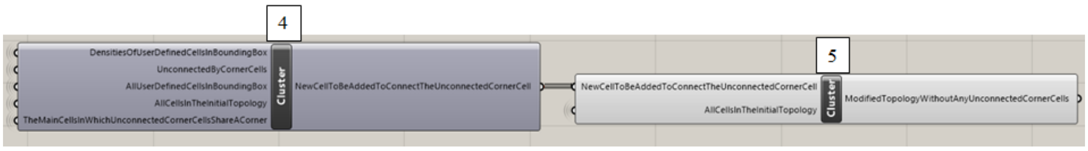

Figure 4.24: Code block to add a new surface neighbor to the unconnected cell (4) and generate a topology without unconnected corner cells (5)

After this step, the topology does not contain any unconnected corner neighbors. In this step, the topology is checked for any unconnected edge neighbors. The cell pairs 1 & 7, 8 & 9 and 10 & 11 shares only an edge, therefore they are unconnected as shown in Figure 4.25.

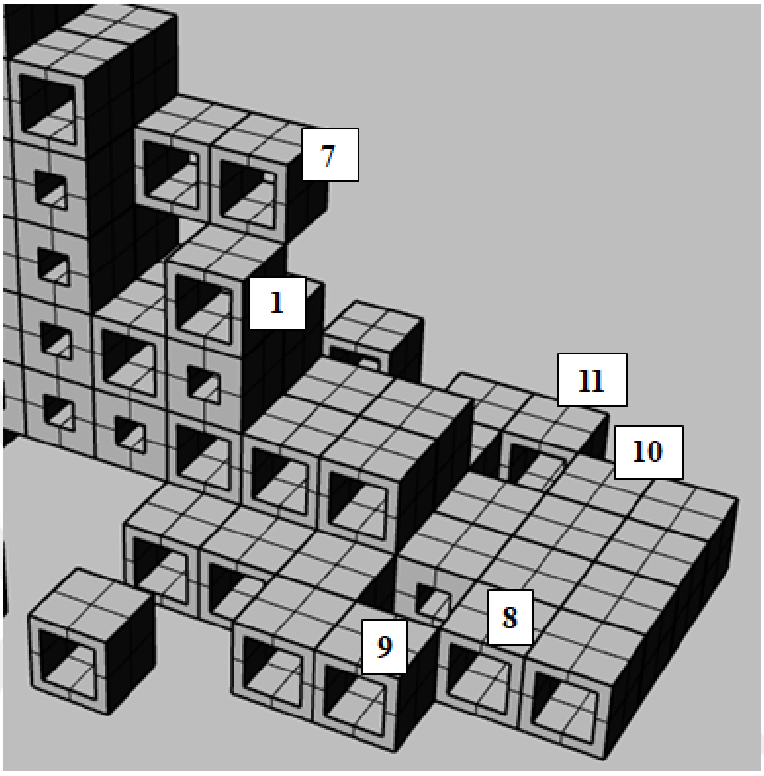

Figure 4.25: Unconnected cell pairs sharing only an edge.

In order to connect the pair of cells to each other, a new surface neighbor is added to the 7^{th}, 9^{th} and 11^{th} cells. In this case, there are two possible surface neighbors to be added for each cell. The surface neighbors that can be added to the cell 7, 9 and 11 are the cell groups 12-13, 14-15 and 16-17 respectively as shown in Figure 4.26.

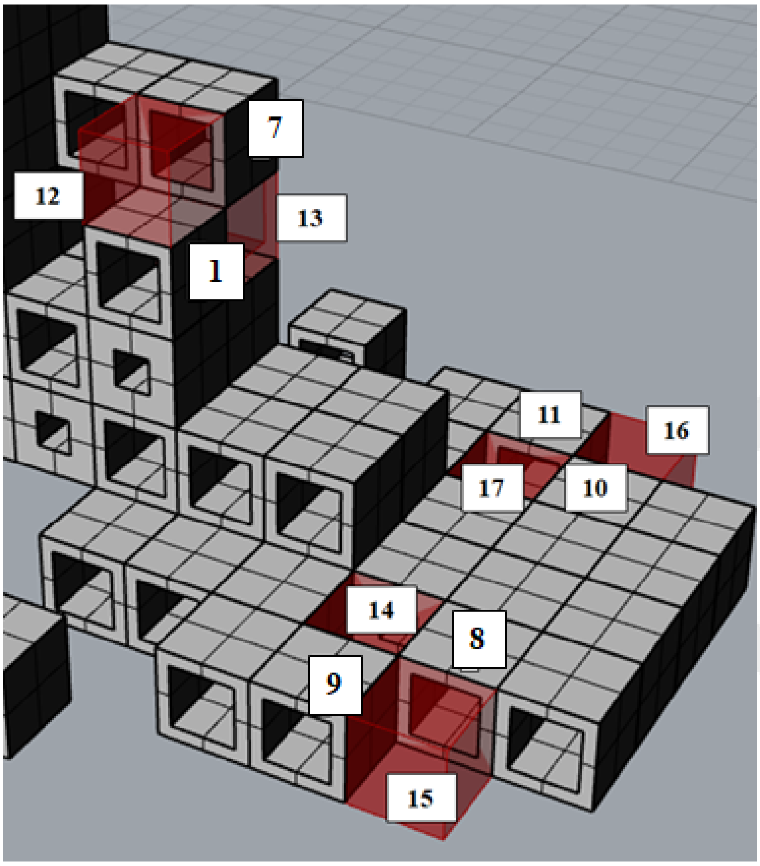

Figure 4.26: Possible surface neighbors (12-13, 14-15, 16-17) to be added to the 7^{th}, 9^{th} and 11^{th} cells to make them connected to the topology

In these group of cells, the cell with the highest density, which are the 12^{th}, 15^{th} and 16^{th}, is selected as the new surface neighbor. After this step, the topology does not contain any unconnected edge neighbors as shown in Figure 4.27. The Grasshopper3D code block to find the unconnected edge neighbor and add a new cell to the topology to connect this neighbor is shown in Figure 4.28.

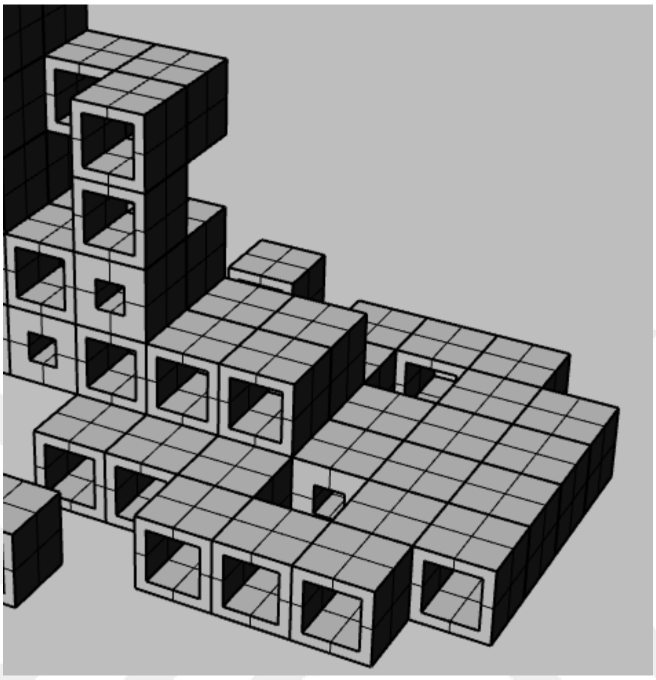

Figure 4.27: Topology without any unconnected corner and edge neighbors.

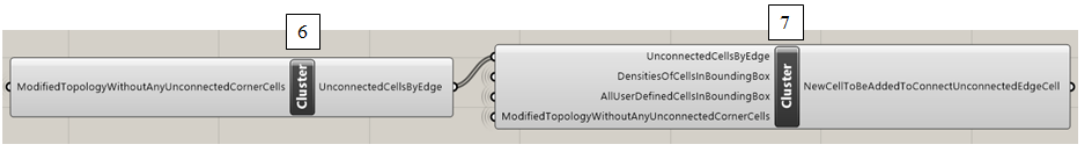

Figure 4.28: Code block to find unconnected edge neighbor (6) and make it connected by adding a new cell to the topology (7)

The last step of the connectivity analysis is to find the cells that do not share any feature with the main topology and are within one cell distance. The cells marked as 18 and 21 shown in Figure 4.29 satisfy this condition, so that they are unconnected.

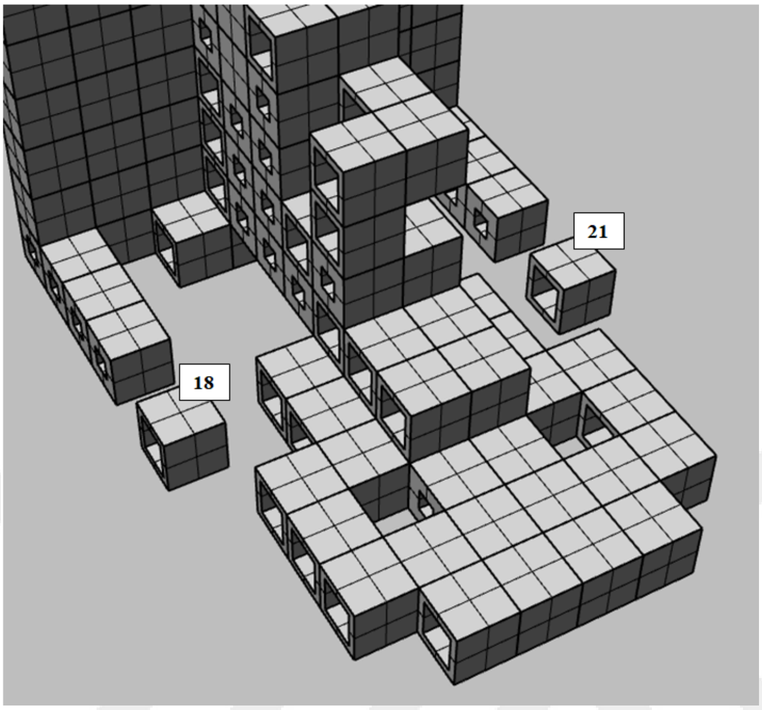

Figure 4.29: Unconnected cells that do not share any feature with the main topology

In order to connect the unconnected cells, the closest cells in the main topology to which the 18^{th} and 21^{th} cells can be connected via a surface neighbor are found. In this case, cells 19-20 and 22-23 are the closest cells to cell 18 and 21 respectively as shown in Figure 4.30.

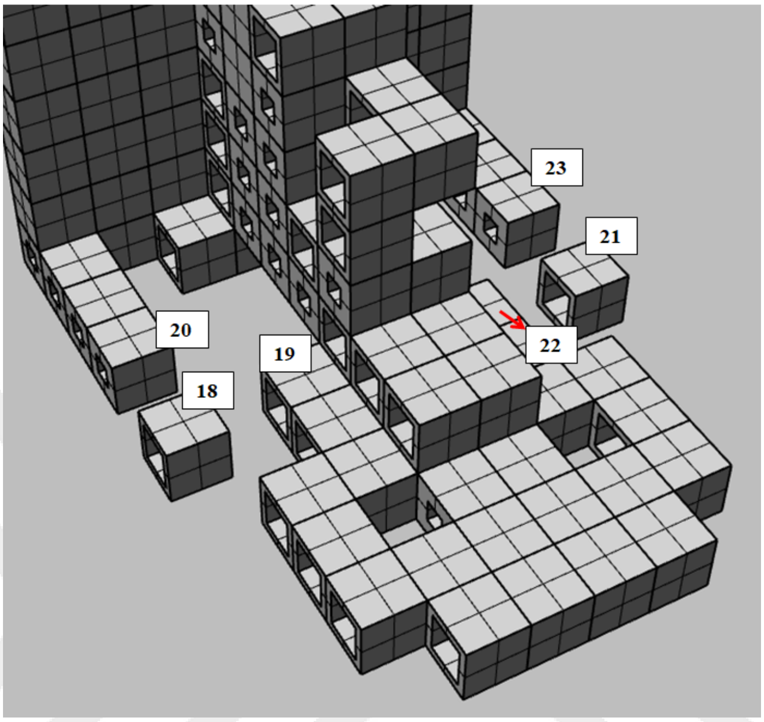

Figure 4.30: Closest cells to the unconnected cells in the main topology

The 18^{th} and 21^{th} cells can be connected to the main topology via the surface neighbors 24-25 and 26-27 respectively as shown in Figure 4.31.

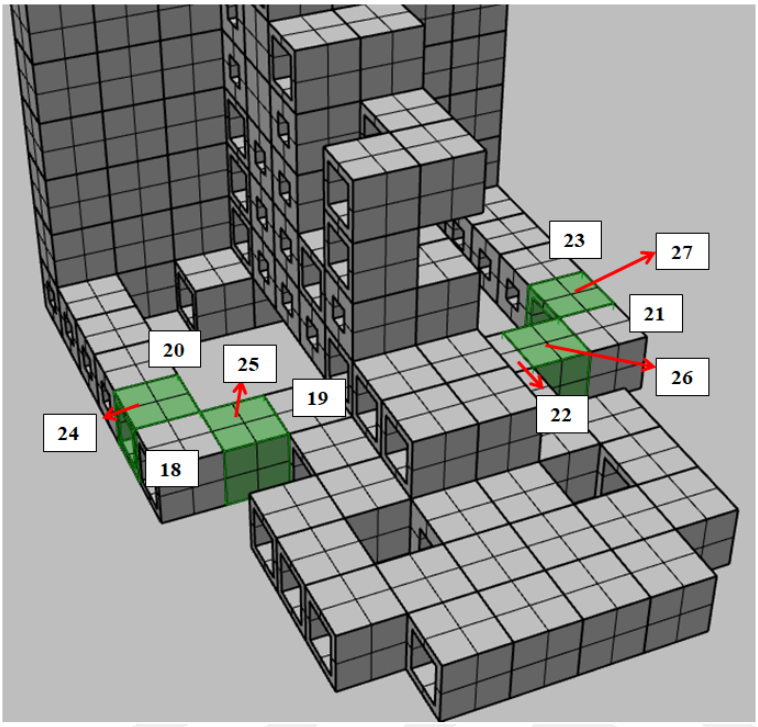

Figure 4.31: Surface neighbors to be added to the unconnected cells to make them connected to the main topology

Then the surface neighbors are added to the unconnected cell and a fully connected topology is obtained. The Grasshopper3D code block to find the unconnected cells that do not share any feature with the topology and connect them to the main topology is shown in Figure 4.32.

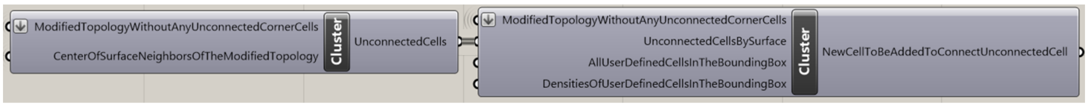

Figure 4.32: The code block to connect the unconnected cells that do not contain any common feature with the main topology

The code block for the generation of the fully connected topology and the illustration of the topology is shown in Figure 4.33 and Figure 4.34 respectively.

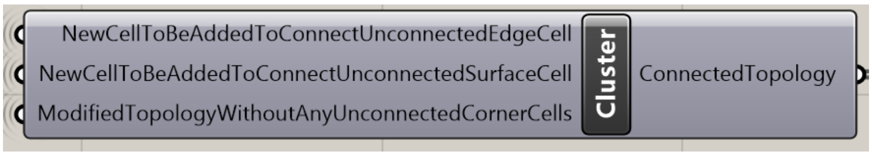

Figure 4.33: The code block to generate fully connected topology

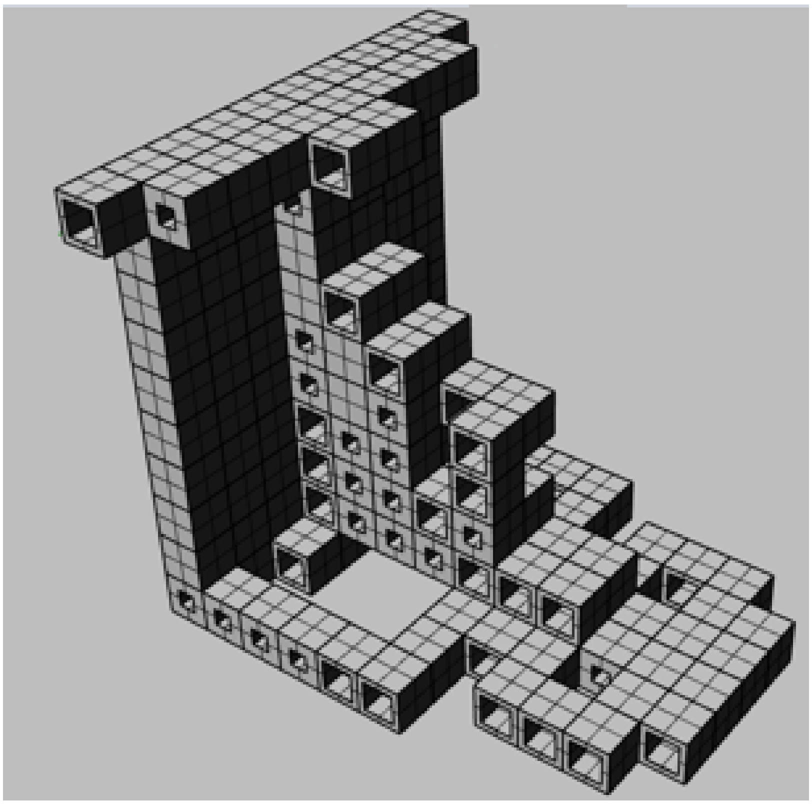

Figure 4.34: Fully connected topology

In the same way, when the connectivity analysis is applied to the original topology shown in Figure 4.18, it is seen that the cells shown as A_1, A_2, A_3 and A_4 in Figure 4.35 are unconnected to the topology.

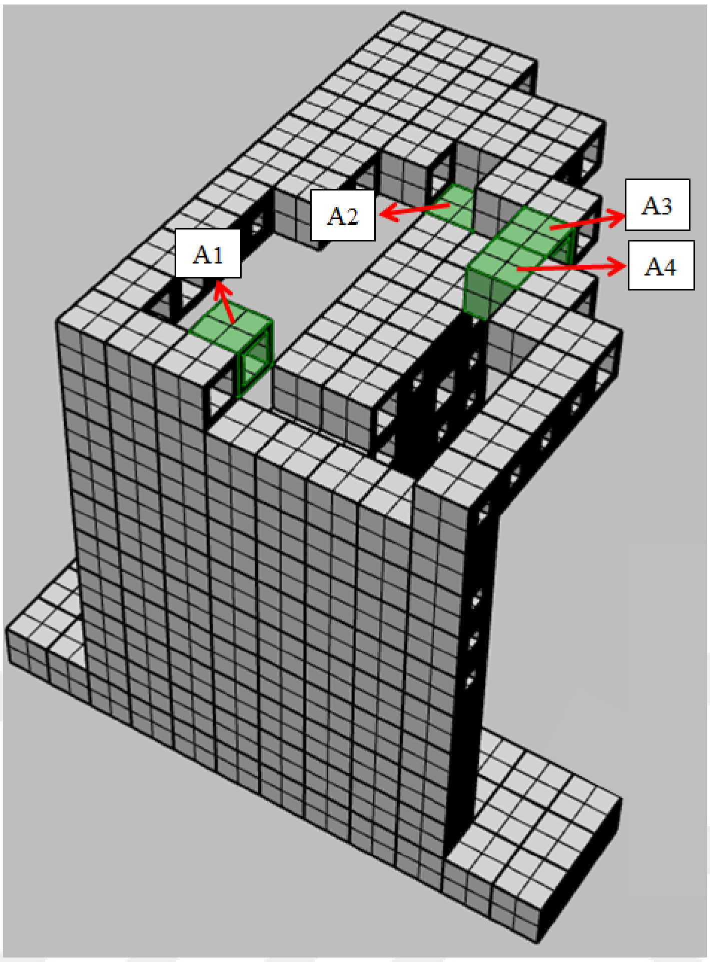

Figure 4.35: Unconnected cells in the original topology

In order to connect the unconnected cells, new cells, shown as B_1, B_2, B_3, B_4 and B_5 are added to the topology as shown in Figure 4.36.

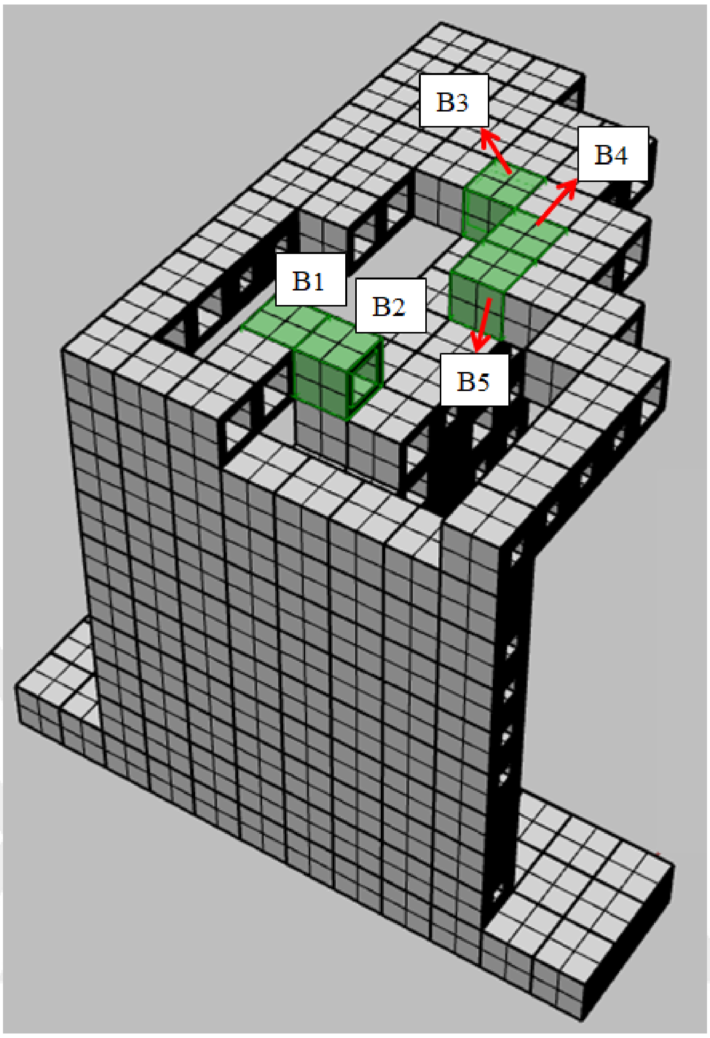

Figure 4.36: Added cells to connect the unconnected cells to the topology

Finally, a fully connected topology is obtained as shown in Figure 4.37.

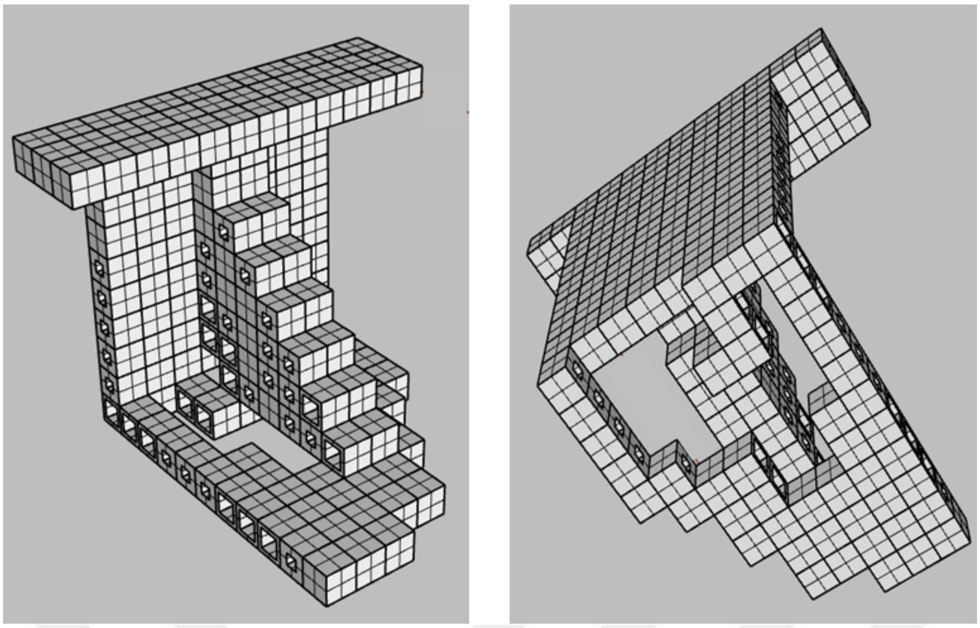

Figure 4.37: Fully connected topology

4.6 Easy Removal of Powder/Resin

In powder-based AM approaches such as SLS, SLM and EBM, and in SLA technologies powder/resin may remain in the internal features of the part which do not have access to the outer space through the holes. It leads to heavier parts than the expected outcomes. One of the focuses of the proposed method is to ensure that the designed topology allows removal of all the excess powder/resin from the part after fabrication is completed. In this regard, firstly, the cells comprising the fully connected topology shown in Figure 4.37 are grouped in a way that all the cells in a group share the same x and z coordinates as illustrated in Figure 4.38. Two of the groups are shown on the geometry as an example. The related Grasshopper3D code block for this step is given in Figure 4.39. It takes the fully connected topology obtained in the previous step as the input and gives the cell groups as an output.

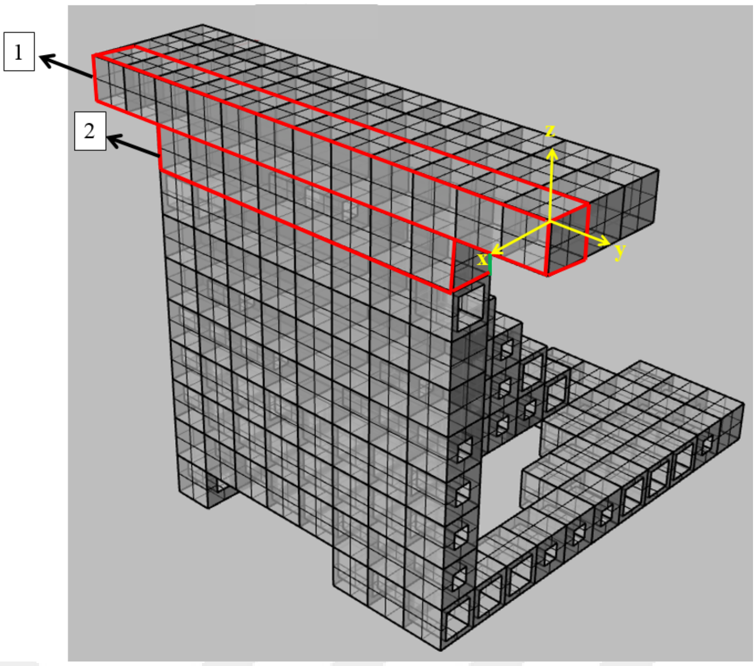

Figure 4.38: Example cell groups marked as 1 & 2 are illustrated on the topology.

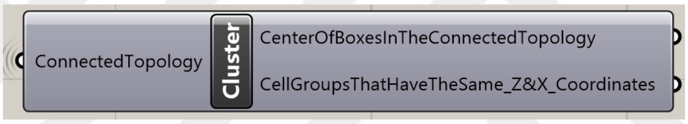

Figure 4.39: Code block for the generation cell groups that contain cells with the same x and z coordinates

The second step is to check all the cells in the cell groups against the possibility of remaining powder/resin. In order to reduce the number of cells to be checked, a filtering operation is performed. Since there is not any possibility for the powder/resin to remain inside a cell group whose all members contain a hole, then this group are excluded from the check group. In a similar way, if all the cells comprising a group not containing any holes, then this group of cell are also excluded from the check group. The cell groups to be checked against excess powder/resin are shown in Figure 4.40 and the related code block is shown in Figure 4.41.

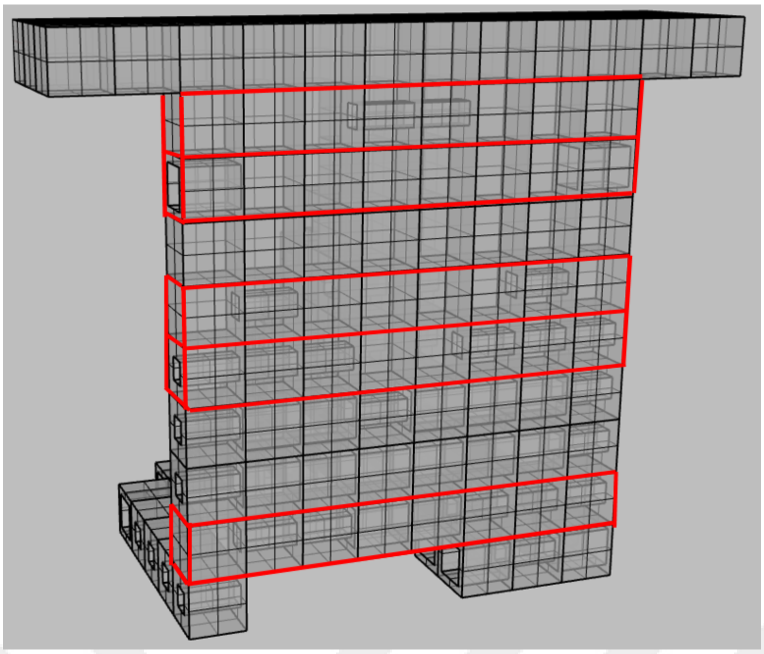

Figure 4.40: Cell groups to be checked against powder/resin

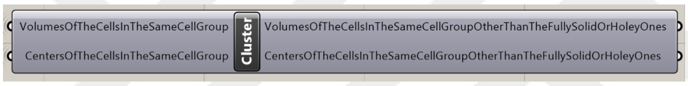

Figure 4.41: Code block to determine cell groups to be checked against powder/resin

The number of cells to be checked can be reduced further. Since powder/resin may only remain inside the cells with a hole, the cells filled full of material do not need to be checked. Therefore, the cells with a hole are selected from each group as shown in Figure 4.42. The related code block is shown in Figure 4.43.

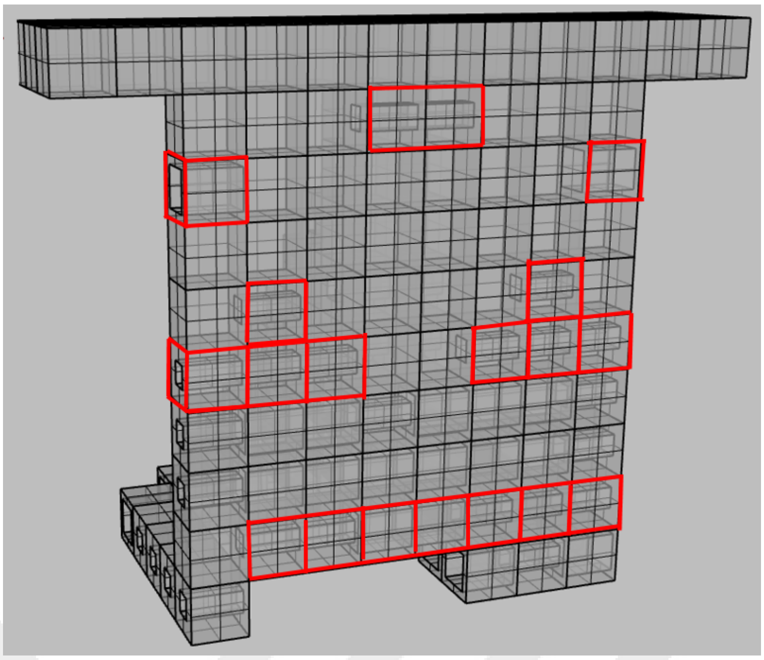

Figure 4.42: The cells in each group in which the excess powder/resin may remain inside

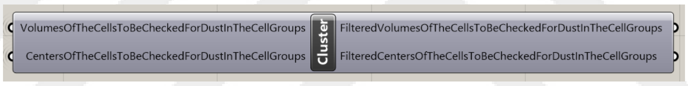

Figure 4.43: Code block to determine the cells in cell groups which have the possibility of containing powder/resin

If the cells specified in Figure 4.42 are between the two solid cells, and there are not any cell interfacing with the outer space between these solid cells, than the powder/resin remains inside the cell with the hole. Some of the cells in Figure 4.42 are analyzed for demonstration purposes as shown in Figure 4.44. The cell numbered as 1, 2 and 3 have a direct interface with the outer space. The cell numbered 4 is not between two solid cells. There is a solid cell numbered as 5 in the y direction but the other side of the cell has an interface with the outer space through the cell numbered 3. In a similar way, there is a solid cell numbered as 6 in the y direction for the 7^{th} cell, but the 7^{th} cell is open to outer space through the other cells in the y direction sharing the same group with it. Therefore, the cells numbered as 1, 2, 3, 4 and 7 do not contain excess powder/resin after fabrication.

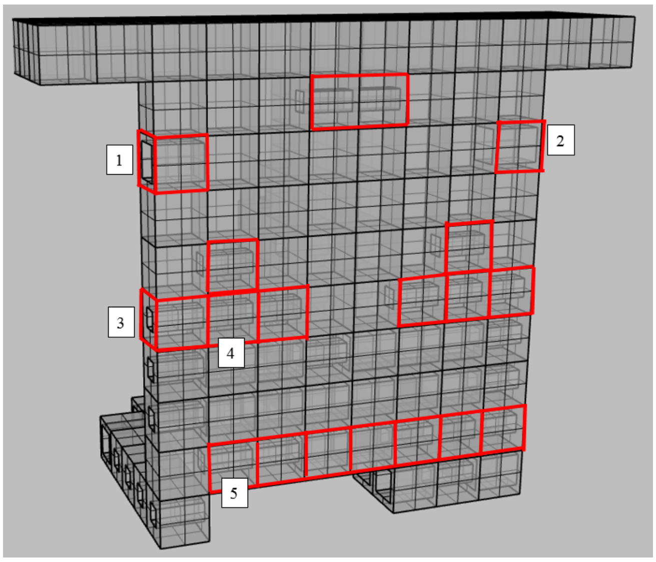

Figure 4.44: Sample cells to be checked against powder/resin

When the entire topology is analyzed in the same way, the cells in which the excess powder/resin remains are obtained and shown in Figure 4.45. The related code block for the determination of these cells are shown in Figure 4.46.

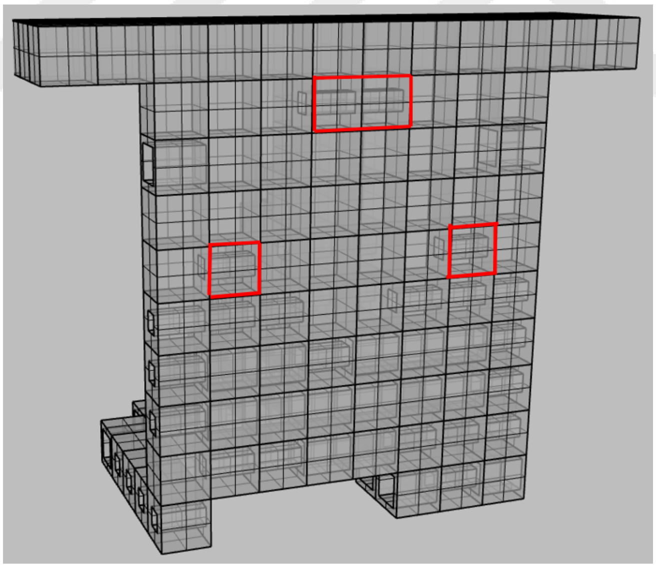

Figure 4.45: Cells in which excess powder/resin remains

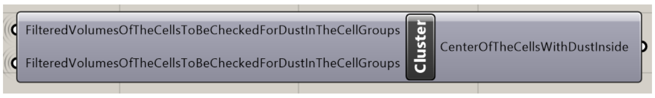

Figure 4.46: Code block to obtain cells with powder/resin inside

The next step is to provide a cavity in the topology to allow the removal of excess powder/resin. In this regard, the closest cells, which have an interface with the outer space, to the cells shown in Figure 4.45 are obtained. Then, a rectangular hole with dimensions identical to the inner dimensions of the second type of cell given in Table 4.2 is generated for the cells obtained in this step. The cells to be hollowed are shown in Figure 4.47 and the related code block is given in Figure 4.48.

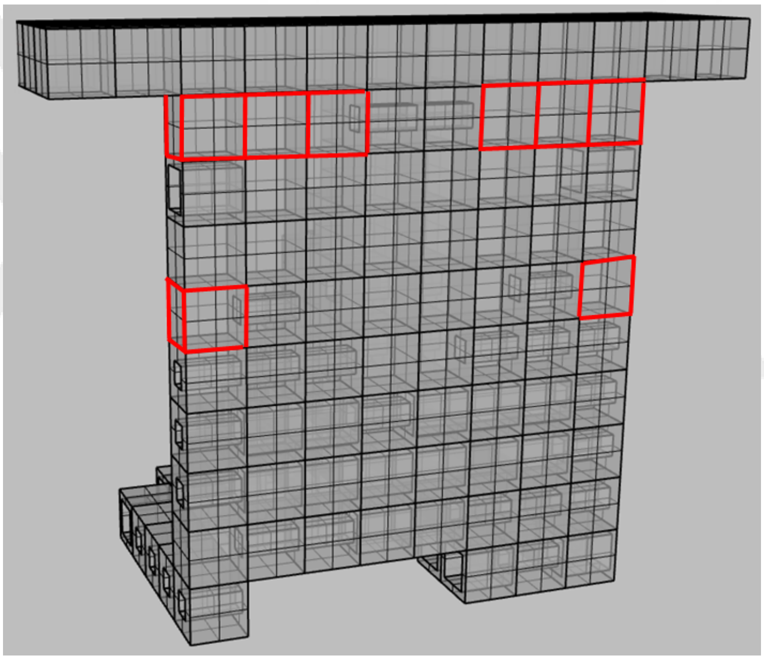

Figure 4.47: Cells to be hollowed out

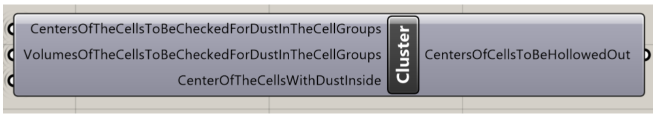

Figure 4.48: Code block to obtain the cells to be hollowed out

The resulting powder/resin-free topology is given in Figure 4.49 and the code block for the generation of the final topology is given in Figure 4.50.

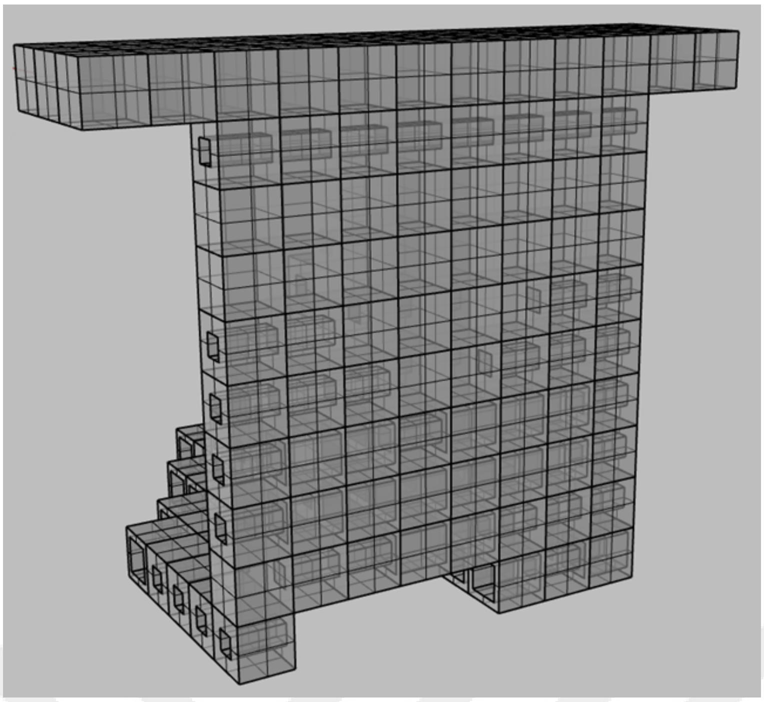

Figure 4.49: Final, fully connected and powder/resin-free topology

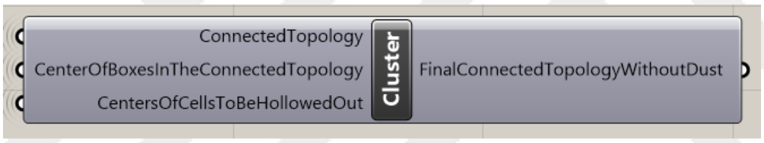

Figure 4.50: Code block to generate final, fully connected and powder/resin-free topology

4.7 Application of the Proposed Method by Using Circular Beams

The proposed method is also applied to the topology shown in Figure 4.3 with different cellular structures. In this case, the fully connected group of boxes shown in Figure 4.51 are filled with structures having circular cross sections rather than the rectangular cells shown in Figure 4.37.

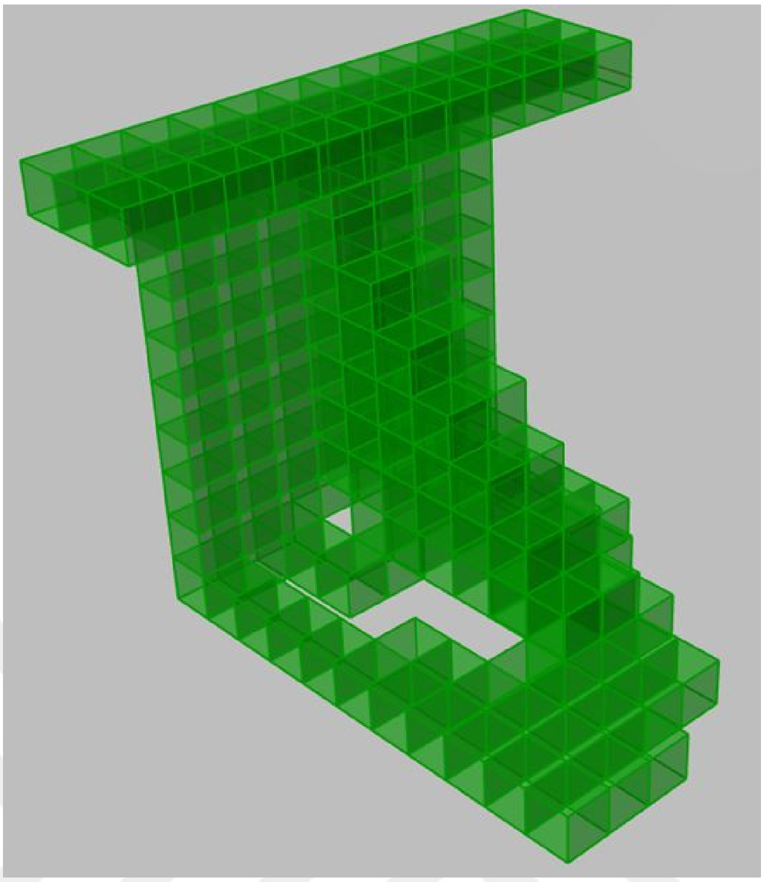

Figure 4.51: Fully connected group of cells

After obtaining the density data for each box in Figure 4.51, the boxes are filled with cellular structures in the shape of circular beams. Three types of cells are used as shown in Figure 4.52.

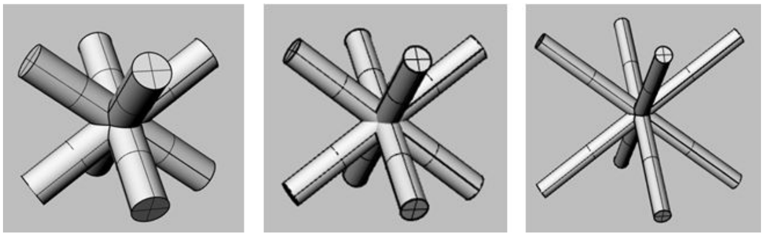

Figure 4.52: Circular beam type structures

The cells are categorized according to the densities of the boxes they belong to. As the density of the box increases, the radius of the beams also increase. The first type of cells are composed of beams having a radius of $1mm$ and are used in the boxes with densities between 0.75 and 1. The second type of cells are composed of beams having a radius of $0.7mm$ and are used in the boxes with densities between 0.5 and 0.75. The third type of cells are composed of beams having a radius of $0.4mm$ and are used in the boxes with densities between 0.25 and 0.5. The properties of the cells are summarized in Table 4.3.

Table 4.3: Properties of the circular beam type structures

Properties	First	Second	Third
Beam radius (mm)	1	0.7	0.4
Density region	0.75 – 1	0.5 – 0.75	0.25-0.5

The resulting topology after filling the each box with the associated circular beam type cells is shown in Figure 4.53. The boxes on which boundary conditions are present are fully filled with material.

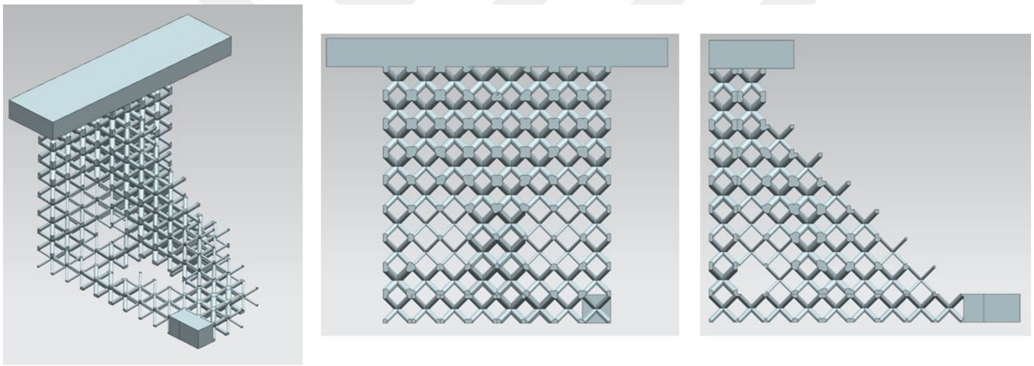

Figure 4.53: Isometric (left), back (middle) and side (right) view of the final topology

CHAPTER 5

ANALYSIS AND TEST RESULTS FOR 2D GEOMETRIES

The proposed method is applied on multiple geometries including a cantilever beam, simply supported beam and a hanger shaped geometry. The beam geometries are taken from the work of Jakiela et al. [42] and the performance of the proposed method for the beams are compared with the methods used in [42], which are the homogenization method and the genetic algorithms. Additionally, the performance of all three geometries are compared with their SIMP optimized forms. While the analysis are done for each geometry, the tests are applied on the cantilever beam only. The results are given in the following sections.

5.1 Cantilever Beam

5.1.1 3D Model Generation

The proposed method is applied on the cantilever beam geometry shown in Figure 3.2 after the beam is optimized by the SIMP method with a penalization factor of 1 and 3. The properties of the cellular structures are the same as in Table 3.1. The resulting geometries are shown in Figure 5.1.

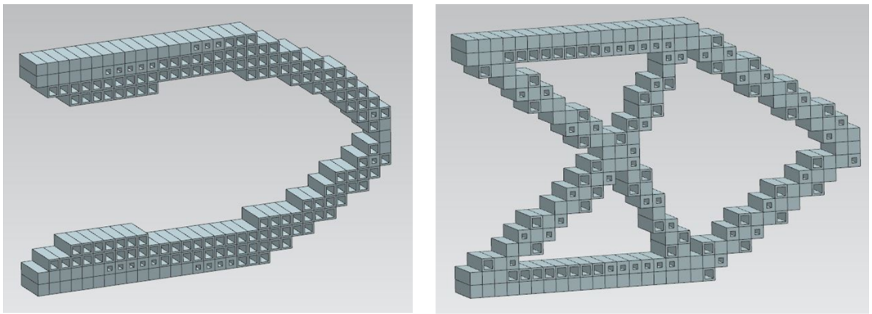

Figure 5.1: Cantilever beams remodelled with cellular structures after it is optimized by the SIMP method with a penalization factor of 1 (left) and 3 (right)

In order to see the effect of intermediate densities in the final topology, the parts with cellular structures are compared with the SIMP optimized parts which are not remodelled with the proposed method. The density limit for the geometries is set to 0.25, which means the elements with densities larger than 0.25 are filled with material while the others are left blank. The geometries after optimization are shown in Figure 5.2.

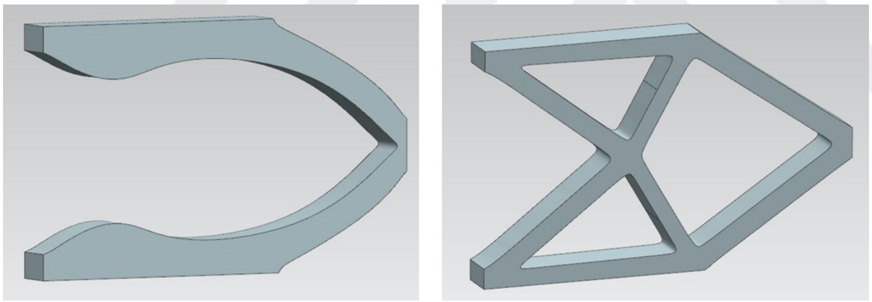

Figure 5.2: Cantilever beams after it is optimized by the SIMP method with a penalization factor of 1 (left) and 3 (right)

The proposed method is also compared with the cantilever geometries optimized by the homogenization method and genetic algorithms in the work of Jakiela et al. [42]. In this regard, the parts shown in Figure 5.3 are generated in Rhino3D. Both geometries are optimized according to the boundary conditions shown in Figure 3.2.

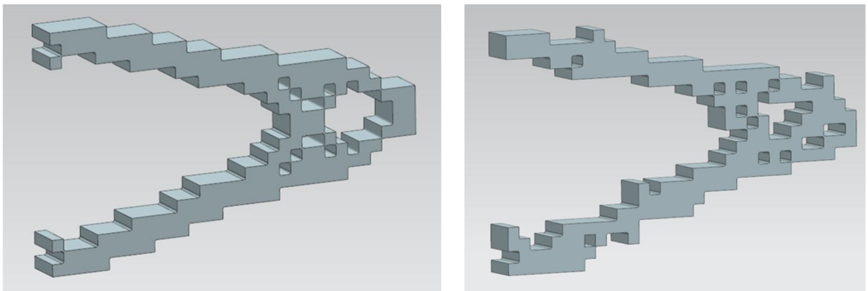

Figure 5.3: Cantilever beams after it is optimized by the homogenization method (left) and genetic algorithms (right)

5.1.2 Fabrication of the Parts and the Test Rig

The parts shown in Figure 5.1, Figure 5.2 and Figure 5.3 are fabricated on Ultimaker 3 Extended, which is an extrusion-based 3D printer, by using PLA as the material. In order to test the parts, the force application side of the geometries are extended to provide a $10mm$ x $10mm$ area. The fabricated geometries are shown Figure 5.4.

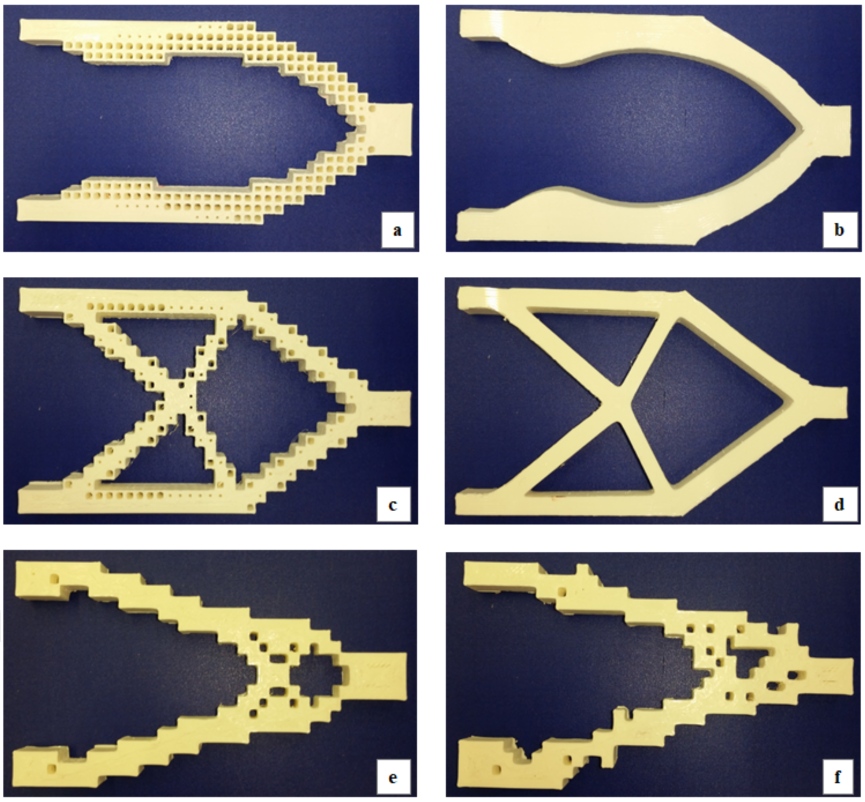

Figure 5.4: Cantilever beams remodelled with the proposed method with a penalization factor of 1 (a) and 3 (c), optimized by the SIMP method with a penalization factor of 1 (b) and 3 (d), optimized by the homogenization method (e) and the genetic algorithm (f)

The test rig used is shown in Figure 5.5. It is made of stainless steel. The cantilever beams are fixed from their left side by squeezing in between the screws.

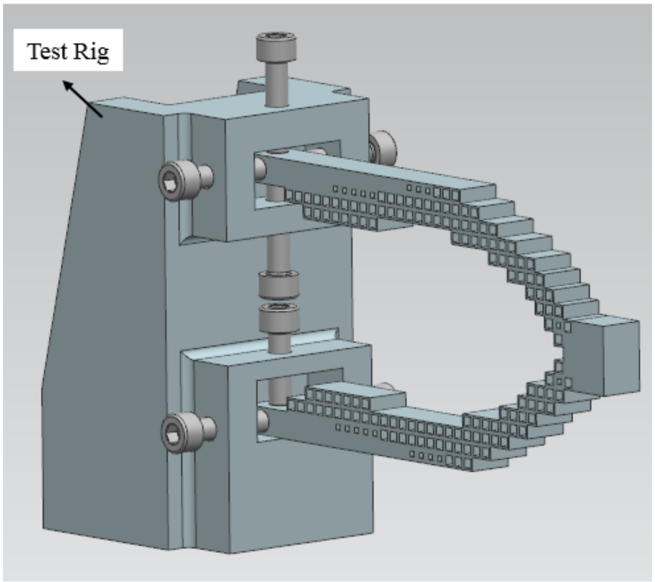

Figure 5.5: Test rig

5.1.3 Tests

The fabricated cantilever parts are tested with Instron 8872 Fatigue Testing Machine. Each part is fixed from the left side by the test rig and a force is applied on the $10mm$ x $10mm$ area at the right side as shown in Figure 5.6. In order to provide the proper load application interface with the surface on the specimen, an apparatus is fabricated to be connected to the cross-head. As the cross-head moves downward, magnitude of the load increases in proportion to the amount of displacement of the cross-head. The load is increased until the specimen is broken.

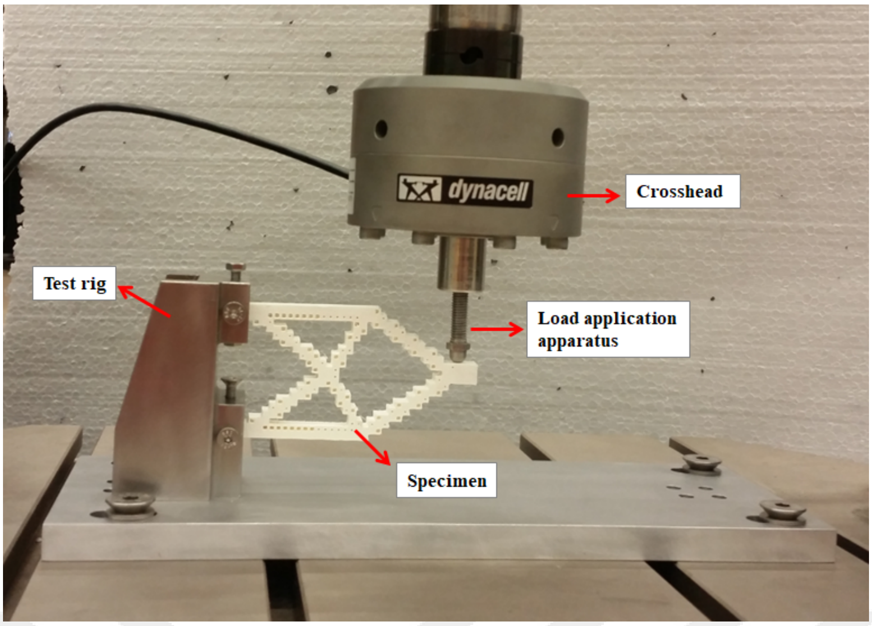

Figure 5.6: Test setup

The images of the parts after yielding are shown in Figure 5.7. The cantilever beam marked as d is not broken during the tests. After a while, it started to slide forward and no further measurements could be taken. The magnitude of the load applied to the part at the moment when the piece started sliding is taken as the $loadatyielding$ for comparison purposes. Therefore, it is important to emphasize that the beam undergoes plastic deformation under greater force. The trail of the screw on the part can be seen in Figure 5.8.

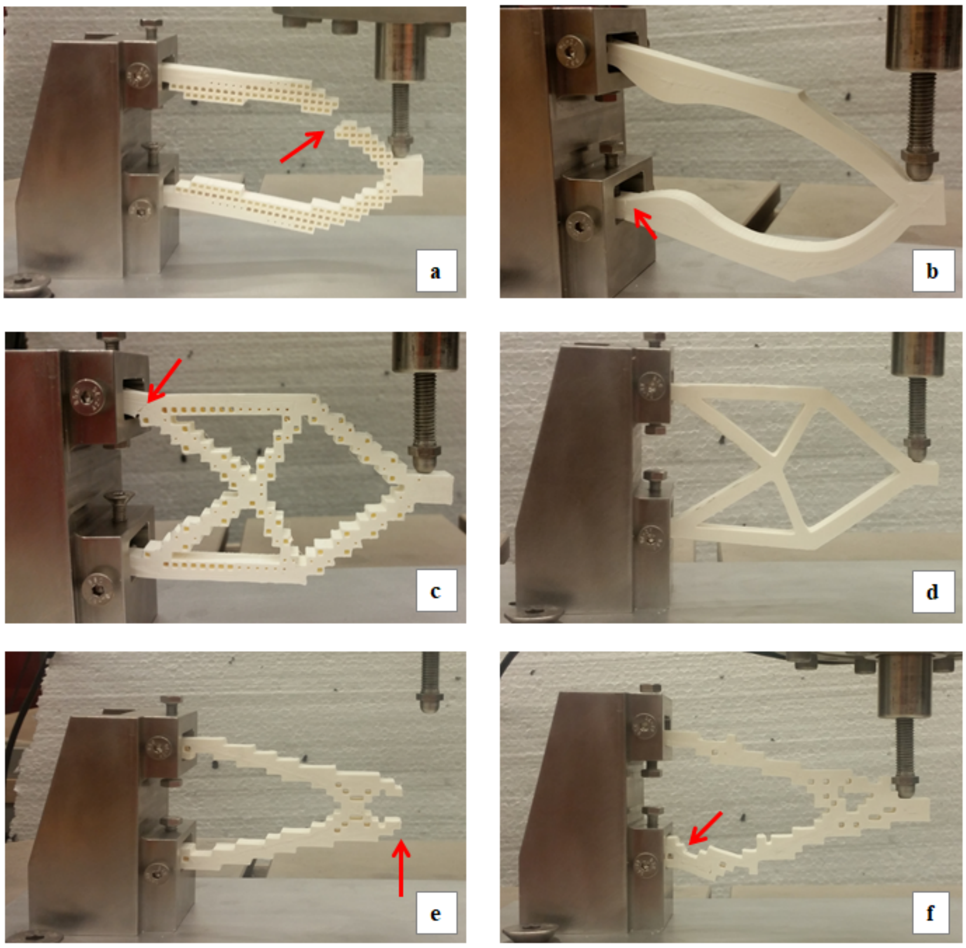

Figure 5.7: The fraction points are shown on the cantilever beam remodelled with the proposed method with a penalization factor of 1 (a) and 3 (c), optimized by the SIMP method with a penalization factor of 1 (b) and 3 (d), optimized by the homogenization method (e) and the genetic algorithm (f)

Figure 5.8: The trail of the screw on the cantilever beam part optimized by the SIMP method with a penalization factor of 3

At the end of the tests, the performances of the specimens are compared in terms of their load carrying capacities. The results of the tests are summarized in Table 5.1.

Table 5.1: Test results for the cantilever beams

Optimization Method	Weight (N)	Load at Yielding (N)	Load/Weight
Proposed Method with a Penalization Factor of 1	0.188	155.5	827.13
SIMP with a Penalization Factor of 1	0.259	210.8	813.9
Proposed Method with a Penalization Factor of 3	0.232	395.7	1705.6
SIMP with a Penalization Factor of 3	0.235	477	2029.8
Homogenization	0.218	274.3	1258.3
Genetic Algorithms	0.217	315.5	1453.9

As it can be seen from the test results, load-to-weight ratio of the proposed method is quite close to the results of the parts optimized by the SIMP method. Although the results are closer, the proposed method provides 27.4% weight reduction with a slightly higher performance for a penalization factor of 1.

Another point to emphasize is that the cantilever beam optimized by the SIMP without penalization was not manufacturable at first as it can be seen from Figure 5.9 since it has many intermediate density regions. In the form of the geometry shown in the figure, the density filter is set to 0.7, which means that the elements with a density lower than 0.7 are empty. It results in discontinuous regions with material through the topology which leads to a non-manifold geometry. The boundaries of the regions with material are shown in Figure 5.9.

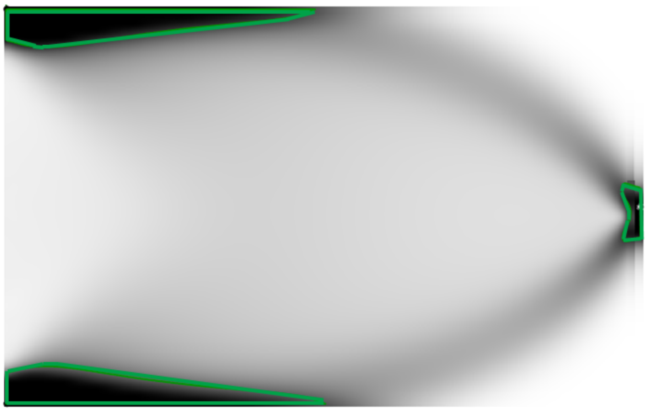

Figure 5.9: Boundaries of the manufacturable regions for a density filter of 0.7

Therefore, the only way to have a manufacturable part is to lower the density filter, for this case, from 0.7 to 0.25. In this case, the majority of the intermediate densities are eliminated. The 3D printable region is shown in Figure 5.10. Thus, the proposed method not only provides a manufacturable topology without eliminating intermediate densities, it also has a slightly better load carrying capacity with a far less weight compared to the solid part.

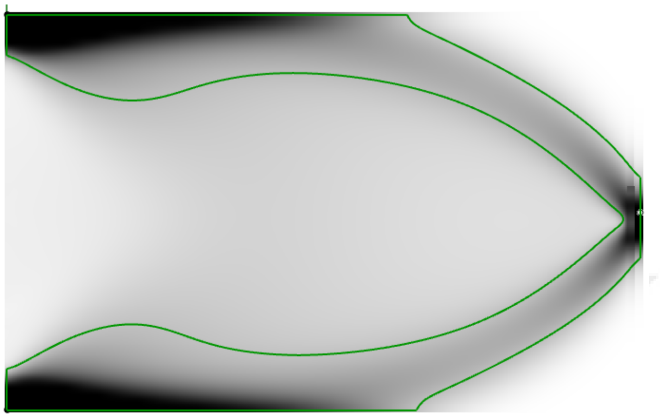

Figure 5.10: Boundary of the manufacturable region for a density filter of 0.25

When the results of the parts for a penalization factor of 3 are compared, it is seen that the proposed method provides a weight reduction of 1.3$\%$ but does not have a better performance than the SIMP method. However, the parts can be used interchangeably since the load carrying capacities of the parts do not differ greatly.

When the whole table of results are evaluated, the performances of the methods can be listed in descending order as follows: SIMP method with a penalization factor of 3, proposed method with a penalization factor of 3, genetic algorithms, homogenization, proposed method with a penalization factor of 1, SIMP method with a penalization factor of 1.

The yielding points of the parts are marked on the graph generated according to the data collected during the test is shown in Figure 5.11.

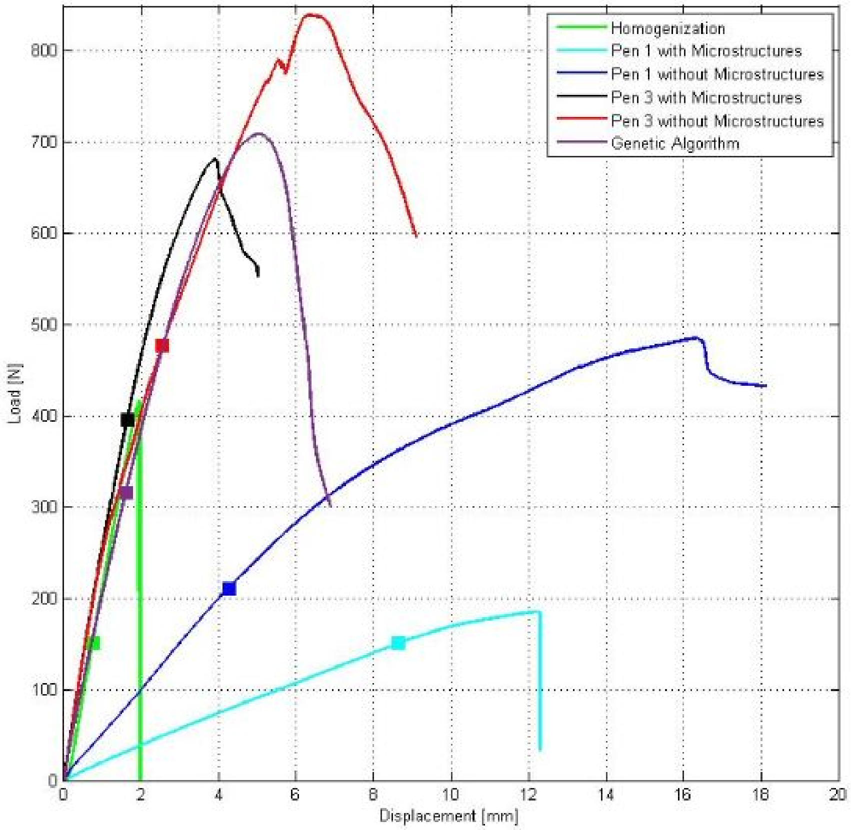

Figure 5.11: Yielding points of the tested parts

5.1.4 Analysis

Structural analysis are done on the cantilever geometries in Ansys software to validate the test results. In order to simulate the tests, the parts are also extended from their right hand side until the edge of the force application surface by $10mm$. All the boundary conditions are set in a way to simulate the test conditions. Force is applied on a $10mm$ x $10mm$ area at the rightmost surface. The contact regions between the squeezing screws and the surfaces of the parts at the left side are defined; and a fixed support condition is set for the interior surfaces of 4 holes providing connection to the ground. PLA is assigned as the material of the parts. The boundary conditions for one of the parts and the material properties of PLA are shown in Figure 5.12 and Table 5.2, respectively.

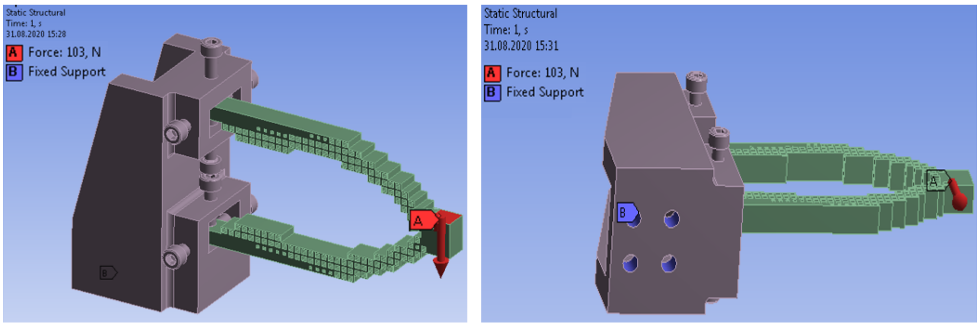

Figure 5.12: Boundary conditions defined for the cantilever beam geometries where A shows the force application surface and B shows the surfaces set as fixed supports

Table 5.2: Mechanical properties of PLA

Properties	PLA
Density	1240 kg/m^3
Young's Modulus	2346.5 MPa
Tensile Yield Strength	49.5 MPa

The analysis problem is solved for the load carrying capacities of the parts. Applied load is increased gradually until the safety factor, which is the ratio of the maximum equivalent stress to the yield strength of the part, reduces under 1. The magnitude of the force just before the reduction of the safety factor under 1 implies the maximum load that can be carried by the part before yielding. The analysis results are given in Table 5.3.

Table 5.3: Analysis results for the cantilever beam geometries

Optimization Method	Weight (N)	Load at Yielding (N)	Load/Weight
Proposed Method with a Penalization Factor of 1	0.174	103	591.9
SIMP with a Penalization Factor of 1	0.252	133	527.8
Proposed Method with a Penalization Factor of 3	0.219	445.5	2034.2
SIMP with a Penalization Factor of 3	0.227	527	2321.6
Homogenization	0.212	192.5	908
Genetic Algorithms	0.209	196	937.8

The success of the proposed method for a penalization factor of 1 is better observed in the analysis results. While the weight of the part remodelled with the proposed method is 30.9% less than the SIMP optimized part, its load carrying capacity is increased by 10.8%. When the whole results are evaluated, it is seen that analysis and test results overlap. The performances of the methods can be listed in descending order as follows: SIMP method with a penalization factor of 3, proposed method with a penalization factor of 3, genetic algorithms, homogenization, proposed method with a penalization factor of 1, SIMP method with a penalization factor of 1. The graphics showing the safety regions of the parts under the loading specified in Table 5.3 is given in Figure 5.13. The color-bar on the left side of the figures shows the safety degree of the material. The regions experiencing large stresses have a safety degree closer to 1. If the safety degree is smaller than 1, then yielding occurs in the corresponding region.

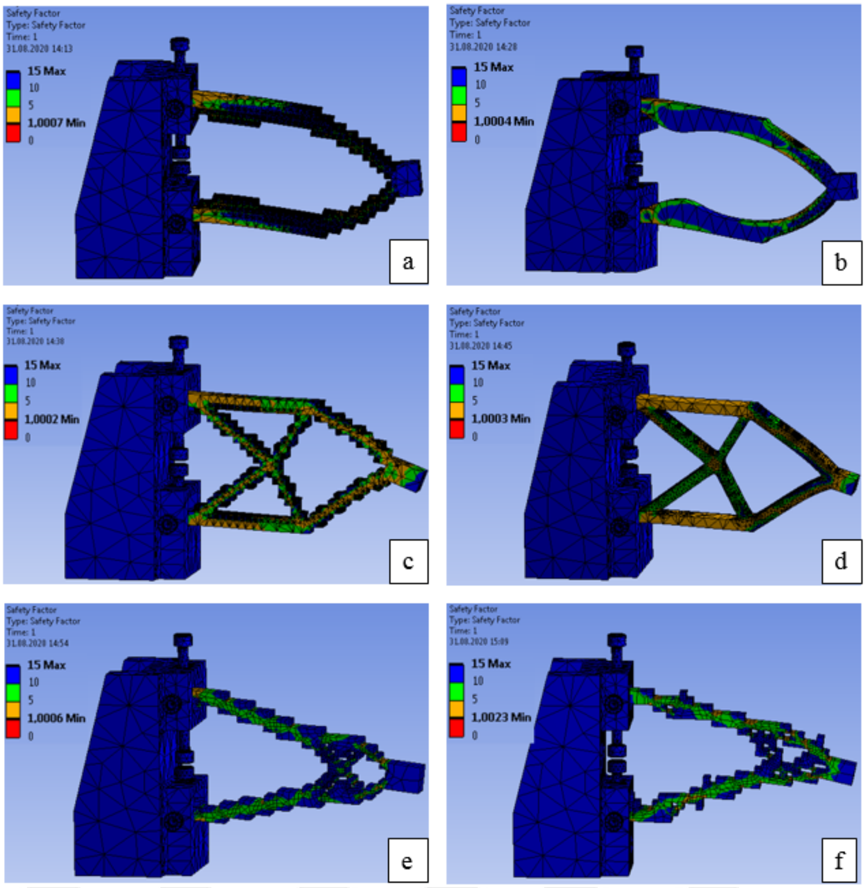

Figure 5.13: The safety regions of the geometries remodelled with the proposed method with a penalization factor of 1 (a) and 3 (c); optimized by the SIMP method with a penalization factor of 1 (b) and 3 (d), the homogenization method (e) and the genetic algorithm (f)

5.2 Simply Supported Beam

5.2.1 3D Model Generation

In this part, a simply supported beam geometry [42] shown in Figure 5.14 is used for the optimization. The beam is fixed from its lower ends and a force with a magnitude of $10kN$ is applied at the middle of the beam.

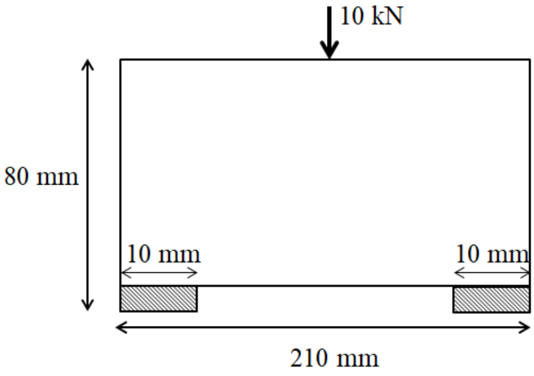

Figure 5.14: Simply supported beam geometry and boundary conditions

The proposed method is applied on the beam geometry after it is optimized by the SIMP method with a penalization factor of 1 and 3. The illustration and the properties of the cellular structures used are given in Figure 5.15 and Table 5.4, respectively. The resulting geometries are shown in Figure 5.16.

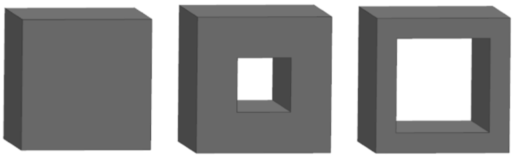

Figure 5.15: Cellular structures filling the design domain

Table 5.4: Properties of cellular structures

Properties	First	Second	Third
Outer dimensions (mm)	10x10	10x10	10x10
Inner dimensions (mm)	NA	4x4	7x7
Wall thickness (mm)	NA	3	1.5
Area ratio (%)	100	84	51
Density region	0.75 – 1	0.5 – 0.75	0.25-0.5

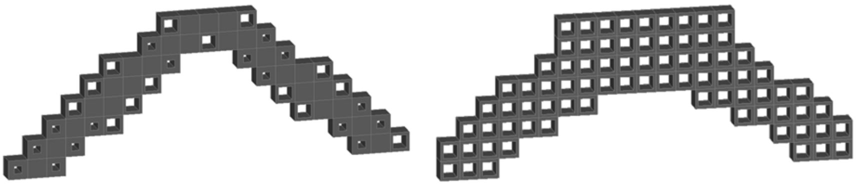

Figure 5.16: Simply supported beams remodelled with cellular structures after they are optimized by the SIMP method with a penalization factor of 1 (left) and 3 (right)

In order to see the effect of including intermediate densities in the final topology, the parts with cellular structures are compared with their SIMP optimized forms. The density limit for the geometries is set to 0.25, which means that the elements with densities larger than 0.25 are filled with material while the others are left empty. The geometries after the optimization is shown in Figure 5.17.

Figure 5.17: Simply supported beams after they are optimized by the SIMP method with a penalization factor of 1 (left) and 3 (right)

The proposed method is also compared with the beam geometry optimized by the genetic algorithm according to the boundary conditions shown in Figure 5.14 in the work of Jakiela et al. [42]. In this regard, the part shown in Figure 5.18 is generated in Rhino3D.

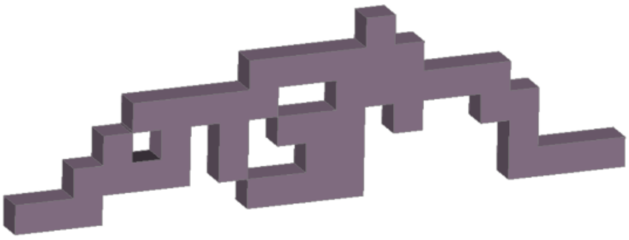

Figure 5.18: Simply supported beam after it is optimized by the genetic algorithm

5.2.2 Analysis

Structural analysis are applied on the beam geometries in Ansys software for comparison purposes. The parts are fixed from the cellular structures at the lower ends and a force is applied to the surface of the cellular structure at the top middle. PLA is assigned as the material for the parts. The boundary conditions for one of the parts and the material properties of the PLA are shown in Figure 5.19 and Table 5.2 respectively.

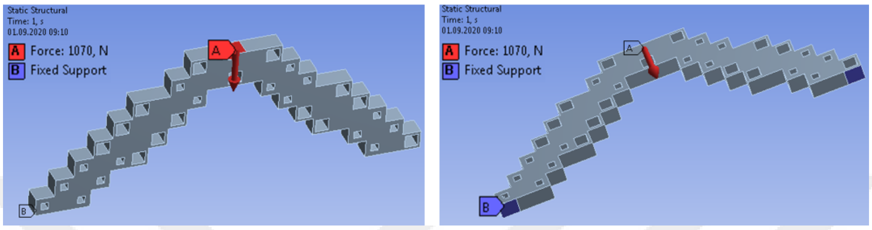

Figure 5.19: Boundary conditions for the simply supported beams. A shows the force application surface and B shows the surfaces set as fixed supports

The analysis problem is solved for the load carrying capacities of the parts and results are given in Table 5.5.

Table 5.5: Analysis results for the simply supported beams

Optimization Method	Weight (N)	Load at Yielding (N)	Load/Weight
Proposed Method with a Penalization Factor of 1	0.554	650	1172.7
SIMP with a Penalization Factor of 1	0.619	1095	1768.9
Proposed Method with a Penalization Factor of 3	0.49	435	887
SIMP with a Penalization Factor of 3	0.981	1025	1045.3
Genetic Algorithms	0.56	405	723.8

As it can be seen from the results, load-to-weight ratio of the proposed method is smaller than the results of the parts optimized by the SIMP method both for penalization factors of 1 and 3. However, the method is still advantageous in terms of the weight reduction it provides, especially for the parts optimized/re-modelled for a penalization factor of 3. While the proposed method provides a weight reduction of 50%, its load to weight ratio decreases by only 15.1% compared to the SIMP optimized part. These ratios change for the proposed method for a penalization factor of 1 as 10.5% reduction in weight and 33.7% loss in load-to-weight ratio. Therefore, the parts remodelled with the proposed method may be preferable for the applications where they satisfy the performance criteria.

When the whole results are evaluated, the performances of the methods can be listed in descending order as follows: SIMP method with a penalization factor of 1, proposed method with a penalization factor of 1, SIMP method with a penalization factor of 3, proposed method with a penalization factor of 3 and genetic algorithms. The graphics showing the safety regions of the parts under the loading specified in Table 5.5 is given in Figure 5.20.

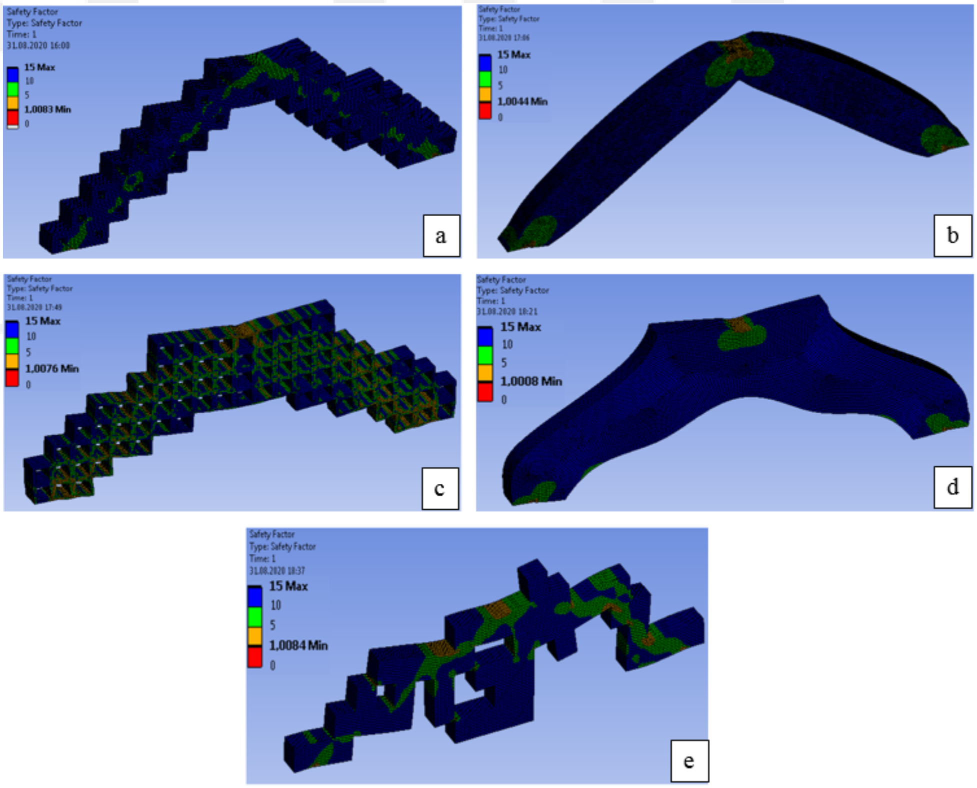

Figure 5.20: The safety regions of the geometries remodelled with the proposed method with a penalization factor of 1 (a) and 3 (c); optimized by the SIMP method with a penalization factor of 1 (b) and 3 (d) and the genetic algorithm (e)

5.3 Hanger

5.3.1 3D Model Generation

In this part, a hanger shaped geometry shown in Figure 5.21 is used for the optimization. The part is fixed from its lower edge and a unit force is applied on the edge in the right side as shown in the figure.

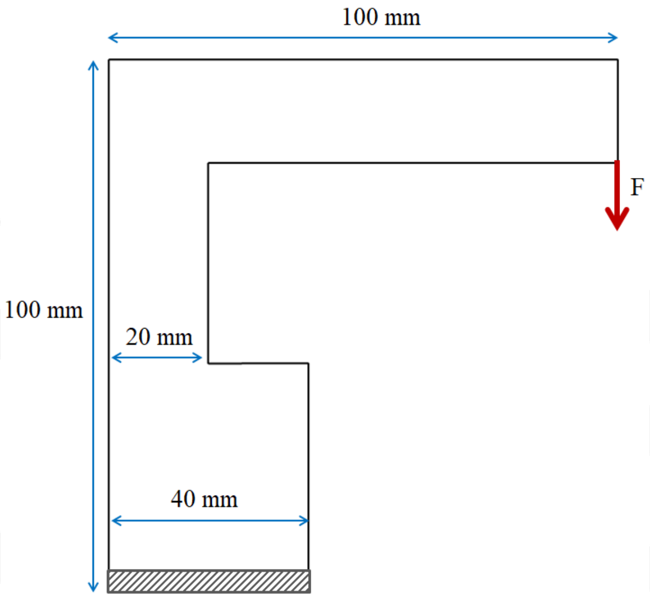

Figure 5.21: Hanger shaped geometry and boundary conditions

The proposed method is applied on the hanger geometry after it is optimized by the SIMP method with a penalization factor of 1 and 3. The cellular structures used are the same as in Figure 5.15. The resulting geometries are shown in Figure 5.22.

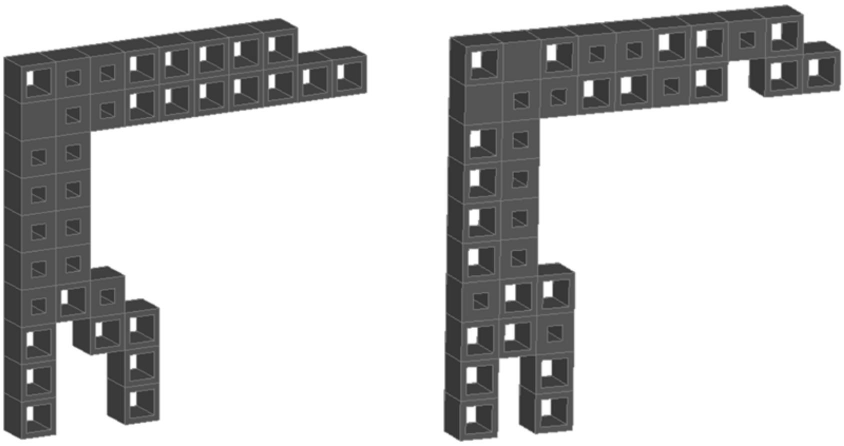

Figure 5.22: Hanger geometries remodelled with cellular structures after they are optimized by the SIMP method with a penalization factor of 1 (left) and 3 (right)

In order to see the effect of including intermediate densities in the final topology, the parts with cellular structures are compared with their SIMP optimized forms. The density limit for the geometries is set to 0.25 for the part optimized with a penalization factor of 1 and 3 respectively, which means that the elements with densities larger than 0.25 are filled with material while the others are left blank. The density limits are set in a way to have a manufacturable topology. The geometries after optimization is shown in Figure 5.23.

Figure 5.23: Hanger geometries after they are optimized by the SIMP method with a penalization factor of 1 (left) and 3 (right)

5.3.2 Analysis

Structural analysis are applied on the hanger geometries in Ansys software for comparison purposes. The parts are fixed from their bottom surfaces and a force is applied to the rightmost surface as shown in Figure 5.24.

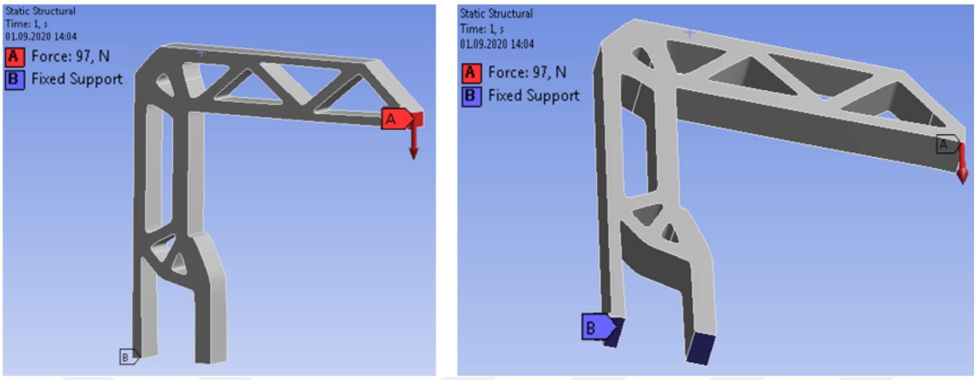

Figure 5.24: Boundary conditions defined for the hanger geometries. A shows the force application surface and B shows the surfaces given fixed support

The analysis problem is solved for the load carrying capacities of the parts and results are given in Table 5.6.

Table 5.6: Analysis results for the hanger geometries

Optimization Method	Weight (N)	Load at Yielding (N)	Load/Weight
Proposed Method with a Penalization Factor of 1	0.286	72	252.2
SIMP with a Penalization Factor of 1	0.281	23.7	84.5
Proposed Method with a Penalization Factor of 3	0.283	67	236.4
SIMP with a Penalization Factor of 3	0.256	97	379.4

It is seen that the performance of the proposed method for a penalization factor of 1 is much better than the SIMP optimized part. Although the remodelled part is heavier than the SIMP optimized part by 1.75%, it provides a 66.5% increase in the load carrying capacity of the part. However, the proposed method for a penalization factor of 3 increases the weight of the part by 9.5% and reduces the load-to-weight ratio by 37.7%, though, it can be used instead of the SIMP optimized part if it satisfies the application's performance criteria. When the whole results are evaluated, the performances of the methods can be listed in descending order as follows: SIMP method with a penalization factor of 3, proposed method with a penalization factor of 1, proposed method with a penalization factor of 3, SIMP method with a penalization factor of 1.

The graphics showing the safety regions of the parts under the loading specified in Table 5.6 is given in Figure 5.25.

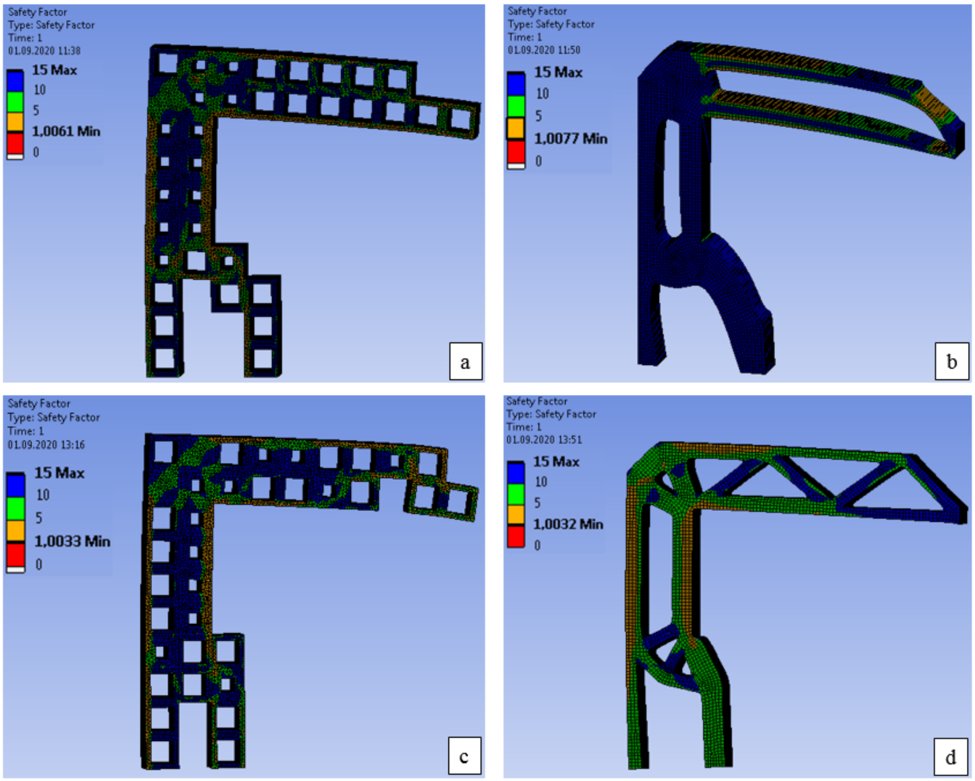

Figure 5.25: The safety regions of the geometries remodelled with the proposed method with a penalization factor of 1 (a) and 3 (c); optimized by the SIMP method with a penalization factor of 1 (b) and 3 (d).

CHAPTER 6

ANALYSIS AND TEST RESULTS FOR 3D GEOMETRIES

In this chapter, the performances of the geometries shown in Figure 6.1 are compared through the analysis and tests. The geometry on the left is the original topology, the middle one is the topology optimized in Ansys software, and the one on the right is the output of the proposed method. The performances of the geometries are measured in terms of their load carrying capacities.

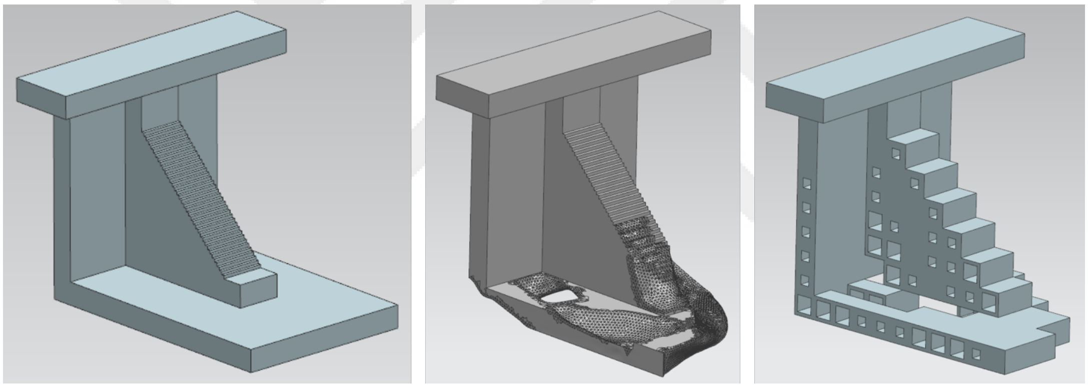

Figure 6.1: The original geometry (Left), the geometry optimized in Ansys (Middle) and the output of the proposed method (Right)

Additionally, the geometry remodelled with circular beams as a result of the proposed method, shown in Figure 6.2, is also compared with the geometries given in Figure 6.1 through analysis.

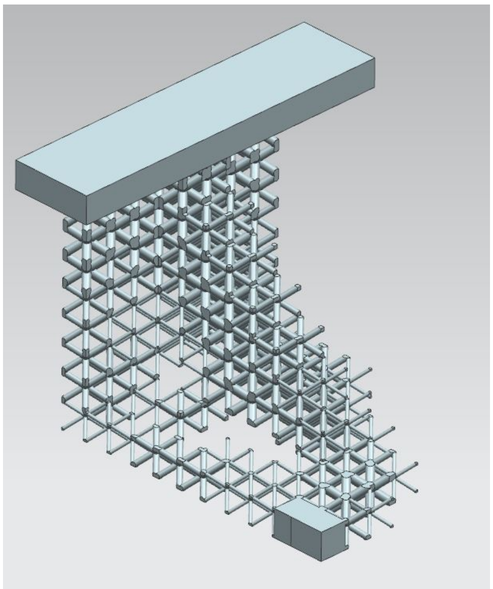

Figure 6.2: The output of the proposed method with circular beams

6.1 Analysis

Static structural analysis is applied on the geometries shown in Figure 6.1 and 6.2. Since the parts are intended to be fabricated with titanium powder (Ti6Al4V) on Arcam EBM machine and photopolymer resin through SLA process, the analysis are done for both materials. The properties of Ti6Al4V and the resin are given in Table 4.1 and 6.1 respectively.

Table 6.1: Properties of rigid resin

Properties	Rigid Resin
Ultimate Tensile Strength	75 MPa
Modulus of Elasticity	4.1 GPa
Elongation at Break	5.6%

The next step is to set the boundary conditions for each geometry. The boundary conditions are set by taking the fixture to be used in tests into consideration. The fixture is shown in Figure 6.3. The parts to be analyzed/tested are placed in the channel indicated with "A" on the fixture and fixed through the components shown as 1 and 2.

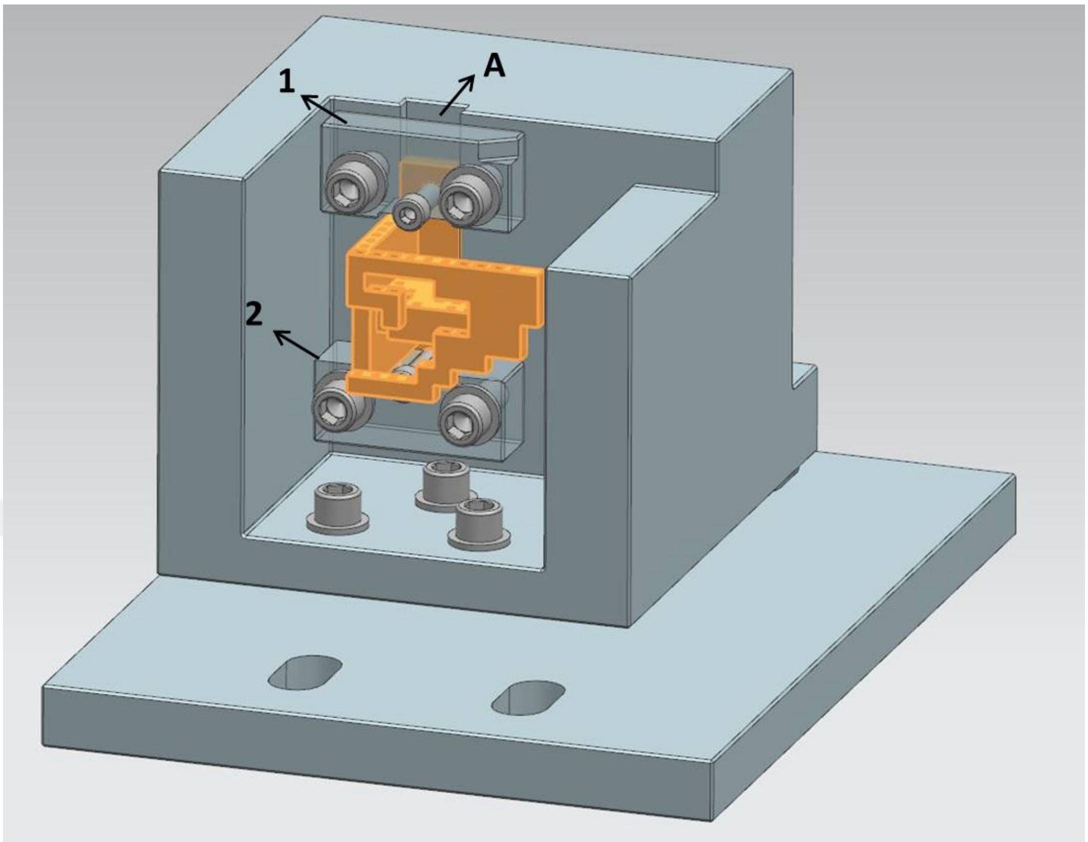

Figure 6.3: The fixture to be used in analysis and tests

The fixture is fixed through the holes on its bottom surface, and a load is applied to a $9mm$ by $9mm$ surface on the parts. The boundary conditions are set as the same for all geometries. An example is shown with the Ansys optimization output in Figure 6.4.

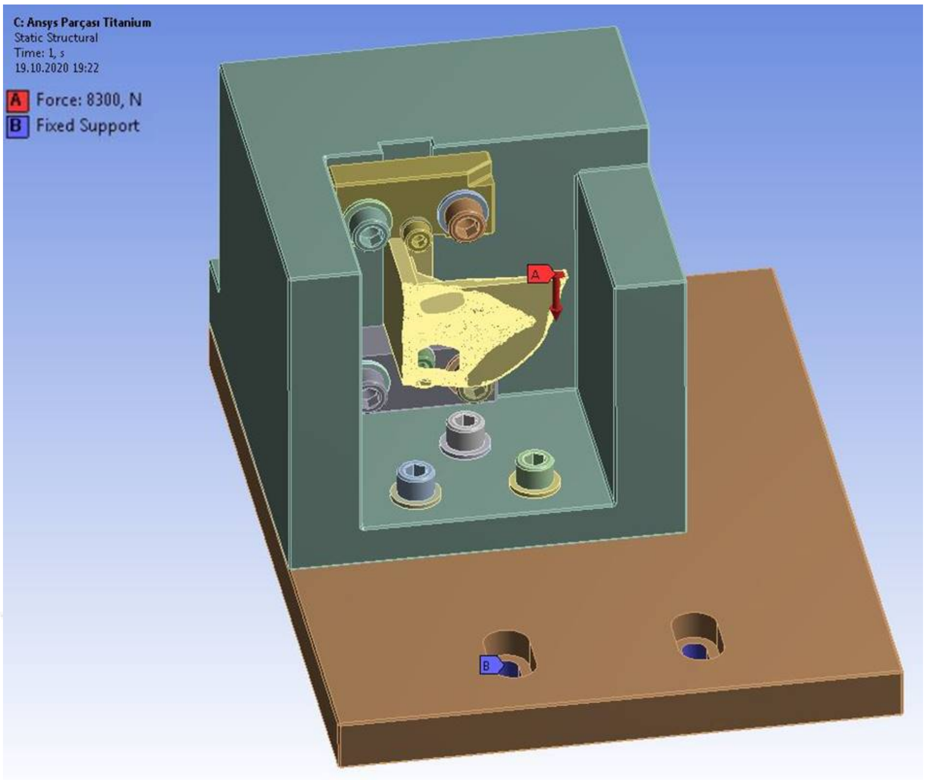

Figure 6.4: Boundary conditions for the geometry optimized in Ansys where the part is fixed from the surface marked as B and a load is applied to the surface marked as A

After the boundary conditions are set, the parts are meshed and the analysis problem is solved for their load carrying capacities. The analysis results for the case using Ti6Al4V are given in Table 6.2.

Table 6.2: Analysis results for 3D geometries made of Ti6Al4V material

Part	Weight (N)	Load at Yielding (N)	Load/Weight
The original geometry	3.80	8800	2313.3
The geometry optimized by Ansys	2.26	8300	3680.5
The geometry remodelled by the proposed method (Rectungular structures)	2.53	7300	2884.4
The geometry remodelled by the proposed method (Circular beam structures)	1.11	145	130.1

As it can be seen from the table, the output of the proposed method with circular beams has the lowest performance among others. When the other three outputs are compared, both optimization methods show better performances than the original part. While the optimization performed in Ansys and the proposed method provide a weight reduction of 40.5% and 33.4% respectively, the performance of the original part is increased by 59.1% and 24.6%.

When the performances of the proposed method and the Ansys optimization result are compared, it is seen that the proposed method shows a lower performance than the optimization output with a higher weight. However, it makes the main contribution in the reduction of operations performed after the optimization to prepare the part for 3D printing and the generation of manufacturable output as explained in the following section.

The graphics showing the safety regions of the parts under the loading specified in Table 6.2 is given in Figure 6.5. The color-bar on the left side of the figures shows the safety degree of the material. The regions experiencing large stresses have a safety degree closer to 1. If the safety degree is smaller than 1, then yielding occurs in the corresponding region.

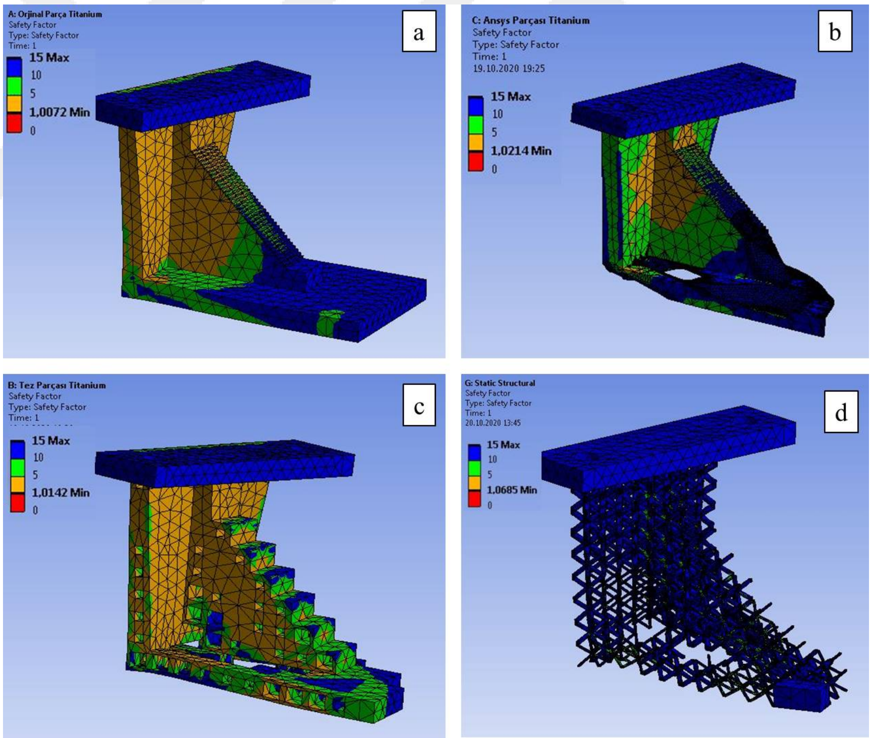

Figure 6.5: The safety regions of the original geometry (a), the output of the optimization done in Ansys (b), the result of the proposed method for rectangular structures (c) and the result of the proposed method for circular beam structures (d) when Ti6Al4V is used as the material

The analysis results for the case using rigid resin are given in Table 6.3.

Table 6.3: Analysis results for 3D geometries (Rigid resin)

Part	Weight (N)	Load at Yielding (N)	Load/Weight
The original geometry	0.99	690	692.7
The geometry optimized by Ansys	0.59	650	1100.7
The geometry remodelled by the proposed method (Rectungular structures)	0.66	550	829.9
The geometry remodelled by the proposed method (Circular beam structures)	0.29	12	41.4

As it can be seen from the table, the output of the proposed method with circular beams has the lowest performance among others. When the other three outputs are compared, both optimization methods show better performances than the original part. While the Ansys output and the proposed method provides a weight reduction of 40.4% and 33.3% respectively, the performance of the original part is increased by 58.9% and 19.8%. The graphics showing the safety regions of the parts under the loading specified in Table 6.2 is given in Figure 6.6.

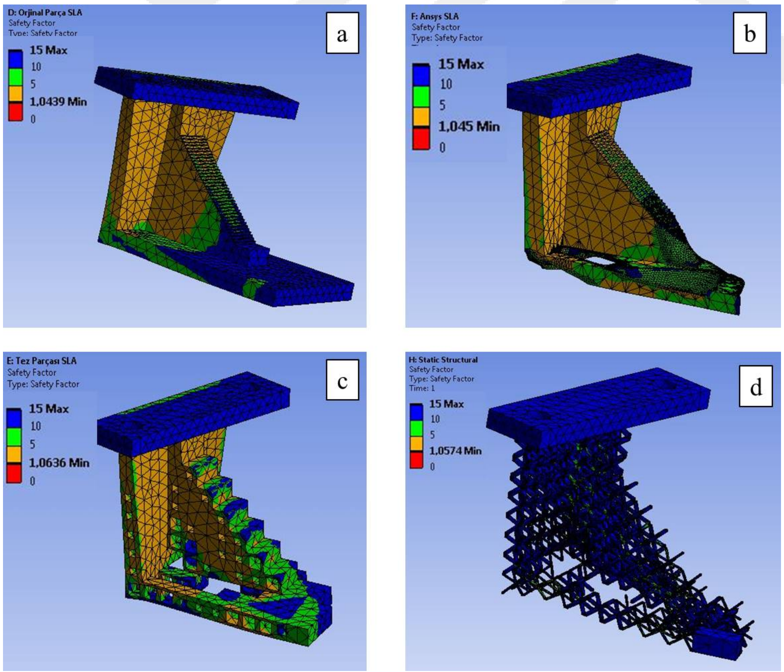

Figure 6.6: The safety regions of the original geometry (a), the output of the optimization done in Ansys (b), the result of the proposed method for rectangular structures (c) and the result of the proposed method for circular beam structures (d) when rigid resin is used as the material

6.2 Fabrication of the Parts

The geometries shown in Figure 6.1 are fabricated to be used in tests for the validation of analysis results. In order to check the powder/resin-free feature of the proposed method, a powder based machine, Arcam EBM and SLA based machine are used as the 3D printers.

One of the main contributions of the proposed method is that it generates a ready to print output while the Ansys method requires several steps to make the optimization output suitable for fabrication. The preparation steps of the Ansys optimization output is given in the following section.

6.2.1 Preparation of the Ansys Optimization Output for Fabrication

After the topology optimization is done in Ansys, the output is conveyed to SpaceClaim, which is a 3D modelling CAD software compatible with Ansys. The user interface of SpaceClaim is shown in Figure 6.7.

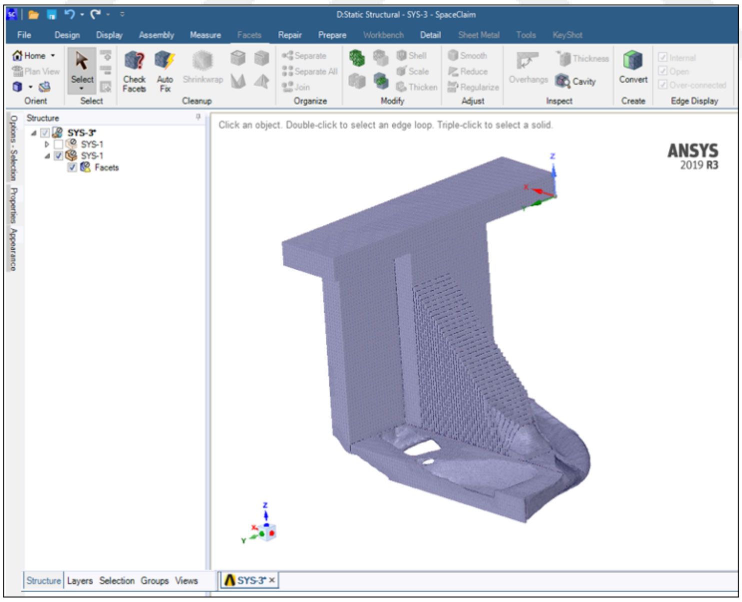

D:Static Structural - SYS-3 - SpaceClaim

Click an object. Double-click to select an edge loop. Triple-click to select a solid.

Figure 6.7: User interface of SpaceClaim

The first step is to check the facets of the geometry to see if there are any errors detected in the mesh. After clicking on the button $CheckFacets$, the errors are listed as shown in Figure 6.8.

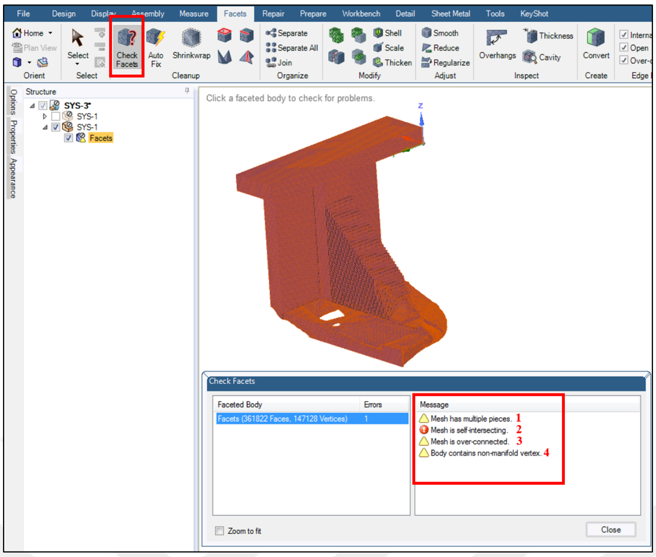

Click a faceted body to check for problems.

Check Facets

Faceted Body	Errors
Facets (361822 Faces, 147128 Vertices)	1

Message
⚠ Mesh has multiple pieces. 1
❗ Mesh is self-intersecting. 2
⚠ Mesh is over-connected. 3
⚠ Body contains non-manifold vertex. 4

☐ Zoom to fit

Close

Figure 6.8: Errors related to the meshes are listed

The next step is to fix the errors. The button marked as $AutoFix$ is clicked and then the facets are checked again to see if there remains any errors related to the meshes, which should be fixed manually. As it can be seen from Figure 6.9, two of the errors, 2 and 3, are fixed while the others are still present.

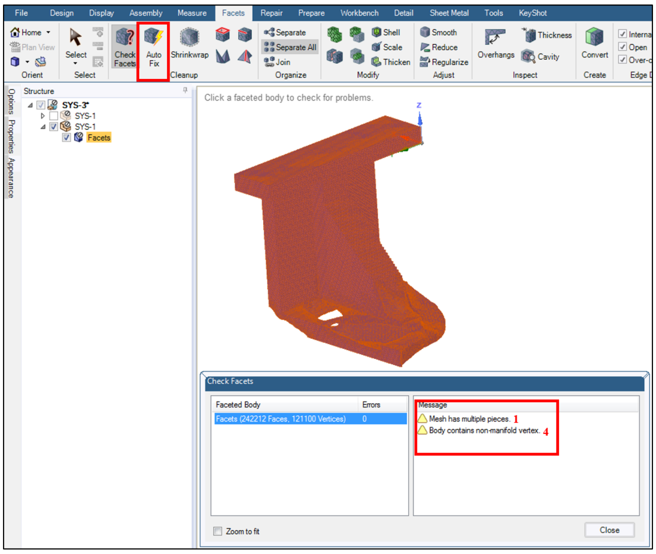

Click a faceted body to check for problems.

Check Facets

Faceted Body	Errors
Facets (242212 Faces, 121100 Vertices)	0

Message
⚠ Mesh has multiple pieces. 1
⚠ Body contains non-manifold vertex. 4

☐ Zoom to fit

Close

Figure 6.9: List of errors after $Autofix$ tool is used on the facets

In order to repair the geometry further, $Shrinkwrap$ tool shown in Figure 6.10 is used with a gap size of $1mm$. It generates a high quality faceted model by detecting the facets with coarser sizes and resizing them according to the value set as the gap size.

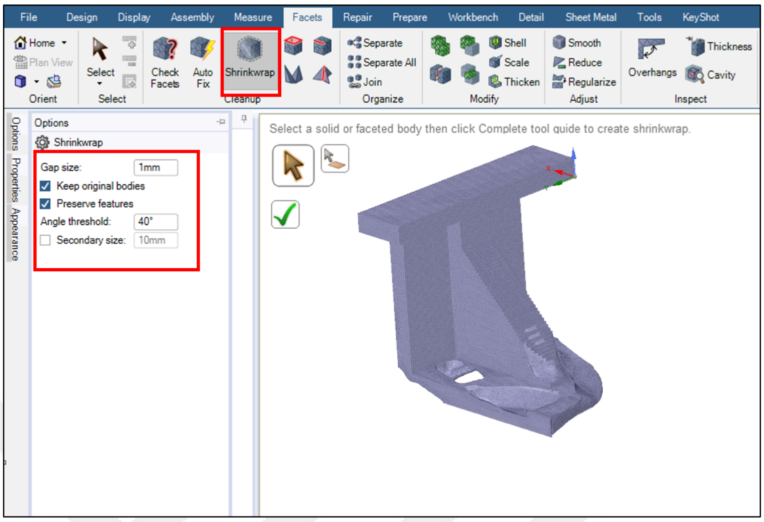

Select a solid or faceted body then click Complete tool guide to create shrinkwrap.

Gap size: 1mm
☑ Keep original bodies
☑ Preserve features
Angle threshold: 40°
☐ Secondary size: 10mm

Figure 6.10: Application of the $Shrinkwrap$ operation on the facets

After the $Shrinkwrap$ operation, the facets are smoothed by using the $Smooth$ tool shown in Figure 6.11, and the geometry is checked again by using the $CheckFacets$ tool. It is seen that there remains no problems related to the geometry as shown in the following figure.

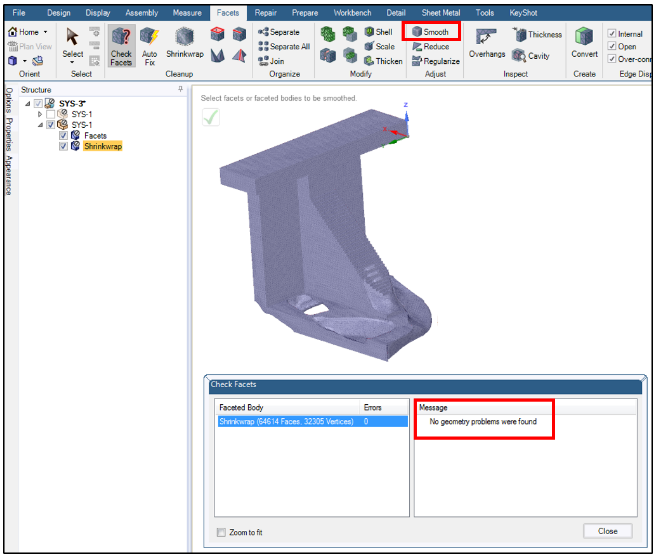

Select facets or faceted bodies to be smoothed.

Faceted Body	Errors
Shrinkwrap (64614 Faces, 32305 Vertices)	0

Message

No geometry problems were found

Figure 6.11: Application of the $Smooth$ tool and checking the geometry against errors

The next step is to convert the error-free facets to a solid body. It is done by right-clicking the $Shrinkwrap$ on the Structure tree and selecting the $Converttosolid$ and $Mergefaces$ options respectively as shown in Figure 6.12.

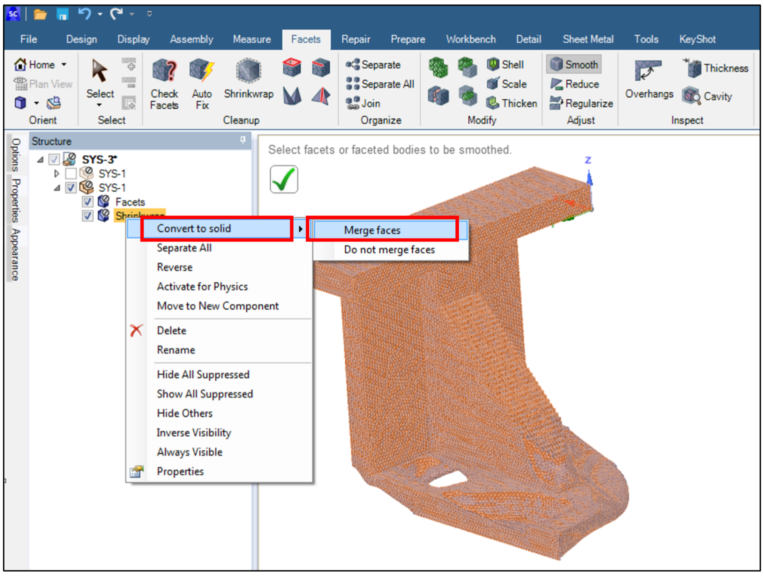

Select facets or faceted bodies to be smoothed.

Figure 6.12: Converting the facets to a solid body

In order to repair the solid body, the tools under the *Repair* section can be used according to the needs. In this case, it is seen that there are some extra edges on the geometry as shown in Figure 6.13.

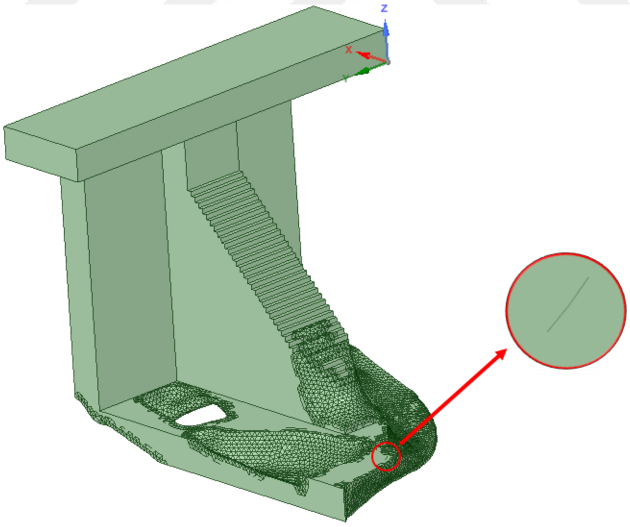

Figure 6.13: Extra edges on the solid body

In order to detect all the extra edges and delete them, the $ExtraEdges$ tool under the $Repair$ section is used. There are total of 52 extra edges as shown in Figure 6.14. After the part is selected and the check mark shown in the figure is clicked, the extra edges are deleted from the geometry.

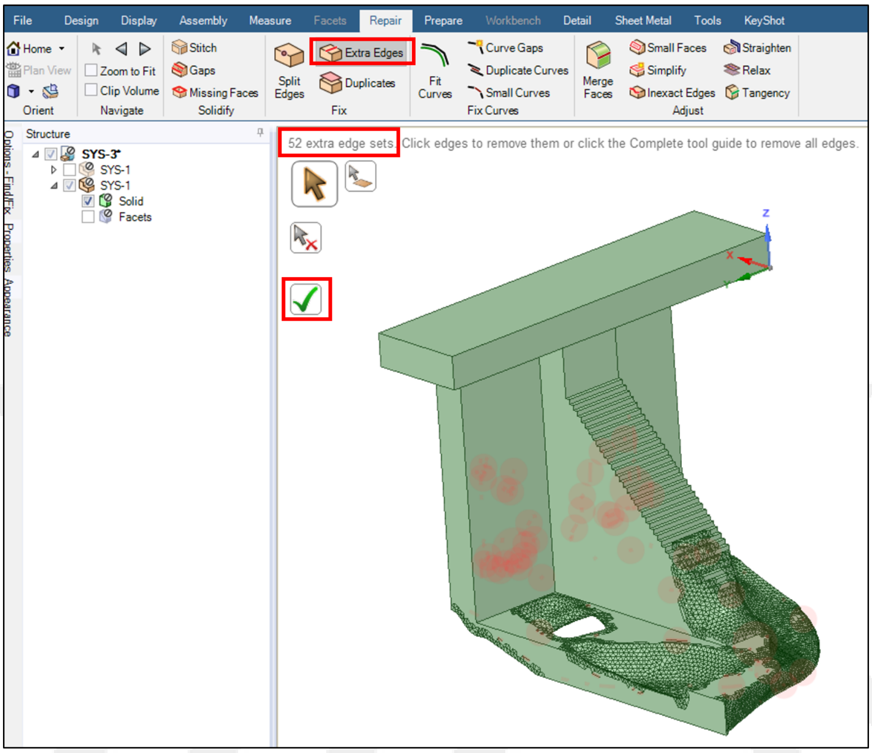

52 extra edge sets Click edges to remove them or click the Complete tool guide to remove all edges.

Figure 6.14: Application of Extra Edges tool to remove extra edges

Finally, the geometry is checked by right clicking on the $Solid$ under the Structure tree and selecting the $CheckGeometry$ button. Since there are not any remaining errors related to this part as shown in Figure 6.15, it can be saved as an STL file to be used for fabrication. It is important to emphasize that different geometries may require further or less operations to be prepared for fabrication.

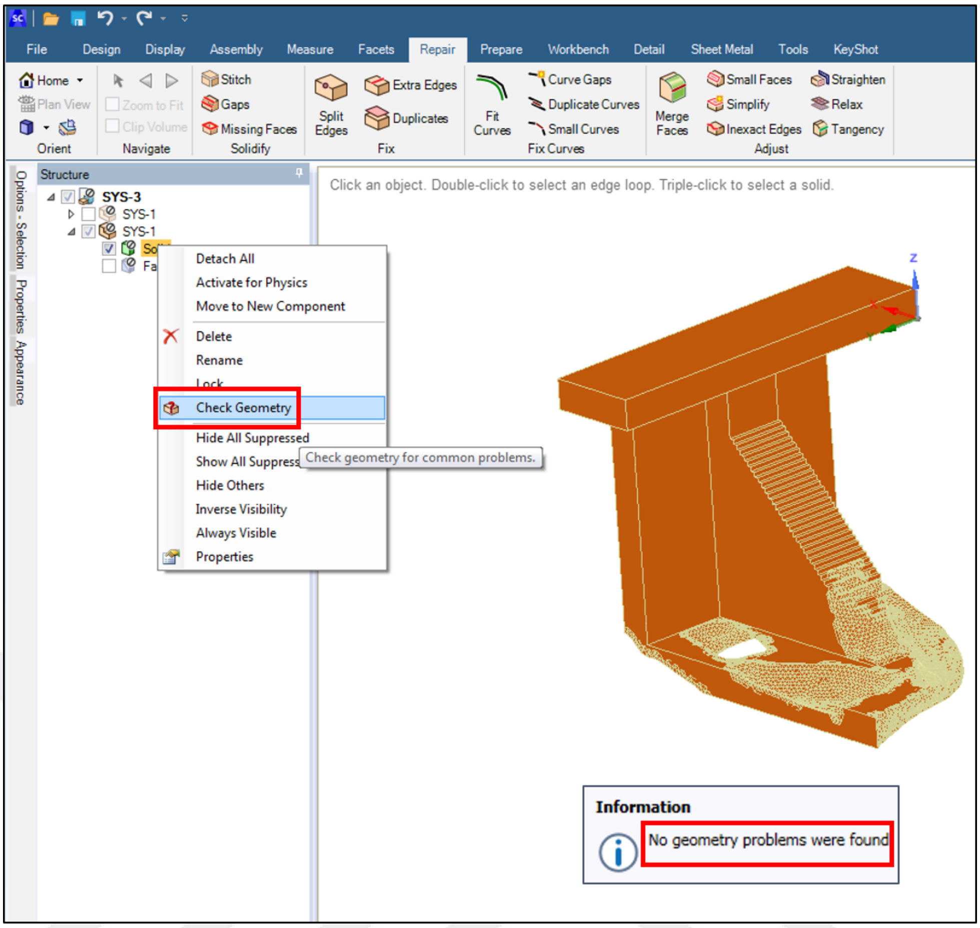

Click an object. Double-click to select an edge loop. Triple-click to select a solid.

Check geometry for common problems.

Information

No geometry problems were found

Figure 6.15: Checking geometry against errors

6.2.2 Fabrication

After the STL files are prepared for each geometry as shown in Figure 6.1, they are transferred to Materialise Magics, which is a software compatible with Arcam EBM machine used for editing the STL files and preparing the build platform [Materialise.com]. There, the support structures are generated and the way the parts are placed on the build platform is adjusted, and then the fabrication is started. The placement of the parts in the platform and the support structures are shown in Figure 6.16.

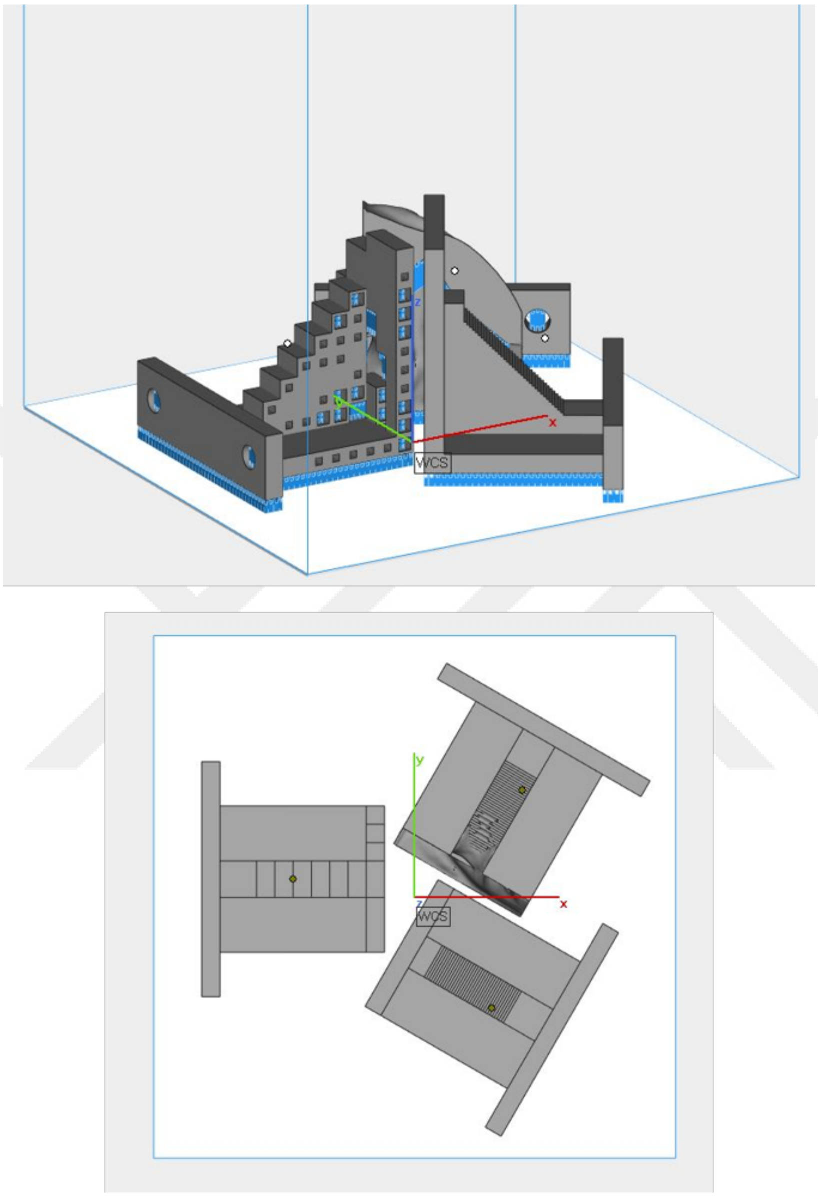

Figure 6.16: Isometric view of the parts in the build platform and support structures (top) and their view from top (bottom)

The fabrication lasts for 18.5 hours. After the process is completed, the parts are removed from the machine in a block of powder. The powder block just before the removal is shown in Figure 6.17.

Figure 6.17: Block of powder containing the fabricated parts

Then, the excess powder on the parts and the powder accumulated inside the parts are removed in a sand blasting machine. A photo taken during the sand blasting process is given in Figure 6.18.

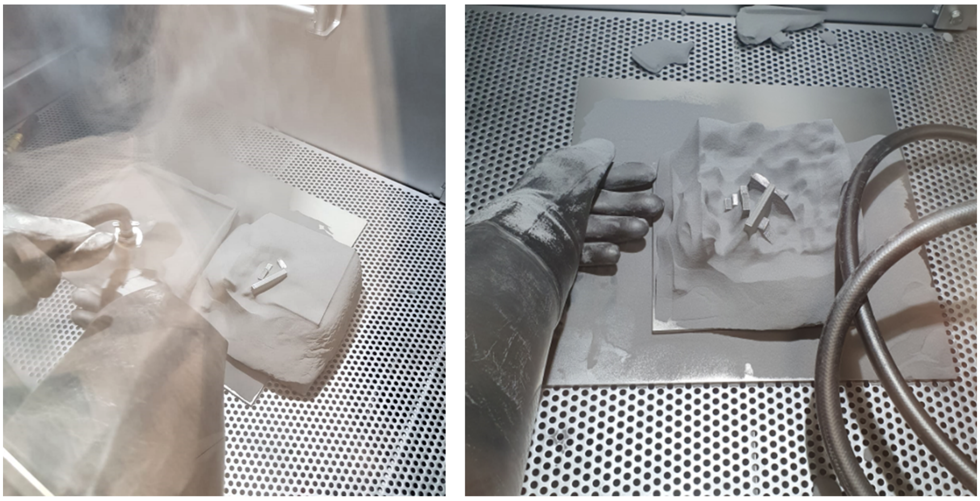

Figure 6.18: Sand blasting process

Finally, the support structures of the parts are broken with the help of a hammer. The images of the parts in their final form can be seen in Figure 6.19, Figure 6.20 and Figure 6.21.

Figure 6.19: Fabricated original topology

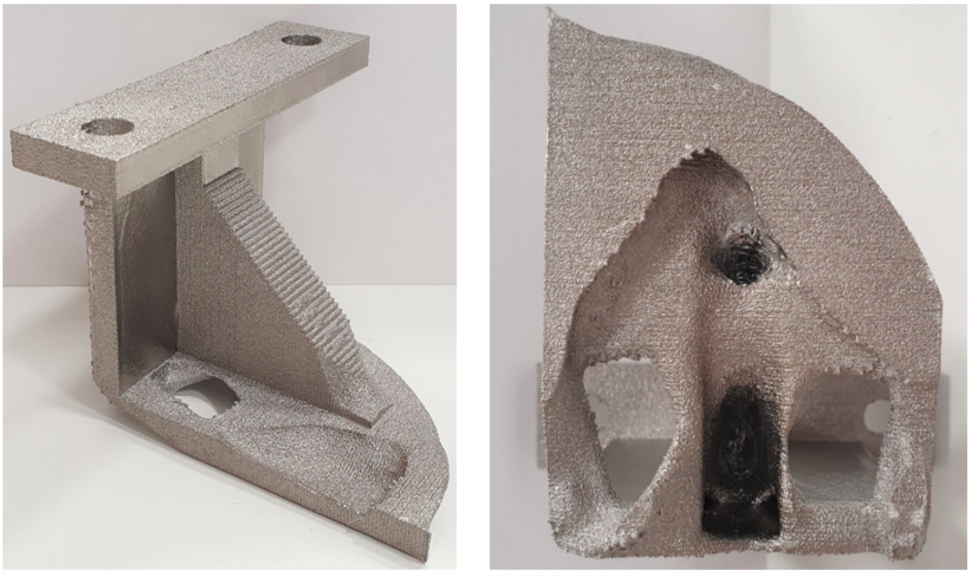

Figure 6.20: Fabricated Ansys optimization output

Figure 6.21: Fabricated proposed method output

Additionally, the parts are fabricated through SLA process by using rigid resin. The fabrication outputs are shown in Figure 6.22.

Figure 6.22: SLA fabricated proposed method output

6.3 Tests

The fabricated parts are tested with Instron 8872 Fatigue Testing Machine. Each part is fixed by the test rig and a force is applied as shown in Figure 6.23. In order to provide the proper load application interface with the surface on the specimen, an apparatus is fabricated to be connected to the cross-head. As the cross-head moves downward, magnitude of the applied force is increased until the part is broken. The speed of the cross-head is set as $5mm/s$ for all the tests.

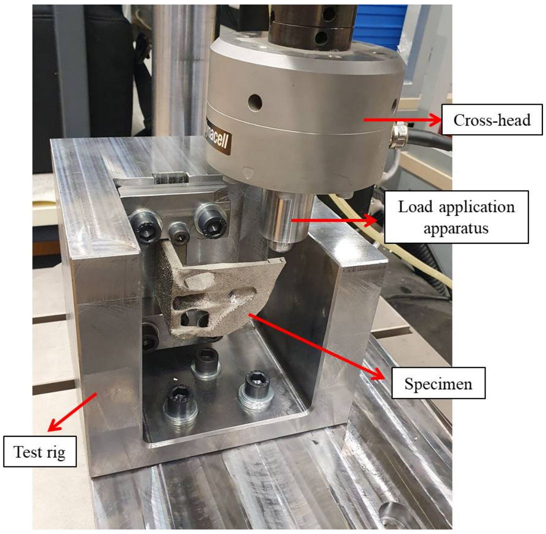

Figure 6.23: Test setup with an EBM fabricated specimen

An example test setup with an SLA output is also shown in Figure 6.24.

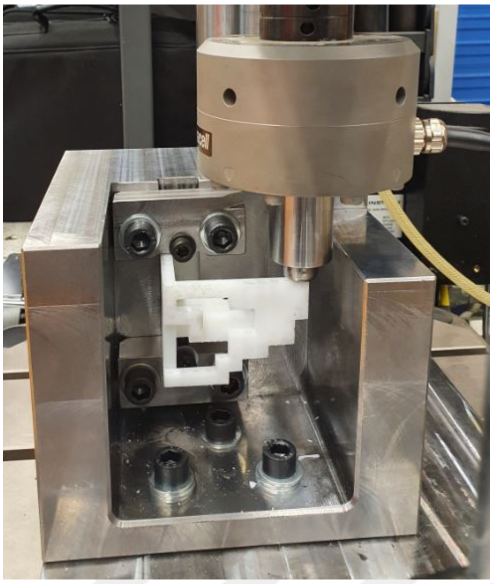

Figure 6.24: Test setup with an SLA fabricated specimen

The images of the deformed parts are shown in Figure 6.25, 6.26, 6.27. Since the SLA outputs are broken into small pieces, only the EBM outputs are shown for demonstration purposes.

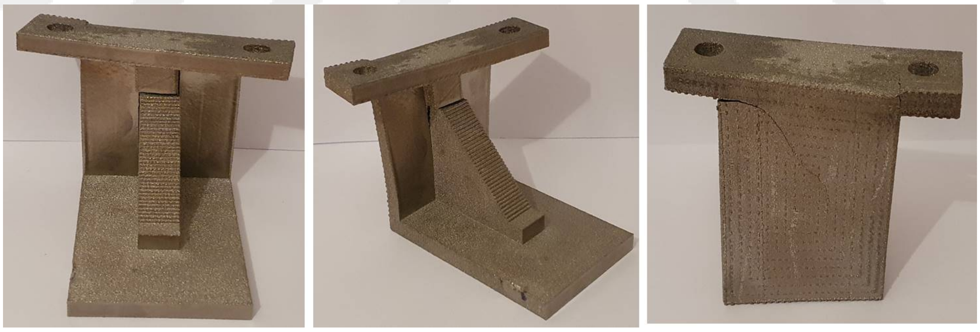

Figure 6.25: Deformed original geometry

Figure 6.26: Deformed output of the proposed method

Figure 6.27: Deformed output of Ansys optimization

The load-displacement curves obtained in the tests for the EBM outputs are shown in Figure 6.28.

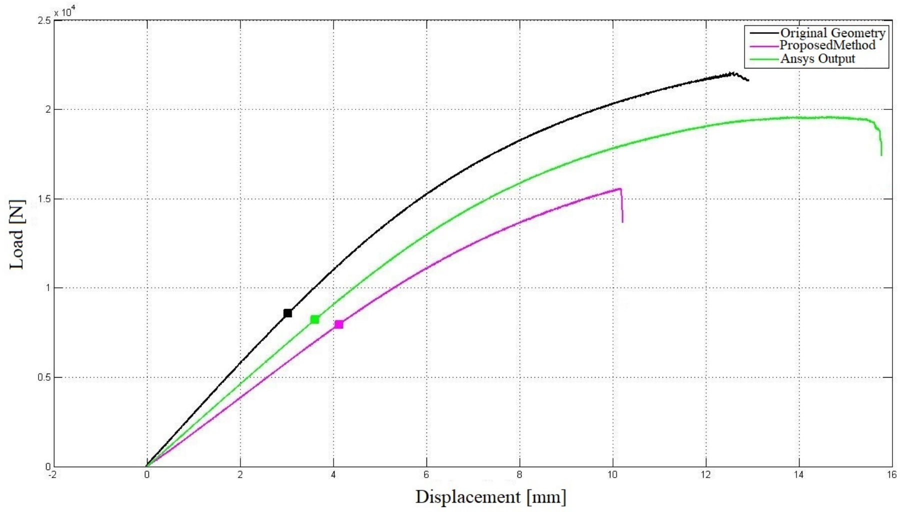

Figure 6.28: Load vs. displacement graph for EBM outputs

The yielding points of the parts are marked on the graph. These points are determined by fitting a curve to the linear portion of the graph and finding the point where the fitted curve deviates from the main curve. The determination of yield point is shown on the load-displacement curve of the proposed method output in Figure 6.29 as an example.

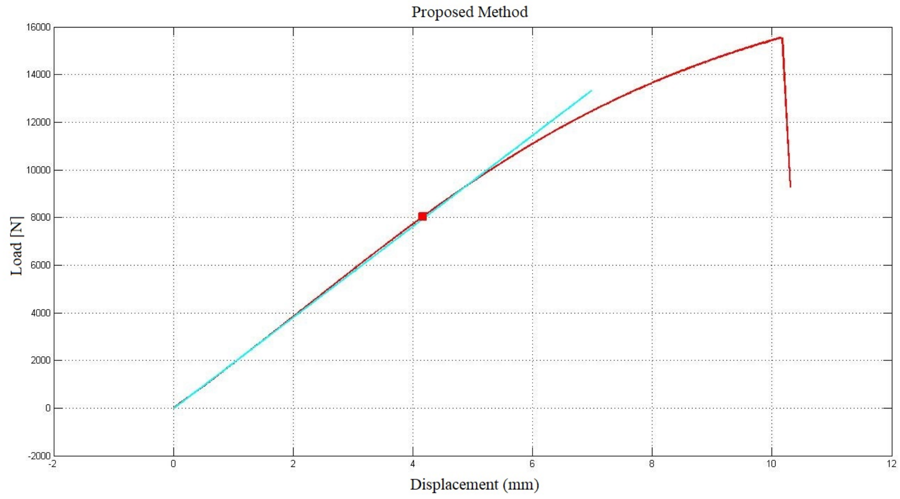

Figure 6.29: Determination of yield point for the proposed method's output

The results of the tests are summarized in Table 6.4.

Table 6.4: Test results for 3D geometries made of Ti6Al4V

Part	Weight (N)	Load at Yielding (N)	Load/Weight
The original geometry	3.70	8563	2315.3
The geometry optimized by Ansys	2.25	8231	3663.94
The geometry remodelled by the proposed method	2.52	8031	3185.4

It is seen that the magnitude of the load at yielding is similar for the parts. When load to weight ratios are compared, both optimization methods show a better performance than the original part. While the optimization performed in Ansys and the proposed method provides a weight reduction of 39.1% and 31.9% respectively, the performance of the original part is increased by 58.2% and 37.6%.

The load-displacement curves obtained in the tests for the SLA outputs are shown in Figure 6.30.

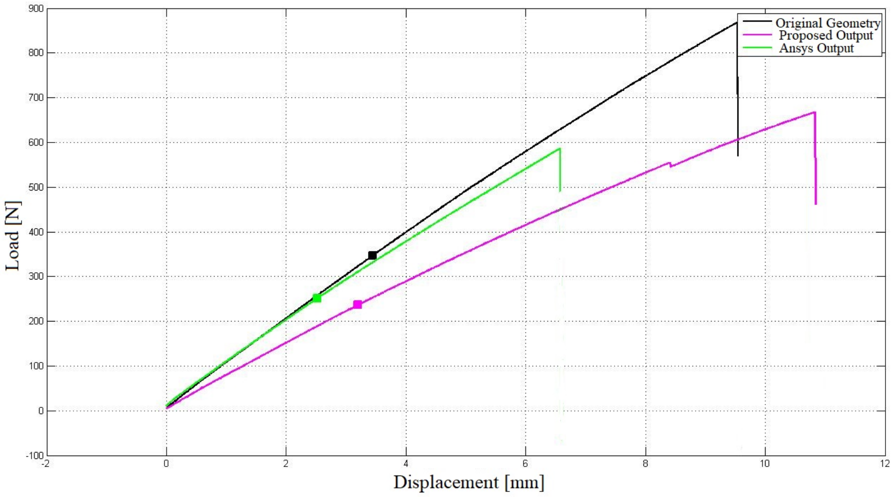

Figure 6.30: Load vs. displacement graph for SLA outputs

The results of the tests are summarized in Table 6.5.

Table 6.5: Test results for 3D geometries made of rigid resin

Part	Weight (N)	Load at Yielding (N)	Load/Weight
The original geometry	1.1	347	315.45
The geometry optimized by Ansys	0.6	251.3	418.83
The geometry remodelled by the proposed method	0.67	236.1	352.39

It is seen that both optimization methods show a better performance than the original part. While the optimization performed in Ansys and the proposed method provides a weight reduction of 45.5% and 39.1% respectively, the performance of the original part is increased by 32.7% and 11.7%.

CHAPTER 7

CONCLUSION

In this thesis, a method has been proposed to enhance the performances of the parts optimized by the SIMP topology optimization method. The proposed method utilizes the intermediate density regions in contrast to many other optimization techniques, which intend to generate topologies consisting of elements with densities either 1 or 0. This method takes the density output of the SIMP optimization, which is obtained for each finite element composing the geometry, and then fills the entire design domain with rectangular cellular structures having user-defined dimensions. The cellular structures are categorized according to the density ranges to which the average density of the finite elements covered by the associated structure belongs. While the cellular structures fully filled with material are used for the regions whose density belongs to the range of high density values, for example, the cellular structures with rectangular holes in the middle are used for regions belonging to density ranges with lower values. The size of the holes are set by multiplying the outer dimensions of the cellular structure with a user-defined scaling factor. The scaling factor, and consequently the hole size, increases as the density range of the region to which the cellular structure belongs decreases.

The proposed method is applicable to both 2D and 3D geometries. A cantilever beam, a simply supported beam and a hanger geometry optimized by the SIMP with penalization factors of 1 and 3 are used as examples for 2D applications. A 3D geometry, which is originally used for connecting a moving body to a slip-ring, is used as an example for 3D applications after it is optimized by a density-based optimization method in Ansys. In order to see the effect of utilizing intermediate density regions, the performances of the 2D and 3D parts are compared with their SIMP and Ansys optimized forms respectively, according to their load carrying capacities through analysis and tests.

It is seen through the test and analysis that the method works best for the SIMP optimized cantilever and hanger geometry when the penalization factor is set to 1. Considering the cantilever case, the weight is reduced by 27.4 % while providing a slightly increased performance, which is about 1.5 %. The method makes its greatest contribution on the hanger geometry with a performance gain of 66.5 %, while increasing the part's weight by 1.75 %.

The advantage of the method is also observed for the SIMP optimized simply supported geometry when the penalization factor is set to 3. It provides a weight reduction of 50 % while decreasing the performance by about 15 %. The result may be advantageous for the applications requiring a light-weight design, if it satisfies the associated performance criteria.

Another contribution of the proposed method is that it generates a fully connected topology by using one of the two alternative methods presented in Chapter 3. In contrast to the majority of techniques in the literature which delete the unconnected elements directly, in this method, only the unconnected elements that are away from a predefined distance from the topology are deleted while the others are connected to the topology by adding new cellular structures.

The performances of the proposed method for 3D geometries made of Ti6Al4V and rigid resin are much better than the original geometry. The load carrying capacity of the proposed method for the parts made of Ti6Al4V is reduced by 13% and the weight is increased by 12% when compared to the part optimized in Ansys. Similarly, for the geometries made of rigid resin, the load carrying capacity of the proposed method is reduced by 15.8% and the weight is increased by 11.7%. Although the Ansys-optimized parts have a better performance, the result of the proposed method may still be advantageous in terms of other benefits it promises.

Firstly, it provides a topology composing of fully connected elements as in the 2D applications. If the unconnected element is within a pre-described distance to the topology, it is connected to the topology by adding new cells to its neighbors. In other case, it is deleted.

Secondly, it offers a solution for a problem common to powder/resin based additive manufacturing processes. Excess powder/resin remains inside the internal cavities of the fabricated geometry, if there is not a channel that can be used for the removal of powder/resin by connecting the cavities to the outside. The proposed method ensures the removal of the excess powder/resin from the geometry by opening channels to the required places inside the part automatically.

Finally, it generates ready to fabricate models as opposed to the optimization output obtained in Ansys. The Ansys optimization output goes through several operations before printing as explained in Chapter 6, Section 6.2.1. Therefore, overall processing time can be decreased by using the proposed method.

One point to emphasize is that the proposed method is only applicable to the 3D geometries that do not have any round or angled features. In order to include these features in the topology, post-processing is required. As a future work, the scope of the proposed method can be expanded in a way that it can be also used for the parts with round or angled features.

REFERENCES

[1] I. Gibson, D. W. Rosen, B. Stucker, *et al.*, *Additive manufacturing technologies*, vol. 17. Springer, 2014.

[2] W. Gao, Y. Zhang, D. Ramanujan, K. Ramani, Y. Chen, C. B. Williams, C. C. Wang, Y. C. Shin, S. Zhang, and P. D. Zavattieri, "The status, challenges, and future of additive manufacturing in engineering," *Computer-Aided Design*, vol. 69, pp. 65–89, 2015.

[3] K. V. Wong and A. Hernandez, "A review of additive manufacturing," *International scholarly research notices*, vol. 2012, 2012.

[4] N. Guo and M. C. Leu, "Additive manufacturing: technology, applications and research needs," *Frontiers of Mechanical Engineering*, vol. 8, no. 3, pp. 215–243, 2013.

[5] H. Bikas, P. Stavropoulos, and G. Chryssolouris, "Additive manufacturing methods and modelling approaches: a critical review," *The International Journal of Advanced Manufacturing Technology*, vol. 83, no. 1-4, pp. 389–405, 2016.

[6] S. H. Huang, P. Liu, A. Mokasdar, and L. Hou, "Additive manufacturing and its societal impact: a literature review," *The International Journal of Advanced Manufacturing Technology*, vol. 67, no. 5-8, pp. 1191–1203, 2013.

[7] S. Daneshmand, R. Adelnia, and S. Aghanajafi, "Design and production of wind tunnel testing models with selective laser sintering technology using glass-reinforced nylon," in *Materials Science Forum*, vol. 532, pp. 653–656, Trans Tech Publ, 2006.

[8] Deloitte, "Challenges of additive manufacturing." Available at `https://www2.deloitte.com/content/dam/Deloitte/de/Documents/operations/Deloitte_Challenges_of_Additive_Manufacturing.pdf` (2020/09/07).

[9] S. K. Moon, Y. E. Tan, J. Hwang, and Y.-J. Yoon, "Application of 3d printing technology for designing light-weight unmanned aerial vehicle wing structures," *International Journal of Precision Engineering and Manufacturing-Green Technology*, vol. 1, no. 3, pp. 223–228, 2014.

[10] H. Wadley, "Ultralight lattice-based materials for multifunctional space structures." Available at `https://www.nasa.gov/sites/default/files/atoms/files/haydn_quad.pdf` (2020/09/07).

[11] T. A. Schaedler, C. J. Ro, A. E. Sorensen, Z. Eckel, S. S. Yang, W. B. Carter, and A. J. Jacobsen, "Designing metallic microlattices for energy absorber applications," *Advanced Engineering Materials*, vol. 16, no. 3, pp. 276–283, 2014.

[12] Z. Ozdemir, E. Hernandez-Nava, A. Tyas, J. A. Warren, S. D. Fay, R. Goodall, I. Todd, and H. Askes, "Energy absorption in lattice structures in dynamics: Experiments," *International Journal of Impact Engineering*, vol. 89, pp. 49–61, 2016.

[13] V. Kumar, G. Manogharan, and D. R. Cormier, "Design of periodic cellular structures for heat exchanger applications," in *20th Annual International Solid Freeform Fabrication Symposium*, 2009.

[14] M. Pelanconi, M. Barbato, S. Zavattoni, G. Vignoles, and A. Ortona, "Thermal design, optimization and additive manufacturing of ceramic regular structures to maximize the radiative heat transfer," *Materials & Design*, vol. 163, p. 107539, 2019.

[15] C. Emmelmann, P. Scheinemann, M. Munsch, and V. Seyda, "Laser additive manufacturing of modified implant surfaces with osseointegrative characteristics," *Physics Procedia*, vol. 12, pp. 375–384, 2011.

[16] R. Huiskes, H. Weinans, and B. Van Rietbergen, "The relationship between stress shielding and bone resorption around total hip stems and the effects of flexible materials," *Clinical orthopaedics and related research*, pp. 124–134, 1992.

[17] Y. Tang, G. Dong, Q. Zhou, and Y. F. Zhao, "Lattice structure design and op-

timization with additive manufacturing constraints," *IEEE Transactions on Automation Science and Engineering*, vol. 15, no. 4, pp. 1546–1562, 2017.

[18] W. Tao and M. C. Leu, "Design of lattice structure for additive manufacturing," in *2016 International Symposium on Flexible Automation (ISFA)*, pp. 325–332, IEEE, 2016.

[19] D. Brackett, I. Ashcroft, and R. Hague, "Topology optimization for additive manufacturing," in *Proceedings of the solid freeform fabrication symposium, Austin, TX*, vol. 1, pp. 348–362, 2011.

[20] T. Zegard and G. H. Paulino, "Bridging topology optimization and additive manufacturing," *Structural and Multidisciplinary Optimization*, vol. 53, no. 1, pp. 175–192, 2016.

[21] M. Langelaar, "An additive manufacturing filter for topology optimization of print-ready designs," *Structural and multidisciplinary optimization*, vol. 55, no. 3, pp. 871–883, 2017.

[22] F. I. for Laser Technology, "Topology-optimized wheel knuckle with internal graded lattice structure." Available at `https://t.ly/G2M0` (2020/09/07).

[23] D. Herzog, V. Seyda, E. Wycisk, and C. Emmelmann, "Additive manufacturing of metals," *Acta Materialia*, vol. 117, pp. 371–392, 2016.

[24] A. LarsKrog, "Application of topology, sizingandshapeoptimizationmethodsto optimal design of aircraft components," *Retrievedfrom Altair productdesign*, 2011.

[25] T. Gao, L. Qiu, and W. Zhang, "Topology optimization of continuum structures subjected to the variance constraint of reaction forces," *Structural and Multidisciplinary Optimization*, vol. 56, no. 4, pp. 755–765, 2017.

[26] J.-H. Zhu, Y. Li, W.-H. Zhang, and J. Hou, "Shape preserving design with structural topology optimization," *Structural and Multidisciplinary Optimization*, vol. 53, no. 4, pp. 893–906, 2016.

[27] M. P. Bendsoe and N. Kikuchi, "Generating optimal topologies in structural design using a homogenization method," 1988.

[28] S. Nishiwaki, M. I. Frecker, S. Min, and N. Kikuchi, “Topology optimization of compliant mechanisms using the homogenization method,” *International journal for numerical methods in engineering*, vol. 42, no. 3, pp. 535–559, 1998.

[29] I. Hagiwara *et al.*, “Eigenfrequency maximization of plates by optimization of topology using homogenization and mathematical programming,” *JSME international journal. Ser. C, Dynamics, control, robotics, design and manufacturing*, vol. 37, no. 4, pp. 667–677, 1994.

[30] G. Allaire, F. Jouve, and H. Maillot, “Topology optimization for minimum stress design with the homogenization method,” *Structural and Multidisciplinary Optimization*, vol. 28, no. 2-3, pp. 87–98, 2004.

[31] J. Yoo and N. Kikuchi, “Topology optimization in magnetic fields using the homogenization design method,” *International Journal for Numerical Methods in Engineering*, vol. 48, no. 10, pp. 1463–1479, 2000.

[32] M. P. Bendsøe, “Optimal shape design as a material distribution problem,” *Structural optimization*, vol. 1, no. 4, pp. 193–202, 1989.

[33] G. I. Rozvany, M. Zhou, and T. Birker, “Generalized shape optimization without homogenization,” *Structural optimization*, vol. 4, no. 3-4, pp. 250–252, 1992.

[34] D. Tcherniak, “Topology optimization of resonating structures using simp method,” *International Journal for Numerical Methods in Engineering*, vol. 54, no. 11, pp. 1605–1622, 2002.

[35] V. Kandemir, O. Dogan, and U. Yaman, “Topology optimization of 2.5 d parts using the simp method with a variable thickness approach,” *Procedia Manufacturing*, vol. 17, pp. 29–36, 2018.

[36] Y. Liu, S. Zhuo, Y. Xiao, G. Zheng, G. Dong, and Y. F. Zhao, “Rapid modeling and design optimization of multi-topology lattice structure based on unit-cell library,” *Journal of Mechanical Design*, vol. 142, no. 9, 2020.

[37] Y. M. Xie and G. P. Steven, “A simple evolutionary procedure for structural optimization,” *Computers & structures*, vol. 49, no. 5, pp. 885–896, 1993.

[38] O. M. Querin, G. P. Steven, and Y. M. Xie, "Evolutionary structural optimisation (eso) using a bidirectional algorithm," *Engineering computations*, 1998.

[39] X. Yang, Y. Xie, G. Steven, and O. Querin, "Bidirectional evolutionary method for stiffness optimization," *AIAA journal*, vol. 37, no. 11, pp. 1483–1488, 1999.

[40] M. P. Bendsøe, A. Ben-Tal, and J. Zowe, "Optimization methods for truss geometry and topology design," *Structural optimization*, vol. 7, no. 3, pp. 141–159, 1994.

[41] C. D. Chapman, K. Saitou, and M. J. Jakiela, "Genetic algorithms as an approach to configuration and topology design," 1994.

[42] M. J. Jakiela, C. Chapman, J. Duda, A. Adewuya, and K. Saitou, "Continuum structural topology design with genetic algorithms," *Computer Methods in Applied Mechanics and Engineering*, vol. 186, no. 2-4, pp. 339–356, 2000.

[43] J. P. Groen and O. Sigmund, "Homogenization-based topology optimization for high-resolution manufacturable microstructures," *International Journal for Numerical Methods in Engineering*, vol. 113, no. 8, pp. 1148–1163, 2018.

[44] W. Zhang, W. Zhong, and X. Guo, "An explicit length scale control approach in simp-based topology optimization," *Computer Methods in Applied Mechanics and Engineering*, vol. 282, pp. 71–86, 2014.

[45] S. Wang, K. Tai, and M. Y. Wang, "An enhanced genetic algorithm for structural topology optimization," *International Journal for Numerical Methods in Engineering*, vol. 65, no. 1, pp. 18–44, 2006.

[46] C. D. Chapman and M. Jakiela, "Genetic algorithm-based structural topology design with compliance and topology simplification considerations," 1996.

[47] A. EBM, "Ti6al4v titanium alloy." Available at `https://pdf.directindustry.com/pdf/arcam/ti6al4v-titanium-alloy/19734-503503.html` (2020/09/08).